High level algorithm definition and physical and mathematical optimisations

MIPAS Level 2 Algorithm Theoretical Baseline Document (MIPAS Level 2 ATBD)

7 January 2020

Issue 7 Rev. 1
(Compliant with ORM Version 8.22)

Delivery of the study:

Support to MIPAS Level 2 processor verification and validation - Phase F

upgrade of the delivery of the original studies:

"Support to MIPAS Level 2 Product Validation" and

"Development of an Optimised Algorithm for Routine P, T and VMR Retrieval from MIPAS Limb Emission Spectra"

Prepared by:

Name	Institute
B. Carli	IFAC-CNR, Firenze, Italy
M. Carlotti	University of Bologna, Italy
S. Ceccherini	IFAC-CNR, Firenze, Italy
M. Höpfner	KIT, Karlsruhe, Germany
P. Raspollini	IFAC-CNR, Firenze, Italy
M. Ridolfi	University of Bologna, Italy
L. Sgheri	IAC-CNR, Firenze, Italy

TABLE OF CONTENTS

1 - INTRODUCTION 7

1.1 Changes from Issue 2A to Issue 3 of the present document 8

1.2 Changes from Issue 3 to Issue 4 of the present document 8

1.3 Changes from Issue 4 to Issue 5 of the present document 9

1.4 Changes from Issue 5 to Issue 6 of the present document 9

1.5 Changes from Issue 6 to Issue 7 of the present document 9

2 - OBJECTIVES OF THE TECHNICAL NOTE 10

3 - CRITERIA FOR THE OPTIMISATION 10

4 - THE INVERSE (OR RETRIEVAL) PROBLEM 11

4.1 Mathematical conventions 11

4.2 Theoretical background 12
4.2.1 The direct problem 12
4.2.2 The Gauss Newton method 13
4.2.3 The Levenberg-Marquardt method 15
4.2.4 Review of the possible convergence criteria 16
4.2.5 Use of external (a-priori) information in the inversion model 17
4.2.6 Use of the optimal estimation, for inclusion of LOS engineering information (LEI) in p,T retrieval 18
4.2.7 Covariance matrix and averaging kernels of the LM solution 21

4.3 The global fit analysis 23

4.4 The forward model 23
4.4.1 The radiative transfer 24
4.4.2 Convolution with the AILS 27
4.4.3 Convolution with the FOV 27
4.4.4 Instrumental continuum 28
4.4.5 Summary of required variables 28

4.5 Calculation of the VCM of the measurements 29
4.5.1 Operations performed on the interferogram to obtain the apodised spectrum 29
4.5.2 Computation of the VCM relating to a single microwindow 31
4.5.3 Computation of the inverse of the VCM 33

4.6 Calculation of the Jacobian matrix **K** *of the simulations* 34

4.7 Generalised inverse 35

4.8 Variance-covariance matrix of tangent height corrections 35

4.9 Tangent heights correction based on ECMWF data 37

5 - SCIENTIFIC ASPECTS AND PHYSICAL OPTIMISATIONS 39

5.1 Choice between retrieval of profiles at fixed levels and at tangent altitude levels 39

5.1.1 Retrieval at tangent altitude and interpolation between retrieved values 39
5.1.2 Retrieval at fixed levels 40
5.1.3 Discussion of the problem 40
5.1.4 Conclusions 41

5.2 Use of a-priori information **41**
5.2.1 - Precision improvement 41
5.2.2 - Systematic errors 42
5.2.3 - Hydrostatic equilibrium and LOS Engineering information 43

5.3 Latitudinal variability **44**
5.3.1 Angular spread of the limb measurements 44
5.3.2 Latitudinal temperature gradients 45
5.3.3 Modeling the latitudinal variability with a horizontal gradient 45

5.4 Earth model and gravity **48**
5.4.1 Earth model 48
5.4.2 Gravity 48

5.5 Ray tracing and atmospheric refraction **50**
5.5.1 Refraction model 52

5.6 Line shape modeling **52**
5.6.1 Numerical calculation of the Voigt profile 53
5.6.2 Approximation of the Voigt profile by the Lorentz function 54
5.6.3 χ-factors in the case of CO_2 and H_2O 54

5.7 Line-mixing **55**

5.8 Pressure shift **55**

5.9 Implementation of Non-LTE effects **56**

5.10 Self broadening **56**

5.11 Continuum **57**
5.11.1 Instrumental continuum 57
5.11.2 Near continuum 57
5.11.3 Far continuum 57

5.12 Interpolation of the profiles in the forward / retrieval model **59**

5.13 Interpolation of the "retrieved" profiles to a user-defined grid **60**

5.14 Optimized algorithm for construction of initial guess profiles and gradients **62**
5.14.1 Initial guess pressure, temperature and VMR profiles, and their horizontal gradients 62
5.14.2 Initial guess continuum profiles 63

5.15 Profiles regularization **63**
5.15.1 The error consistency (EC) method 63
5.15.2 The Iterative Variable Strength (IVS) regularization method 67

5.16 Cloud filtering **70**

6 - MATHEMATICAL OPTIMISATIONS **72**

6.1 Radiative Transfer integral and use of Curtis-Godson mean values **72**
6.1.1 Layering of the atmosphere 75

6.2 Secant law approximation for the calculation of Curtis-Godson quantities and definition of paths (not used in the ORM v.8) **77**

6.2.2 Sequence of the operations *81*

6.3 Interpolation of cross sections for different geometries ***82***

6.4 Calculation of the spectrum: spherical symmetries (not used in the ORM v.8) ***83***

6.5 Use of interpolation for the calculation of Planck function ***84***

6.6 Finite instrument field of view. ***85***

6.7 Analytical derivatives ***89***
6.7.1 General considerations *89*
6.7.2 Derivative with respect to the volume mixing ratio *91*
6.7.3 Derivative with respect to temperature *92*
6.7.4 Derivative with respect to the atmospheric continuum *93*
6.7.5 Derivative with respect to the tangent pressure *93*
6.7.6 Independence of retrieved variables *94*
6.7.7 New choice of continuum variables in the MIPAS processor starting from V.7.0. *94*

6.8 Convergence criteria ***96***

6.9 Pre-calculation of line shapes ***97***

6.10 Different grids during the cross-section calculation ***98***

6.11 Cross-section look-up tables ***98***

6.12 Variable frequency grids for radiative transfer computation ***99***

REFERENCES **100**

APPENDIX A: DETERMINATION OF THE VCM OF ENGINEERING TANGENT HEIGHTS IN MIPAS **103**

APPENDIX B: EVALUATION OF RETRIEVAL ERROR COMPONENTS AND TOTAL ERROR BUDGET **112**

APPENDIX C: GENERATION OF MW DATABASES AND OCCUPATION MATRICES **114**

APPENDIX D: GENERATION OF LUTS AND IRREGULAR FREQUENCY GRIDS (IG) **116**

APPENDIX E: GENERATION OF MW-DEDICATED SPECTRAL LINELISTS **117**

APPENDIX F: MIPAS OBSERVATION MODES **121**

ACRONYMS LIST	
AILS	Apodised Instrument Line Shape
ATBD	Algorithm Theoretical Baseline Document
ATMOS	Atmospheric Trace MOlecule Spectroscopy experiment
BAe	British Aerospace
CKD	Clough-Kneizys-Davies
CPU	Central Processing Unit
EC	Error Consistency
ECMWF	European Centre for Medium-range Weather Forecasts
ENVISAT	ENVironment SATellite
ESA	European Space Agency
FM	Forward Model
FOV	Field Of View
FR	Full Resolution measurements acquired by MIPAS in the first two years of operations (2002 – 2004)
FTS	Fourier Transform Spectrometer
FWHM	Full Width at Half Maximum
GN	Gauss Newton (minimization method)
HITRAN	HIgh-resolution TRANsmission molecular absorption database
HWHM	Half Width at Half Maximum
IAPTs	Implemented Atmospheric Pressures and Temperatures,
IFOV	Instantaneous Field Of View
IG	Irregular Grid
ILS	Instrument Line Shape
IMK	Institut für Meteorologie und Klimaforschung
IVS	Iterative Variable Strength (regularization method)
LEI	LOS Engineering Information
LM	Levenberg-Marquardt (minimization method)
LOS	Line Of Sight
LS	Lower Stratosphere
LSF	Least Squares Fit
LTE	Local Thermal Equilibrium

LUT	Look Up Table
MIPAS	Michelson Interferometer for Passive Atmospheric Sounding
ML2PP	MIPAS Level 2 Processor Prototype
MPD	Maximum Path Difference
MW	spectral MicroWindow
NESR	Noise Equivalent Spectral Radiance
NLSF	Non-linear Least Squares Fit
NLTE, Non-LTE	Non Local Thermal Equilibrium
NRT	Near Real Time
OFM	Optimized Forward Model
OR	Optimized Resolution measurements acquired by MIPAS from January 2005 to April 2012
ORM	Optimised Retrieval Model
PDS	Payload Data Segment
POEM	Polar Orbit Earth Mission
REC	Residuals and Errors Correlation analysis
RFM	Reference Forward Model
RMS	Root Mean Square
SVD	Singular Value Decomposition
TA	Tangent Altitude
UTLS	Upper Troposphere / Lower Stratosphere
VCM	Variance Covariance Matrix
VMR	Volume Mixing Ratio
VS	Variable Strength (regularization method)
ZFPD	Zero-Filled Path Difference
ZPD	Zero Path Difference

1 - Introduction

MIPAS (Michelson Interferometer for Passive Atmospheric Sounding) is an ESA developed instrument that operated on board of the ENVISAT satellite launched on a polar orbit on March 1st, 2002, as part of the first Polar Orbit Earth Observation Mission program (POEM-1). MIPAS measured the atmospheric limb-emission spectrum in the middle infrared (670 – 2410 cm^{-1}) from April 2002 until 8 April 2012, i.e. the day in which the contact with ENVISAT was lost. The first measurement acquired by MIPAS dates back to 24 March 2002. Starting from July 2002 nearly continuous measurements were acquired during the first two years of operations. In this mission phase, most of the measurements were acquired with a spectral resolution of 0.025 cm^{-1}, in the nominal scanning mode, consisting of 17 sweeps per limb scan, with tangent heights ranging from 6 to 68 km and steps of 3 km from 6 to 42 km, of 5 km from 42 to 52 km and of 8 km from 52 to 68 km. In this period only few measurements were acquired using the so called "special modes". The measurements relating to the first two years (2002 – 2004) of operations are referred to as Full-Resolution (FR) measurements.
Due to problems with the mirror driver of the interferometer, MIPAS measurements were discontinued at the end of March of 2004. In January 2005 MIPAS operations were resumed with a reduced maximum interferometric optical path difference (corresponding to a lower spectral resolution of 0.0625 cm^{-1} instead of the original 0.025 cm^{-1}) and with a finer vertical sampling step of the limb measurements. These measurements acquired from January 2005 onward are referred to as Optimized Resolution (OR) measurements. Several new special measurement modes were devised for this mission phase and a significant fraction of measurements was actually acquired in this configuration. Appendix F includes a detailed description of the measurement modes employed during the whole MIPAS mission.
The raw interferograms acquired by MIPAS are transformed into geo-located and radiometrically calibrated spectral radiances by the Level 1b processing chain. Subsequently, the Level 2 processor inverts the calibrated radiances to infer the vertical distribution profiles of numerous trace gases and atmospheric state variables.
Starting from 1995, in the frame of the ESA project "Development of an Optimised Algorithm for Routine P, T and VMR Retrievals from MIPAS Limb Emission Spectra" a scientific code referred to as the Optimized Retrieval Model (ORM) was developed for near real time (NRT) Level 2 analysis of MIPAS. The code was developed by optimizing the accuracy of the Level 2 products, with the limitations owing to the strong computing time constraint set by the needs of NRT processing. The results of the study were used by industry as an input for the development of a prototype for the Level 2 code, the so called ML2PP. In turn, the algorithms of the ML2PP were re-coded by a second industrial contractor and implemented in the ENVISAT payload data segment (PDS). MIPAS Level 2 products up to Version 5.x were generated by the ENVISAT PDS Level 2 processor. In the time frame from 2002 to 2004, MIPAS measurements were processed by ESA both Near-Real Time (NRT) and, subsequently, off-line (OFL) with the same PDS processor, but using different auxiliary data to get more accurate results at the expenses of an increased computing time. MIPAS Level 2 products Versions 6.x and 7.x were generated by ESA, using the ML2PP. The final reprocessing of MIPAS data, Version 8, was obtained using directly the ORM Version 8. This last version of the ORM differs significantly as compared to the older versions: the original NRT computing time requirements do not hold for this version, allowing the implementation of much more sophisticated and accurate algorithms. Moreover, while the earliest ESA Level 2 processor versions were able to handle only nominal mode MIPAS measurements, ORM version 8 is able to handle all measurement modes. The processing of the modes including tangent heights above 75 km is however limited to the sweeps with tangent altitudes lower than this bound. This choice prevents the assumption of Local Thermodynamic Equilibrium (LTE), still present in the ORM v8, from introducing too large model errors in the simulated radiances.

Using a pre-defined set of auxiliary data, the ORM v8 processor retrieves from MIPAS limb radiances the pressure at the tangent points of the limb measurements and the vertical profiles of temperature and of Volume Mixing Ratio (VMR) of the following atmospheric constituents: H_2O, O_3, HNO_3, CH_4, N_2O, NO_2, F11, F12, N_2O_5, $ClONO_2$, F22, F14, COF_2, CCl_4, HCN, C_2H_2, CH_3Cl, $COCl_2$, C_2H_6, OCS, HDO.

The present document describes the theoretical baseline of the algorithms implemented in the ORM Version 8. Physical and mathematical optimizations that were implemented in former ORM versions and are no longer used in Version 8 are still described in this document for future records. In these cases, however, the title of the related section is extended with the remark "not used in ORM v8".

1.1 Changes from Issue 2A to Issue 3 of the present document

The main changes consist in the introduction of new sections regarding the description of items that previously were either described in sparse memorandums and small notes or not described at all. Namely, the following new sections have been introduced:

- Sect. 5.13: Interpolation of the retrieved profiles to a user-defined grid,
- Sect. 5.14: Optimized algorithm for construction of initial guess profiles (including generation of continuum profiles described in sub-sect 5.14.1),
- Sect. 5.15: Profiles regularization
- Appendix A: Determination of the VCM of the engineering tangent heights in MIPAS,
- Appendix B: Evaluation of retrieval error components and total error budget (includes pT error propagation approach),
- Appendix C: Algorithm for generation of MW databases and occupation matrices,
- Appendix D: Algorithm for generation of LUTs and irregular frequency grids,
- Appendix E: Algorithm for generation MW-dedicated spectral linelists.

Furthermore, Sect. 4.5 regarding the calculation of the VCM of the measurements was strongly modified in order to be consistent with baseline modifications. A new sub-section, 4.5.3, describing the method used to calculate the inverse of the VCM of the measurements was introduced. This sub-section replaces the old Sect. 6.13 (now removed).
Additional sparse modifications were introduced in order to remove obsolete statements and make the document in line with the current status of the study.

1.2 Changes from Issue 3 to Issue 4 of the present document

The main change consists in the update of the section 5.15 describing the regularization adopted, that was modified as a consequence of the change of the observation scenario after January 2005.
Additional sparse modifications were introduced in order to remove obsolete statements and make the document in line with the current status of the study.
A notation change concerning adopted symbols for the used variables and parameters has been performed.
Some mismatchings have been corrected.

Introduction has been updated and modified according to changes occurred in instrument measurement mode.

Appendix C has been updated; a figure reporting a summary of the total error for the profiles retrieved from measurements acquired after January 2005 has been introduced.

Appendix F with the description of the MIPAS observation modes has been introduced.

A list of the used acronyms has been added together with a list of the main quantities with the adopted symbols.

1.3 Changes from Issue 4 to Issue 5 of the present document

Document modified in order to be compliant with ORM_ABC_PDS_V2.01 and IPF V. 6.0. In particular:

- Section 1, Introduction: adapted for compliance with the current study status.
- Sect. 4.2.3 new information included about the Levenberg-Marquardt method.
- Sect.s 4.2.4 and 6.8, new convergence criteria included.
- Sect. 4.2.7 new section regarding the calculation of covariance matrix and averaging kernels of the Levenberg-Marquardt solution.

Beyond these main modifications, the whole document has been revised to remove or update outdated sentences.

1.4 Changes from Issue 5 to Issue 6 of the present document

Document modified in order to comply with ORM_ABC_PDS_V3.0 / ML2PP V7.0. The main algorithm updates from ML2PP V6.0 to V7.0 concern the following areas:

a) The implementation of a self-adapting altitude-dependent regularization scheme that is very effective also when applied to the most difficult profiles, such as the H_2O VMR, that show strong variations across the altitude retrieval range.
b) Implementation of a change in continuum retrieval variables. The new selected variables make the retrieval more stable, and permit to reach a deeper minimum of the cost function optimized in the inversion.

The new implemented features are described in sections:

5.16 The Iterative Variable Strength (IVS) regularization method.
6.7.7 New choice of continuum variables in the MIPAS processor starting from V.7.0.

A few minor additional changes are spread throughout the whole document, as necessary to keep it aligned with the current status of the activities.

1.5 Changes from Issue 6 to Issue 7 of the present document

We describe the algorithms that are new in the ORM v8.22 as compared to the previous processor version (ORM_ABC_PDS_V3.0 / ML2PP V7.0). Note that at high level, the algorithms implemented in the ORM versions 8.0 and 8.22 do not differ, thus in this document we simply refer to ORM v.8, while alle the considerations made here apply also to ORM v.8.22. The present issue of the document includes modifications to pre-existing Sections as well as some new Sections. For future memory, we keep in the document also the description of some optimizations that were particularly important in the previous processor versions and that are no longer used in the ORM v8. In these cases, we explicitly mention “not used in the ORM v.8” in the related Section title and, at the end of the Section itself, we explain why the optimization is no longer used in the ORM v.8.

2 - Objectives of the technical note

The main objective of the present document is to provide a description of the equations implemented in the ORM algorithm. Whenever several options are possible for implementation, we outline the individual options and, for each of them, we assess advantages and disadvantages. We also provide a rationale for the choice of the preferred option for implementation in the code and identify a strategy for its validation.

For a further high-level description of the algorithms implemented in the Level 2 scientific code of MIPAS, the reader should also refer to the following published papers: *Ridolfi et al. (2000)*, *Raspollini et al. (2006)*, *Ceccherini et al. (2007, 2010), Raspollini et al. (2013), Ridolfi and Sgheri (2009, 2011, 2013, 2014)*.

3 - Criteria for the optimisation

In the implementation of the ORM code, the requirements that were considered with highest priority are due to:

- characteristics of input data,
- scientific requirements of output data,
- correctness of the atmospheric model,
- correctness of the instrument model,
- numerical accuracy,
- robustness in presence of erroneous observational data,
- reduced computing time.

The main difficulty was due to the last requirement, which, in presence of the others, imposed the search for physical and mathematical optimisations.
For the development of the initial ORM versions, some choices have been made on a purely theoretical basis. Subsequently, tests performed with real data have in some cases consolidated the results of theoretical tests, and in some other cases have suggested a different approach.
In the initial ORM code develpments, the ESA acceptance criterion, and therefore our choices, were based on the combined development of the ORM, an Optimised Forward Model (OFM) and a Reference Forward Model (RFM).

Retrievals with the ORM from spectra simulated with the OFM and the RFM, with and without measurement noise, allow the identification of errors due to:

1. measurement,
2. convergence or minimization,
3. approximations in the forward model, due to the optimisations.

Tests performed with different computing accuracy and with different profile discretizations allow assess, respectively:

4. the numerical accuracy
5. and the smoothing error.

The acceptance criterion required the ORM to limit errors 2. and 3. so that the overall error budget including errors from 1. to 5. as well as systematic error, is kept below the following requirements:

- 3% error in tangent pressure retrieval,
- 2 K error in temperature retrieval,
- 5% error in VMR retrievals,

in the tangent altitude range 8 - 53 km.
These were the requirements established at the beginning of the study in absence of specific indications regarding the ultimate accuracy attainable from MIPAS measurements. However, test retrievals performed later have shown that the above requirements cannot be met in the whole altitude range explored by the MIPAS scan and for all the constituents retrieved by the ESA Level 2 processor.

The problem of assessing the ultimate retrieval accuracy attainable from MIPAS measurements has been tackled in the framework of the study for the selection of optimized spectral intervals (microwindows, MW) for MIPAS retrievals (see Appendix C and Bennett et al.,(1999)).
An acceptance test for the code, on the basis of actual retrieval error has been performed by using the complete OFM/ORM chain as well as the reference spectra generated by the RFM.

In general, the strategy adopted to operate a choice for implementation in the code has been the following one:

- since an altitude error is directly connected to a pressure error, which in turn corresponds also to a VMR error, whenever an approximation corresponds to an altitude error the approximation is accepted if the error is less than 0.15 km (corresponding to a 2% pressure error). Actually, this is not a very conservative criterion but it is still satisfactory because it is applied only for the evaluation of approximations to model the instrument Field-Of-View (FOV) and line self-broadening.
- If the approximation does not correspond to an altitude error, the approximation is accepted on the basis of the radiance error it generates. Random error components must be smaller than the NESR (Noise Equivalent Spectral Radiance), systematic errors must be smaller than NESR divided by the square root of the multiplicity of the effect. If individual approximations behave as either random or systematic errors can only be assessed by the full retrieval process. An educated compromise is made by using an acceptance threshold equal to NESR/4.

In Sect. 4 we summarize the mathematics of the inverse problem. Sect. 5 is dedicated to the scientific aspects that affect the atmospheric and the instrument model and to the corresponding physical optimisations. Sect. 6 is dedicated to the choices related to the implementation of the calculations in the computing software and to the corresponding mathematical optimisations.

4 - The inverse (or retrieval) problem

4.1 Mathematical conventions

The mathematical conventions used in the present technical note are herewith summarised.
The functions may have the following attributes:

- Qualifiers: are given only as subscripts (or as superscript if subscript is not possible) and consist of a note that helps to distinguish the different functions (e.g. the Variance Covariance matrix S of different quantities) or the same function at different levels of the calculation (e.g. the iteration

number of a retrieved quantity). Parentheses are used to separate the qualifier from the other mathematical operations that can be confused with the qualifiers (e.g. to separate qualifiers from transpose or inversion operation).

- The variables of the functions can appear either as a subscript or as arguments. In order to provide a representation consistent with the convention of matrices and vectors, whenever possible, the variables relative to which the variability of the function is explicitly sampled within the code are shown as a subscript, while variables relative to which a dependence only exists implicitly in the equations are shown as arguments.

When dealing with matrices and vectors, bold symbols are used.
The operation of convolution is indicated with an asterisk.

4.2 Theoretical background

The problem of retrieving the altitude distribution of a physical or chemical quantity from limb-scanning observations of the atmosphere, drops within the general class of problems that require the fitting of a theoretical physical / mathematical model (or Forward Model, FM), that describes the behaviour of a given system, to a set of observations of the system itself. The theoretical model describes the system through a set of parameters (or the so called state vector $\mathbf{x}$) so that the retrieval procedure consists in the search for the set of values of the parameters $\mathbf{x}$ that produce the "best" simulation of the observations. The most commonly adopted criterion to accomplish the objective is the minimisation of a cost function, referred to as the $\chi^2(\mathbf{x})$ function. In the Least Squares Fit (LSF) approach, $\chi^2(\mathbf{x})$ is defined as the summation of the squared error-weighted differences between observations and simulations. When the forward model does not depend linearly on the unknown parameters the problem is called Non-linear Least Squares Fit (NLSF). In this case, the minimum of $\chi^2(\mathbf{x})$ cannot be found directly, by using a solution formula, and a numerical iterative minimization method must be used instead. Several methods exist for the NLSF, the one selected for our purposes is the Gauss Newton (GN) method modified according to the Levenberg-Marquardt (LM) criterion (see *Levenberg, 1944* and *Marquardt, 1963*). In the literature, this method is considered the most effective and robust in all the cases in which the calculation of the forward model implies a significant computational effort. The method requires also the computation of the forward model Jacobian, however, this additional effort is usually over-compensated by the extremely fast convergence rate of the method (very few iterations required) and by its accuracy in finding the local minimum of $\chi^2(\mathbf{x})$. In order to provide the framework of the subsequent discussion, the general mathematical formulation of the problem is herewith briefly reviewed. The formalism adopted here is described with full details in *Carlotti and Carli, (1994)*. A more general and comprehensive monography on inverse methods for atmospheric sounding is included in *Rodgers, (2000)*, with a slightly different formalism.

4.2.1 The direct problem

The spectral radiance reaching the spectrometer can be modelled, by means of the radiative transfer equation (described in Sect. 4.6), as a function $S = S(\mathbf{b}, x(z))$ of the observational parameters $\mathbf{b}$ and of the vertical distribution profile $x(z)$ of the atmospheric quantity to be retrieved (z being the altitude coordinate). The function $S(\mathbf{b},x(z))$ is called *forward model*. Since the radiative transfer does not represent a linear transformation, the problem of deriving the distribution $x(z)$ from the observed values of S cannot be solved through the analytical inversion of the radiative transfer equation.

A linear transformation connecting S and x(z) can be obtained by operating a first-order Taylor expansion of the radiative transfer equation, around an assumed profile $\tilde{x}(z)$. In the hypothesis that $\tilde{x}(z)$ is close enough to the true profile to drop in a linear behaviour of the function S, the Taylor expansion can be truncated to the first term to obtain:

$$S(\mathbf{b}, x(z)) = S(\mathbf{b}, \tilde{x}(z)) + \left[\frac{\partial S(\mathbf{b}, x(z))}{\partial x(z)}\right]_{x(z)=\tilde{x}(z)} \cdot \left[x(z) - \tilde{x}(z)\right] \quad , \quad \forall z \qquad (4.2.1)$$

Note that the profile x(z) here is considered as a continuous function. Equation (4.2.1) can be written as:

$$\Delta_S(\mathbf{b}) = \int_0^\infty K(\mathbf{b}, \tilde{x}(z))\left[\Delta_x(z)\right] dz \qquad (4.2.2)$$

where:

$$\Delta_S(\mathbf{b}) = S(\mathbf{b}, x(z)) - S(\mathbf{b}, \tilde{x}(z)) \qquad (4.2.3)$$

$$K(\mathbf{b}, \tilde{x}) = \left[\frac{\partial S(\mathbf{b}, x(z))}{\partial x(z)}\right]_{x(z)=\tilde{x}(z)} \qquad (4.2.4)$$

$$\Delta_x(z) = \left[x(z) - \tilde{x}(z)\right]. \qquad (4.2.5)$$

Equation (4.2.2) is an integral equation that represents a linear transformation of the unknown $\Delta_x(z)$ leading to the observations $\Delta_S(\mathbf{b})$ by way of the kernel $K(\mathbf{b}, \tilde{x})$.

4.2.2 The Gauss Newton method

In the case of practical calculations, the mathematical entities defined in Sect. 4.2.1 are represented by discrete values. Actually, we will deal with a finite number (*M*) of observations and a finite number (*N*) of values to represent, in a vector x(z), the altitude distribution of the unknown quantities (these *N* values will be denoted as "parameters" from now on).
As a consequence, the integral operator of Eq. (4.2.2) becomes a summation and the equation itself can be expressed in matrix notation as:

$$\mathbf{\Delta_S} = \mathbf{K}\,\mathbf{\Delta_x} \qquad (4.2.6)$$

In equation (4.2.6):

- $\mathbf{\Delta_S}$ is a column vector of dimension *M*. The entry m_j of $\mathbf{\Delta_S}$ is the difference between observation *j* and the corresponding simulation calculated using the assumed profile $\tilde{x}(z)$ (Eq. 4.2.3).

- **K** is a matrix (the Jacobian of the forward model) of *M* rows and *N* columns. The entry k_{ij} of **K** is the derivative of forward model simulation *i* with respect to element *j* of parameter vector **x** (Eq. 4.2.4)
- $\mathbf{\Delta_x}$ is a column vector of dimension *N*. The entry $(\mathbf{\Delta_x})_i$ of $\mathbf{\Delta_x}$ is the correction to be applied to the assumed value of parameter $\tilde{x}(z)$ in order to obtain its correct value $x(z)$. The goal of the retrieval is the determination of this vector.

The problem is therefore that of the search for a "solution matrix" **G** (of *N* rows and *M* columns) that, multiplied by vector $\mathbf{\Delta_S}$ provides $\mathbf{\Delta_x}$.
If the vector $\mathbf{\Delta_S}$ is characterised by the variance-covariance matrix (VCM) $\mathbf{S_m}$ (square matrixx of dimension *M*), the χ^2 function which must be minimised is defined as:

$$\chi^2 = \mathbf{\Delta_S}^T(\mathbf{S_m})^{-1}\mathbf{\Delta_S} \qquad (4.2.7)$$

and matrix **G** is equal to:

$$\mathbf{G} = (\mathbf{K}^T\mathbf{S}_m^{-1}\mathbf{K})^{-1}\mathbf{K}^T\mathbf{S}_m^{-1} \quad . \qquad (4.2.8)$$

The superscript “T” denotes the transpose and the superscript “-1” denotes the matrix inverse, if the inverse of $\mathbf{S_m}$ does not exist, its generalised inverse can be used instead (see *Kalman (1976)* and Sect. 4.7). If the unknown quantities are suitably chosen, matrix $(\mathbf{K}^T\mathbf{S}_m^{-1}\mathbf{K})$ is not singular, thought it might be ill-conditioned.
If the absolute minimum of the χ^2 function is found and $\mathbf{S}_m$ is a correct estimate of the measurement errors, the quantity defined by equation (4.2.7) has expectation value equal to (*M* - *N*) and a standard deviation equal to $\sqrt{M-N}$. The value of the quantity $\frac{\chi^2}{M-N}$ (the so called *normalized* or *reduced* chi-square) provides therefore a good estimate of the quality of the fit. Values of $\frac{\chi^2}{M-N}$ significantly deviating from unity, indicate the presence of incorrect assumptions in the retrieval.

The unknown vector $\mathbf{\Delta_x}$ is then computed as:

$$\mathbf{\Delta_x} = \mathbf{G}\,\mathbf{\Delta_S} \qquad (4.2.9)$$

and the new estimate of the parameters as:

$$x_e(z) = \tilde{x}(z) + \Delta_x(z) \qquad (4.2.10)$$

The errors associated with the solution to the inversion procedure can be characterised by the variance-covariance matrix ($\mathbf{S_x}$) of x(z) given by:

$$\mathbf{S_x} = \mathbf{G}\mathbf{S_m^T}\mathbf{G}^T = \left(\mathbf{K}^T\mathbf{S_m^{-1}}\mathbf{K}\right)^{-1} \qquad (4.2.11)$$

Matrix $\mathbf{S}_x$ permits to estimate how the experimental random errors map into the uncertainty of the retrieved parameters. Actually, the square roots of the diagonal elements of $\mathbf{S}_x$ measure the root mean square (r.m.s.) error of the corresponding parameter. The off-diagonal element s_{ij} of matrix $\mathbf{S}_x$,

normalised to the square root of the product of the two diagonal elements s_{ii} and s_{jj}, provides the correlation coefficient between parameters *i* and *j*.
If the hypothesis of linearity made in Sect. 4.2.1 about the behaviour of function S is satisfied, Eq. (4.2.10) provides the result of the retrieval process. If the hypothesis is not satisfied, the minimum of the χ^2 function has not been reached but only a step has been done towards the minimum and the vector x(z) computed by Eq. (4.2.10) represents a better estimate of the parameters with respect to $\tilde{x}(z)$. In this case the whole procedure must be reiterated starting from the new estimate of the parameters which is used to produce a new Jacobian **K**. Convergence criteria are therefore needed in order to establish when the minimum of the χ^2 function has been approached with sufficient accuracy to stop the iterations.

4.2.3 The Levenberg-Marquardt method

The Levenberg-Marquardt (LM) method introduces a modification to the procedure described in the previous sub-section. This modification permits to achieve the convergence also in the case of strongly non-linear problems. The LM method consists in modifying matrix $(\mathbf{K}^T\mathbf{S}_m^{-1}\mathbf{K})$ before using it in (4.2.8) for the calculation of **G**. The modification consists in amplifying the diagonal elements of matrix $\mathbf{A} \equiv (\mathbf{K}^T\mathbf{S}_m^{-1}\mathbf{K})$ according to:

$$(\mathbf{K}^T(\mathbf{S}_m)^{-1}\mathbf{K})_{ii} \Leftarrow (\mathbf{K}^T(\mathbf{S}_m)^{-1}\mathbf{K})_{ii} * (1+\lambda_M) \qquad (4.2.12)$$

where λ_M is a positive scalar with the effect of damping the norm of the correction vector $\mathbf{\Delta_x}$, thus reducing the risk of projecting the parameters vector far away from the local linearity region. The modification (4.2.12) also rotates the correction vector $\mathbf{\Delta_x}$, from the GN direction towards the direction of $-\nabla\chi^2$, thus increasing the chance of obtaining a smaller χ^2 with the updated parameters vector.

The algorithm proceeds as follows:

1. calculate the χ^2 function and matrix **A** for the initial values of the parameters,
2. set λ_M to a initial "small" value (e.g. 0.001) and modify **A** according to Eq. (4.2.12),
3. calculate the new estimate of the parameters for the current choice of λ_M using equation (4.2.9),
4. calculate the new value of χ^2 using equation (4.2.7),
5. if χ^2 calculated at step 4 is greater than that calculated at step 1, then increase λ_M by an appropriate factor (e.g. 10) and repeat from step 3 (micro iteration),
6. if χ^2 calculated at step 4 is smaller than that calculated at step 1, then decrease λ_M by an appropriate factor (e.g. 10), adopt the new set of parameters to compute a new matrix **A** and proceed to step 3 (macro iteration).

The (macro) iterations are stopped when a pre-defined convergence criterion is fulfilled. An advantage of using the LM method is that the calculation of the Jacobian matrix can be avoided in the micro-iterations. For the development of the ORM code, however, since most operational retrievals do not to deal with a strongly non-linear problem and since the calculation of the Jacobian matrix is faster when performed within the forward model, simultaneously with the calculation of the limb-radiances, the ORM is optimized for a Gauss Newton loop (macro-iteration), i.e. the Jacobian matrix is computed also in the micro-iterations loops.

As a "side effect" the LM modification (4.2.12) improves the conditioning of matrix **A** and introduces a regularizing effect that is mostly lost during the iterations, whenever sufficient information on the retrieved parameters in present in the observations. This feature permits to avoid the risk of introducing biases in the solution. More details on the regularizing effect of the LM method can be found in *Doicu et al. (2010)*. The behaviour of the LM method is critically reviewed and compared to the Tikhonov regularization with constant strength in *Ridolfi et al. (2011)*. For a deeper understanding of the regularizing LM method we still recommend *Ridolfi et al. (2011)* and especially all the pertinent references cited therein.

4.2.4 Review of the possible convergence criteria

Here we review several conditions which can be considered for the definition of a convergence criterion.

1. The relative variation of the χ^2 function obtained in the present iteration with respect to the previous iteration is less than a given threshold t_1 i.e.:

$$\left|\frac{\chi^2(\mathbf{x}^{iter-1}) - \chi^2(\mathbf{x}^{iter})}{\chi^2(\mathbf{x}^{iter})}\right| < t_1 \qquad (4.2.14)$$

   where *iter* is the current iteration index.

2. The maximum correction to be applied to the parameters for the next iteration is below a fixed threshold t_2 i.e.:

$$\mathrm{Max}_j \left|\frac{(\mathbf{x}^{iter-1})_j - (\mathbf{x}^{iter})_j}{(\mathbf{x}^{iter})_j}\right| < t_2 \qquad (4.2.15)$$

   different thresholds can be eventually used for the different types of parameters (T, p, and VMR). The absolute variations of the parameters can also be considered instead of the relative variations, whenever an absolute accuracy requirement is present for a parameter (as for the case of temperature). Auxiliary parameters, such as continuum and instrumental offset, that are retrieved to improve the quality of the inversion should not be included in this check.

3. Since the expression (4.2.15) is singular whenever a parameter is equal to zero, an alternative formula which can be considered is:

$$\varsigma^2 = \frac{\left(\mathbf{x}^{\mathrm{iter}} - \mathbf{x}^{iter-1}\right)^{\mathrm{T}} \left(\mathbf{S}_{\mathbf{x}}\right)^{-1}_{iter} \left(\mathbf{x}^{\mathrm{iter}} - \mathbf{x}^{iter-1}\right)}{N} < t_3 \qquad (4.2.15\text{bis})$$

   Here ς^2 represents the normalized chi-square, testing the compatibility of $\mathbf{x}_{\mathrm{iter}}$ with $\mathbf{x}_{\mathrm{iter\text{-}1}}$ within the error described by the covariance matrix $\left(\mathbf{S}_{\mathbf{x}}\right)_{iter}$. The quantity $f = \sqrt{\varsigma^2}$ roughly represents the average distance between of $\mathbf{x}_{\mathrm{iter}}$ and $\mathbf{x}_{\mathrm{iter\text{-}1}}$ measured as a fraction of the error bar $\left(\mathbf{S}_{\mathbf{x}}\right)_{iter}$. Unless a secondary minimum of the cost function has been approached, f measures also the convergence error. This consideration can be used to set the threshold t_3 on the basis of the maximum acceptable

convergence error. For example, if we require the convergence error to be smaller than 1/10 of the error due to measurement noise, then we should select $t_3 = (1/10)^2 = 0.01$. The reason that discouraged using (4.2.15bis) since the very beginning of the ORM development, is that $(\mathbf{S_x})_{iter}$ does not really represent the noise error of the solution when the retrieval is far from convergence. The experience gained in retrievals from real data, however, showed that the inter-iteration changes of $\mathbf{S_x}$ are usually marginal and (4.2.15bis) can be generally used with satisfaction.

4. The difference between the real χ^2 and the chi-square computed in the linear approximation (χ^2_{LIN}) is less than a fixed threshold t_3:

$$\left| \frac{\chi^2(\mathbf{x}^{iter}) - \chi^2_{LIN}(\mathbf{x}^{iter})}{\chi^2(\mathbf{x}^{iter})} \right| < t_4 \qquad (4.2.16)$$

where χ^2_{LIN} is computed using the expression:

$$\chi^2 = \left((\mathbf{1} - \mathbf{KG})\boldsymbol{\Delta}_S\right)^T \mathbf{S}_\mathbf{m}^{-1}\left((\mathbf{1} - \mathbf{KG})\boldsymbol{\Delta}_S\right) \qquad (4.2.17)$$

4. The iteration index has reached a maximum allowed value (t_4):

$$iter \geq t_4 \qquad (4.2.18)$$

The choice of the most appropriate logical combination of the above conditions (which provides the convergence criterion) is discussed in the section of mathematical optimisations (see Sect. 6.8).

4.2.5 Use of external (a-priori) information in the inversion model

When some a-priori information on the retrieved parameters is available from sources external to the MIPAS interferometer, the error of retrieved parameters can be improved by including this information in the retrieval process. Assuming the a-priori information to consist both of an estimate $\mathbf{x_A}$ of the state vector and of its variance covariance matrix $\mathbf{S_A}$, the combination of the retrieved vector with the externally provided vector $\mathbf{x_A}$ can be made, after the convergence has been reached, by using the following Bayesian formula (of the weighted average):

$$\mathbf{x_{oe}} = \left(\mathbf{S_x^{-1}} + \mathbf{S_A^{-1}}\right)^{-1}\left(\mathbf{S_x^{-1}}\left(\mathbf{G}\boldsymbol{\Delta}_S + \tilde{x}\right) + \mathbf{S_A^{-1}}\mathbf{x_A}\right) \qquad (4.2.19)$$

Introducing the explicit expressions of $\mathbf{G}$ and $\mathbf{S_x}$ given respectively by equations (4.2.8) and (4.2.11), equation (4.2.19) becomes:

$$\mathbf{x^{oe}} = \left(\mathbf{K}^T\mathbf{S_m^{-1}}\mathbf{K} + \mathbf{S_A^{-1}}\right)^{-1}\left(\mathbf{K}^T\mathbf{S_m^{-1}}\boldsymbol{\Delta}_S + \mathbf{S_x^{-1}}\tilde{\mathbf{x}} + \mathbf{S_A^{-1}}\mathbf{x^A}\right) \qquad (4.2.20)$$

This is the so called “optimal estimation” or “Maximum A-posteriori Probability, MAP) formula (see *Rodgers (1976)* and *Rodgers (2000)*). Eq. (4.2.20) can be used also at each retrieval iteration step, in place of eq. (4.2.9), to derive the new estimate of the unknowns. When equation (4.2.20) is used in the

iterations of the retrieval, the a-priori estimate of the retrieved parameters provides information on the unknown quantities also at the altitudes where the measurements may contain only poor information. In this case the retrieval process is more stable (see also Sect. 5.2).
However, when using equation (4.2.20) in the retrieval iterations, the external information and the retrieval information are mixed during the minimisation process and therefore they cannot be individually accessed at any time. This prevents to easily estimate the correction and the bias introduced by the a-priori information on the retrieved quantities.
The decision on whether to use equation (4.2.20) during the retrieval iterations or to use (4.2.9) during the retrieval and (4.2.20) after the convergence has been reached, chiefly depends on the type of a-priori information we are dealing with. In the cases in which the used a-priori information is expected not to bias the results of the retrieval (e.g. in the cases in which independent a-priori estimates are available for different retrievals), equation (4.2.20) can be profitably used during the retrieval iterations.
Further advantages and disadvantages of the use of a-priori information are described as a scientific aspect in Sect. 5.2.

4.2.6 Use of the optimal estimation, for inclusion of LOS engineering information (LEI) in p,T retrieval

Engineering LOS data are updated at each scan and therefore constitute an effective and independent source of information which can be routinely used in p,T retrievals and does not bias the retrieved profiles. In this case it is really worth to use formula (4.2.20) at each iteration step and let the LOS information to help the convergence of the retrieval. In this case the a-priori information does not provide directly an estimate of the unknowns of the retrieval, but a measurement of a quantity related to the unknowns by way of the hydrostatic equilibrium law.
The engineering information on the pointing consists of a vector $\Delta\mathbf{z}$ containing the tangent height increments between the sweeps of the current scan and of a VCM $\mathbf{V}_z$ estimating the actual error of the vector $\Delta\mathbf{z}$. The components of the vector $\Delta\mathbf{z}$ are defined as:

$$\begin{aligned} \Delta z_1 &= z_2 - z_1 \\ &\vdots \\ \Delta z_{N_{sw}-1} &= z_{N_{sw}} - z_{N_{sw}-1} \end{aligned} \qquad (4.2.21)$$

where N_{sw} is the number of sweeps of the considered scan. If we define the vector $\mathbf{\Delta_{S1}}$ as:

$$\mathbf{\Delta_{S1}} = \Delta z - \Delta \mathbf{z}_{tg} \qquad (4.2.22)$$

where $\Delta \mathbf{z}_{tg}$ is the vector of the differences between the tangent altitudes at the current iteration; instead of equation (4.2.6) we have a couple of equations defining the retrieval problem:

$$\begin{aligned} \mathbf{\Delta_S} &= \mathbf{K}\ \mathbf{\Delta_x} \\ \mathbf{\Delta_{S,L}} &= \mathbf{K_L}\ \mathbf{\Delta_{x,L}} \end{aligned} \qquad (4.2.23)$$

where the matrix $\mathbf{K_L}$ is the jacobian that links the differences between tangent altitudes with the vector of the unknowns. This matrix has to be re-computed at each retrieval iteration (as matrix $\mathbf{K}$); the recipe for the calculation of this matrix is given in Sect. 4.2.6.1. The χ^2 function to be minimised becomes:

$$\chi^2 = \boldsymbol{\Delta}_S^T \mathbf{S}_m^{-1} \boldsymbol{\Delta}_S + \boldsymbol{\Delta}_{S1}^T \mathbf{S}_z^{-1} \boldsymbol{\Delta}_{S1} \tag{4.2.24}$$

and the vector $\boldsymbol{\Delta}_{x,L}$ which minimises this χ^2 is given by:

$$\boldsymbol{\Delta}_{x,L} = \left[\mathbf{K}^T \mathbf{S}_m^{-1} \mathbf{K} + \mathbf{K}_L^T \mathbf{S}_z^{-1} \mathbf{K}_L\right]^{-1} \left[\mathbf{K}^T \mathbf{S}_m^{-1} \boldsymbol{\Delta}_S + \mathbf{K}_L^T \mathbf{S}_z^{-1} \boldsymbol{\Delta}_{S1}\right] \tag{4.2.25}$$

Therefore, if we define matrices **A**, **B**, and $\mathbf{B}_L$ as:

$$\begin{aligned} \mathbf{A} &= \left[\mathbf{K}^T \mathbf{S}_m^{-1} \mathbf{K} + \mathbf{K}_L^T \mathbf{S}_z^{-1} \mathbf{K}_L\right] \\ \mathbf{B} &= \mathbf{K}^T \mathbf{S}_m^{-1} \\ \mathbf{B}_L &= \mathbf{K}_L^T \mathbf{S}_z^{-1} \end{aligned} \tag{4.2.26}$$

equation (4.2.25) becomes:

$$\boldsymbol{\Delta}_{x,L} = (\mathbf{A})^{-1} \left[\mathbf{B}\boldsymbol{\Delta}_S + \mathbf{B}_L \boldsymbol{\Delta}_{S1}\right] \tag{4.2.27}$$

In the linear regime, this equation provides the solution of the retrieval problem. At each retrieval iteration the retrieval program has to compute matrices **K**, $\mathbf{K}_L$, **A**, **B** and $\mathbf{B}_L$, then, since LM algorithm is used, matrix **A** has to be modified accordingly to equation (4.2.13) and afterwards used in equation (4.2.27) in order to derive $\hat{\mathbf{y}}$.

In this approach, the equation which defines the linear chi-square χ^2_{LIN} is:

$$\chi^2_{LIN} = \left[\boldsymbol{\Delta}_S - \mathbf{K}\boldsymbol{\Delta}_x\right]^T \mathbf{S}_m^{-1} \left[\boldsymbol{\Delta}_S - \mathbf{K}\boldsymbol{\Delta}_x\right] + \left[\boldsymbol{\Delta}_{S1} - \mathbf{K}_L \boldsymbol{\Delta}_{x1}\right]^T \mathbf{S}_z^{-1} \left[\boldsymbol{\Delta}_{S1} - \mathbf{K}_L \boldsymbol{\Delta}_{x1}\right] \tag{4.2.28}$$

this is the equation to be used instead of equation (4.2.17).

4.2.6.1 Calculation of the jacobian matrix $\mathbf{K}_L$ of the engineering tangent altitudes (TA)

Let's explicitly write the second component of equation (4.2.23):

$$\Delta \boldsymbol{z} = \Delta \boldsymbol{z}_{tg} + \mathbf{K}_L \boldsymbol{\Delta}_x \tag{4.2.29}$$

It is clear from this relation that the component *i,j* of $\mathbf{K}_L$ is:

$$\mathbf{K}_L(i,j) = \frac{\partial \Delta z_i}{\partial x_j} \quad \text{with } i=1, \ldots, N_{sw}\text{-}1 \text{ and } j=1, \ldots, I_{top} \tag{4.2.30}$$

where I_{top} is the total number of fitted parameters in the current retrieval.

Now, being $\mathbf{x}_{pT}$ the vector of the unknowns of p,T retrieval, it is composed as follows:

- The first N_{sw} elements represent the tangent pressures,
- The elements from $N_{sw}+1$ up to $2*N_{sw}$ represent the tangent temperatures,

- The elements from $2*N_{sw}+1$ up to I_{top} represent atmospheric continuum and instrumental offset parameters.

Since engineering tangent altitudes do not depend on continuum and offset parameters $\mathbf{K_L}(i,j)=0$ for $i=1, .., N_{sw}-1$ and $j=2*N_{sw}+1, ..., I_{top}$.
On the other hand, the engineering tangent altitudes are connected with tangent pressures and tangent temperatures through hydrostatic equilibrium law.

The transformation which leads to $\Delta\mathbf{z}$ starting from P,T is defined by the hydrostatic equilibrium:

$$\Delta z_i = -\frac{T_{i+1}+T_i}{2\gamma_I}\ln\left(\frac{P_{i+1}}{P_i}\right) \quad \text{for } i=1,...,N^{sw}-1 \tag{4.2.31}$$

where P and T indicate, as usual, pressure and temperature and γ_i is equal to:

$$\gamma_i = g_0(\bar{z},\varphi)\cdot\frac{M}{R} \tag{4.2.32}$$

where g_0 is the acceleration of gravity at the mean altitude of the layer $\bar{z}=(z_{i+1}+z_i)/2$ and latitude Φ_s; M is the air mass and R the gas constant. If the altitudes are measured in km and T in Kelvin, we get $M/R = 3.483676$.
The jacobian matrix $\mathbf{J}_1$ associated with the transformation (4.2.31) is a $(N_{sw}-1;\ 2N_{sw})$ matrix containing the derivatives:

$$\begin{aligned}
\mathbf{J}_1(i,j) &= \frac{\partial\Delta z_i}{\partial P_j} \qquad \text{for } i=1,...,N_{sw}-1 \text{ and } j=1,...,N_{sw} \\
\mathbf{J}_1(i,j) &= \frac{\partial\Delta z_i}{\partial T_{j-N^{sw}}} \qquad \text{for } i=1,...,N_{sw}-1 \text{ and } j=N_{sw}+1,...,2N_{sw}
\end{aligned} \tag{4.2.33}$$

Therefore, deriving equations (4.2.31) we obtain:

$$\mathbf{J}_1(i,j) = -\frac{T_{i+1}+T_i}{2\gamma}\left[\frac{1}{P_{i+1}}\delta_{j=i+1}-\frac{1}{P_i}\delta_{j=i}\right]$$
$$\text{for } i=1,\ldots N_{sw}-1 \text{ and } j=1,\ldots N_{sw} \tag{4.2.34}$$

$$\mathbf{J}_1(i,j) = -\frac{1}{2\gamma}\ln\left(\frac{P_{i+1}}{P_i}\right)\left[\delta_{j-N^{sw}=i+1}+\delta_{j-N^{SW}=i}\right]$$
$$\text{for } i=1,\ldots N_{sw}-1 \text{ and } j=N_{sw}+1,\ldots 2N_{sw}$$

where the function δ is defined as:

$$\delta_{\text{arg}} = \begin{cases} 1 \text{ if } [\text{arg}] = \text{TRUE} \\ 0 \text{ if } [\text{arg}] = \text{FALSE} \end{cases} \tag{4.2.35}$$

Considering that the original vector of the unknowns of p,T retrieval contains also continuum and offset parameters, matrix $\mathbf{K_L}$ can be obtained by extending matrix $\mathbf{J}_1$ with as many columns as required to

reach the dimension (N_{sw}-*1*; I_{top}). As mentioned earlier, these extra columns contain only zeroes due to the fact that the tangent altitudes do not depend on continuum and offset parameters.

For what concerns the variance-covariance matrix $\mathbf{S}_z$ of MIPAS tangent heights required for the implementation of the equations reported in Sect. 4.2.6, this matrix is derived using a simple algorithm based on MIPAS pointing specifications. This algorithm is described in Appendix A.

4.2.7 Covariance matrix and averaging kernels of the LM solution

The covariance matrix (VCM) and the averaging kernels (AKs, *Rodgers, 2000*) are diagnostic tools commonly used to characterize the solution of the retrieval. In particular, the VCM describes the mapping of the measurement noise error onto the solution, while the AKs describe the response of the system (instrument and retrieval algorithm) to infinitesimal variations in the true atmospheric state, hence characterizes the vertical resolution of the retrieved profiles. Three different algorithms are implemented in the ORM to calculate VCM and AKs of the LM solution. The three methods represent different levels of sophistication and are selectable via a switch.

Method 1): VCM and AKs of the LM solution, in the GN approximation.

If matrix $(\mathbf{K}^T\mathbf{S}_m^{-1}\mathbf{K})$ of Eq. (4.2.12) is well-conditioned (for the inversion involved in Eq. (4.2.8)) and if the iterative process converges within the machine numerical precision, then the LM solution coincides with the GN solution, therefore its VCM ($\mathbf{S}_x$) and AK ($\mathbf{A}_x$) are calculated as (see *Rodgers (2000)*):

$$\mathbf{S}_x = (\mathbf{K}^T\mathbf{S}_m^{-1}\mathbf{K})^{-1} \quad (4.2.36)$$

$$\mathbf{A}_x = \mathbf{I} \quad (4.2.37)$$

where $\mathbf{I}$ is the identity matrix of dimension equal to the number of elements in the state vector $\mathbf{x}$.

Method 2): VCM and AKs of the LM solution, in the single-iteration approximation.

If matrix $(\mathbf{K}^T\mathbf{S}_m^{-1}\mathbf{K})$ of Eq. (4.2.12) is ill-conditioned and / or the retrieval iterations are stopped by some physically meaningful criterion before the exact numerical convergence is reached, then the expressions (4.2.36) and (4.2.37) may be a rough approximation, as the LM and the GN solutions do differ. In this case the LM damping term must be taken into account. The LM solution $\mathbf{x}_{\mathrm{LM}}$ at the last iteration can be written as:

$$\mathbf{x}_{\mathrm{LM}} = \mathbf{x}_i + \left(\mathbf{K}^T\mathbf{S}_m^{-1}\mathbf{K} + \lambda_M\mathbf{D}\right)^{-1} \cdot \mathbf{K}^T\mathbf{S}_m^{-1}\left(\mathbf{y} - \mathbf{f}(\mathbf{x}_i)\right) \quad (4.2.38)$$

where $\mathbf{x}_i$ is the state vector estimate at the second-last iteration, $\mathbf{y}$ the observations vector with VCM $\mathbf{S}_m$, $\mathbf{f}$ the forward model and $\mathbf{K}$ its Jacobian evaluated at $\mathbf{x}_i$. We also introduced $\mathbf{D} \equiv \mathrm{diag}\left[\mathbf{K}^T\mathbf{S}_m^{-1}\mathbf{K}\right]$, where the symbol diag[...] indicates a diagonal matrix with diagonal elements equal to those of the matrix reported within the squared brackets [...]. If we assume $\mathbf{x}_i$ to be independent of $\mathbf{y}$ (single iteration approximation), for the VCM and AKs of the LM solution we easily get:

$$\mathbf{S}_x = \left(\mathbf{K}^T\mathbf{S}_m^{-1}\mathbf{K} + \lambda_M\mathbf{D}\right)^{-1} \cdot \mathbf{K}^T\mathbf{S}_m^{-1}\mathbf{K} \cdot \left(\mathbf{K}^T\mathbf{S}_m^{-1}\mathbf{K} + \lambda_M\mathbf{D}\right)^{-1} \quad (4.2.39)$$

$$\mathbf{A}_{\mathbf{x}} = \left(\mathbf{K}^T\mathbf{S}_m^{-1}\mathbf{K} + \lambda_M\mathbf{D}\right)^{-1}\mathbf{K}^T\mathbf{S}_m^{-1}\mathbf{K} \tag{4.2.40}$$

Method 3): VCM and AKs of the LM solution, taking into account the whole minimization path.
The limiting approximations of methods 1) and 2) illustrated above can be avoided with a mathematical trick. We start by rewriting the generic form of the iterative Eq.(4.2.38) as:

$$\mathbf{x}_{i+1} = \mathbf{x}_i + \left(\mathbf{K}_i^T\mathbf{S}_m^{-1}\mathbf{K}_i + \lambda_i\mathbf{D}_i\right)^{-1}\cdot\mathbf{K}_i^T\mathbf{S}_m^{-1}\left(\mathbf{y}-\mathbf{f}(\mathbf{x}_i)\right) \equiv \mathbf{x}_i + \mathbf{G}_i\left(\mathbf{y}-\mathbf{f}(\mathbf{x}_i)\right) \tag{4.2.41}$$

here we explicitly added a subscript i to all quantities depending on the iteration count i, and we introduced the gain matrix:

$$\mathbf{G}_i \equiv \left(\mathbf{K}_i^T\mathbf{S}_m^{-1}\mathbf{K}_i + \lambda_i\mathbf{D}_i\right)^{-1}\cdot\mathbf{K}_i^T\mathbf{S}_m^{-1} \tag{4.2.42}$$

If we introduce the iteration-dependent matrix $\mathbf{T}_i$ as:

$$\left(\mathbf{T}_i\right)_{jk} \equiv \frac{\partial\left(\mathbf{x}_i\right)_j}{\partial\mathbf{y}_k} \tag{4.2.43}$$

and we assume the retrieval is stopped (by some meaningful criterion) at iteration $i+1=r$, then formally, the VCM and the AK of the LM solution can be written as:

$$\mathbf{S}_{\mathbf{x}} = \mathbf{T}_r\mathbf{S}_y\mathbf{T}_r^T \tag{4.2.44}$$

$$\mathbf{A}_{\mathbf{x}} \equiv \frac{\partial\mathbf{x}_r}{\partial\mathbf{x}} = \frac{\partial\mathbf{x}_r}{\partial\mathbf{y}}\frac{\partial\mathbf{y}}{\partial\mathbf{x}} = \mathbf{T}_r\mathbf{K}_r \tag{4.2.45}$$

Matrices $\mathbf{T}_i$ can be calculated as the derivative of Eq. (4.2.41) with respect to $\mathbf{y}$. Neglecting the derivatives of $\mathbf{K}_i$ with respect to $\mathbf{x}_i$ (hypothesis already exploited in the Gauss-Netwon approach itself), and consequently with respect to $\mathbf{y}$, we get:

$$\mathbf{T}_{i+1} = \mathbf{T}_i + \mathbf{G}_i\left(\mathbf{I}-\mathbf{K}_i\mathbf{T}_i\right) \tag{4.2.46}$$

Rearranging Eq. (4.2.46) and considering that the initial guess $\mathbf{x}_0$ does not depend on the observations $\mathbf{y}$, we obtain the following recursive formula for the matrices $\mathbf{T}_i$:

$$\mathbf{T}_{i+1} = \mathbf{G}_i + (\mathbf{I} - \mathbf{G}_i\mathbf{K}_i)\mathbf{T}_i \qquad \text{with} \qquad \mathbf{T}_0 = \mathbf{0} \tag{4.2.47}$$

Equation (4.2.47) for $i=0,1, \ldots, r-1$ determines $\mathbf{T}_r$. This matrix is then used in Eq.s (4.2.44) and (4.2.45) to provide the VCM and the AK of the solution $\mathbf{x}_r$.
Eqs. (4.2.44) and (4.2.45) show that both the VCM and the AK depend on $\mathbf{T}_r$ which, in turn, as shown by Eq. (4.2.47), depends on the path in the parameter space followed by the minimization procedure, from the initial guess to the solution. Note that, if an iteration step is done with $\lambda_i = 0$ (Gauss-Newton iteration) from Eq. (4.2.42) we get $\mathbf{G}_i\mathbf{K}_i=\mathbf{I}$ and from Eq. (4.2.47) it follows that $\mathbf{T}_r$ is independent of the steps performed before the considered iteration. Therefore, we can say that a Gauss-Netwon iteration resets the memory of the path followed before that iteration.

This last method 3) was first introduced in *Ceccherini and Ridolfi (2010)*, it does not use hypotheses such as well-conditioned inversion, exact numerical convergence or single-iteration retrieval, therefore in general it is far more accurate than the more usual methods 1) and 2) described earlier. The relative accuracy of methods 1) 2) and 3) is critically reviewed and tested in *Ceccherini and Ridolfi (2010)*.

4.3 The global fit analysis

In the global-fit introduced by *Carlotti, (1988),* the whole altitude profile is retrieved from simultaneous analysis of all the selected limb-scanning measurements. The retrieval is based on the least-squares criterion and looks for a solution profile that has a number *p* of degrees of freedom smaller than or equal to the number of the observed data points. In practice the profile is retrieved at *p* discrete altitudes and at intermediate altitudes an interpolated value is used.
In this approach, the vector $\mathbf{\Delta}_S$ that appears in Eq. (4.2.9) is the difference between all the selected observations and the corresponding simulations (all the spectral intervals and all the limb-scanning measurements are included in this vector, eventually also a-priori information can be included).
The unknown vector $\mathbf{\Delta}_x$ may contain a different variable depending on the retrieval we are performing, in general it is, however, an altitude dependent distribution which is sampled at a number of discrete altitudes as well as some spectroscopic and instrumental parameters (e.g. atmospheric continuum).
The use of the LM method for the minimisation of the χ^2 function requires the computation of the quantities that appear in the equations (4.2.8) and (4.2.9), namely:

- simulations for all the limb-scanning measurements and all the selected microwindows,
- the variance covariance matrix $\mathbf{S}_y$ of the observations,
- the Jacobian $\mathbf{K}$ of the forward model

The simulation of the observed spectra is made using the forward model described in Sect. 4.4.
The variance covariance matrix related to the apodised spectral data (observations) is derived starting from noise levels, apodisation function and zero filling information, using the algorithm described in Sect. 4.5.
The Jacobian matrix containing the derivatives of the simulated spectra with respect to the unknown parameters is computed as described in Sect. 4.6.

4.4 The forward model

The task of the forward model is the simulation of the spectra measured by the instrument in the case of known atmospheric composition. Therefore, this model consists of:

1. the simulation of the radiative transfer through the Earth's atmosphere for an ideal instrument, with infinitesimal field of view (FOV), infinite spectral resolution and no distortions in the line-shape.
2. the convolution of this spectrum with the apodised instrument line shape (AILS) to obtain the apodised spectrum which includes line shape distortions.
3. the convolution with the FOV of the instrument.

Note that while step 1. provides a model of the atmospheric signal entering the instrument, steps 2. and 3. simulate instrument effects. Not all the instrumental effects are however simulated in the forward model, since the retrieval is performed from calibrated spectra, instrument responsivity and phase errors are corrected in Level 1b processing. The AILS which includes the effects of finite spectral resolution, instrument line-shape distortions and apodization is provided by Level 1b processing.

4.4.1 The radiative transfer

In order to obtain the spectral radiance $S(\sigma, z_g)$ (i.e. the intensity as a function of the wavenumber σ) for the different limb geometries (denoted by the tangent altitude z_g of the observation g), the following radiative transfer integral has to be calculated:

$$S(\sigma, z_g) = \int_{s^b}^{1} B(\sigma, T(s_g)) d\tau(\sigma, s_g) \qquad (4.4.1)$$

Where:

σ	= wavenumber
z_g	= tangent altitude of the optical path g
s_g	= co-ordinate along the line of sight (LOS) belonging to the optical path with the tangent altitude z_g
$S(\sigma,z_g)$	= spectral intensity
$T(s_g)$	= temperature along the Line of Sight
$B(\sigma,T)$	= source function
$\tau(\sigma,s_g)$	= transmission between the point s_g on the LOS and the observer located at s_0. This quantity depends on the atmospheric composition, pressure and temperature through the co-ordinate s.
b	= indicator for the farthest point that contributes to the signal

Under the assumption of local thermodynamic equilibrium (LTE), and in the absence of scattering (e.g. from cloud particles), B(σ,T) is the Planck function:

$$B(\sigma, T) = \frac{2hc^2\sigma^3}{\exp\left[\frac{hc\sigma}{K_B T}\right] - 1} \qquad (4.4.2)$$

with
h = Planck's constant
c = speed of the light in vacuum
K_B = Boltzmann's constant

The transmission can be expressed as a function of s_g:

$$\tau(\sigma, s_g) = \exp\left[-\int_{s_0}^{s_g} \overline{k(\sigma, s')}\eta(s')ds'\right] \qquad (4.4.3)$$

with $\eta(s_g) = \frac{p(s_g)}{K_B T(s_g)}$ = number density of the air

$p(s_g)$ = pressure

and the weighted absorption cross section:

$$\overline{k(\sigma, s_g)} = \sum_{m=1}^{N^{ms}} k_m(\sigma, s_g) x_m^{VMR}(s_g) \qquad (4.4.4)$$

where N^{ms} = number of different molecular species that absorb in the spectral region under consideration
$x_m^{VMR}(s_g)$ = volume mixing ratio (VMR) of the species m at the point s_g
$k_m(\sigma,s_g)$ = absorption cross sections of the chemical species m

In the retrieval model the atmospheric continuum emission is taken into account as an additional species with VMR = 1 and the corresponding cross section is fitted as a function of altitude and microwindow (see Sect. 5.11.3). For the continuum calculation in the self standing forward model the cross sections are taken from a look up table and the real VMR of the continuum species is used (see Sect. 5.11.3).

Equation (4.4.1) can now be written as:

$$\begin{aligned} S(\sigma, s_g) &= \int_{s_0}^{s_g^b} B(\sigma, T(s_g)) \frac{d\tau(\sigma, s_g)}{ds_g} ds_g = \\ &= \int_{s_0}^{s_g^b} B(\sigma, T(s_g)) \overline{k(\sigma, s_g)} \eta(s_g) \tau(\sigma, s_g) ds_g \end{aligned} \qquad (4.4.5)$$

In order to determine the integral (4.4.5) two basic steps are necessary:

- the ray tracing, i.e. the determination of the optical path s_g and, consequently, the temperature $T(s_g)$, the pressure $p(s_g)$ and the volume mixing ratio $x^{VMR}{}_m(s_g)$ along the LOS and
- the calculation of the absorption cross sections $k_m(\sigma,s_g)$

Ray tracing

The line of sight in the atmosphere is determined by the position and the viewing direction of the instrument, and by atmospheric refraction. The refractive index of air depends mainly on pressure, temperature and water vapour content, therefore it is a function of the position within the atmosphere. An assessment of a few ray-tracing and air refraction models is presented in Sect. 5.5.

Absorption cross section calculation

The absorption cross section of one molecular species m as a function of temperature and pressure is given by the following sum over all lines of the species:

$$k_m(\sigma, T, p) = \sum_{l=1}^{lines} L_{m,l}(T) A_{m,l}^{A}(\sigma - \sigma_{m,l}, T, p) \qquad (4.4.6)$$

where $L_{m,l}(T)$ = line strength of line l of species m
$\sigma_{m,l}$ = central wavenumber of line l of species m

$A^{A}_{m,l}\ (\sigma\text{-}\sigma_{m,l},T,p)$ = line profile (line-shape)

The line strength is calculated by the formula:

$$L_{m,l}(T) = L_{m,l}(T_0)\frac{Q_m(T_0)}{Q_m(T)}\cdot\frac{\exp\left[-\frac{hcE''_{m,l}}{K_B T}\right]}{\exp\left[-\frac{hcE''_{m,l}}{K_B T_0}\right]}\cdot\frac{1-\exp\left[-\frac{hc\sigma_{m,l}}{K_B T}\right]}{1-\exp\left[-\frac{hc\sigma_{m,l}}{K_B T_0}\right]} \qquad (4.4.7)$$

with $L_{m,l}(T_0)$ = line strength at reference temperature T^0
$Q_m(T)$ = total internal partition function
$E''_{m,l}$ = lower state energy of the transition

The basic line shape is the Voigt function $A^{V}_{m,l}(\sigma-\sigma_{m,l},T,p)$ - the convolution of the Doppler $A^{D}_{m,l}(\sigma-\sigma_{m,l},T)$ and the Lorentz profile $A^{L}_{m,l}(\sigma-\sigma_{m,l},T,p)$:

$$A^{V}_{m,l}(\sigma-\sigma_{m,l},T,p) = A^{D}_{m,l}(\sigma-\sigma_{m,l},T) * A^{L}_{m,l}(\sigma-\sigma_{m,l},T,p) \qquad (4.4.8)$$

The Doppler profile is given by the formula

$$A^{D}_{m,l}(\sigma-\sigma_{m,l},T) = \sqrt{\frac{\ln 2}{\pi}}\frac{1}{\alpha^{D}_{m,l}}\exp\left[-\ln 2\frac{(\sigma-\sigma_{m,l})^2}{\alpha^{D\ 2}_{m,l}}\right] \qquad (4.4.9)$$

with the half width at half maximum (HWHM) of the line:

$$\alpha^{D}_{m,l} = \sigma_{m,l}\sqrt{2\ln 2\frac{K^B T}{M_m c^2}} \qquad (4.4.10)$$

where

M_m = molecular mass of species m

The Lorentz function is:

$$A^{L}_{m,l}(\sigma-\sigma_{m,l},T,p) = \frac{1}{\pi}\frac{\alpha^{L}_{m,l}}{\alpha^{L\ 2}_{m,l}+(\sigma-\sigma_{m,l})^2} \qquad (4.4.11)$$

and the Lorentz HWHM:

$$\alpha^{L}_{m,l} = \alpha^{L_0}_{m,l}\frac{p}{p^0}\left[\frac{T^0}{T}\right]^{\gamma_{m,l}} \qquad (4.4.12)$$

with :

$\alpha^{L_0}_{m,l}$ = Lorentz half width at reference temperature T_0 and reference pressure p_0
$\gamma_{m,l}$ = coefficient of temperature dependence of the half width

Using the substitutions:

$$x_{m,l} = \sqrt{\ln 2}\,\frac{\sigma - \sigma_{m,l}}{\alpha^{D}_{m,l}} \tag{4.4.13}$$

and

$$y_{m,l} = \sqrt{\ln 2}\,\frac{\alpha^{L}_{m,l}}{\alpha^{D}_{m,l}} \tag{4.4.14}$$

the Voigt function can be rewritten as:

$$A^{V}_{m,l}(\sigma - \sigma_{m,l}, T, p) = \sqrt{\frac{\ln 2}{\pi}}\,\frac{1}{\alpha^{D}_{m,l}}\,K(x_{m,l}, y_{m,l}) \tag{4.4.15}$$

with:

$$K(x_{m,l}, y_{m,l}) = \frac{y_{m,l}}{\pi}\int_{-\infty}^{+\infty}\frac{e^{-t^2}}{(x_{m,l} - t)^2 + y_{m,l}^{\;2}}\,dt \tag{4.4.16}$$

4.4.2 Convolution with the AILS

In order to take into account the

- finite spectral resolution of the instrument
- distortion of the line-shape by the instrument
- the apodisation of the observed spectra,

the spectrum $S(\sigma,z_g)$ is convolved with $AILS(\sigma)$, giving:

$$S_A(\sigma, z_g) = S(\sigma, z_g) * AILS(\sigma) \tag{4.4.16}$$

$AILS(\sigma)$ is the Apodised Instrument Line Shape that is obtained by convoluting the measured ILS with the apodisation function used for the apodisation of the observed spectra.

4.4.3 Convolution with the FOV

The responsivity of the instrument to the incident radiance depends on the inclination with which the light beams within the FOV, travel with respect to the instrument optical axis. In the case of MIPAS, since the atmosphere is assumed homogeneous in the across-track direction, only the variations of the responsivity as a function of the elevation angle are relevant. Moreover, the distance between the satellite and the tangent points of the limb measurements is much greater than the vertical range of the limb scan, thus, the angular response function of the instrument can be represented using a limb-scanning-angle-invariant altitude distribution.
$FOV(z_g,z)$ describes the instrument responsivity within the finite FOV of MIPAS as a function of the altitude z. In the case of MIPAS, $FOV(z_g,z)$ is represented by a piecewise linear curve tabulated in the

input files. For the simulation of the spectrum affected by the finite FOV ($S_{FA}(\sigma,z_g)$) the following convolution is calculated:

$$S_{FA}(\sigma, z_g) = S_A(\sigma, z) * FOV(z_g, z) \qquad (4.4.17)$$

4.4.4 Instrumental continuum

For the simulation of the instrumental continuum an additional (microwindow dependent and sweep independent) term is added to $S_F(\sigma, z_g)$. This term is fitted in the retrieval program.

4.4.5 Summary of required variables

For the atmospheric model:

- pressure along the line of sight g — $p(s_g)$
- temperature along the line of sight g — $T(s_g)$
- volume mixing ratio along the line of sight g — $x^{VMR}(s_g)$

For the ray tracing:

- altitude and viewing direction of the instrument or
- tangent altitude (in case of homogeneously layered and spherical atmosphere) — z_g

For the cross section calculation:

- central wavenumber of transition *l* of species *m* — $\sigma_{m,l}$
- reference line strength of transition *l* of species *m* — $L_{m,l}(T^0)$
- lower state energy of transition *l* of species *m* — $E''_{m,l}$
- total internal partition function of species *m* — $Q_m(T)$
- molecular mass of species *m* — M_m
- reference Lorentz half width of transition *l* of species *m* — $\alpha^{L_0}_{m,l}$
- coefficient of temperature dependence of the half width — $\gamma_{m,l}$

For the AILS convolution:

- apodised instrument line shape — $AILS(\sigma)$

For the FOV convolution:

- field of view function — $FOV(z_g,z)$

Note: The forward model implemented in the ORM processor (Sect. 4.4) is not designed to simulate limb emission radiances when scattering and absorption processes are relevant, as in the presence of

clouds. For this reason, MIPAS spectral radiance measurements are filtered out for the presence of clouds before Level 2 processing. The cloud-filtering algorithm employed in the ORM pre-processing stage is described in Sect. 5.17.

4.5 Calculation of the VCM of the measurements

The variance covariance matrix (VCM) of the residuals $\mathbf{S_m}$, used in Eq. (4.2.24), is in principle given by the summation of the VCM of the observations $\mathbf{S_y}$ and the VCM of the forward model $\mathbf{S_{FM}}$:

$$\mathbf{S_m} = \mathbf{S_y} + \mathbf{S_{FM}} \tag{4.5.1}$$

However, since:

- the amplitude of the forward model error is not accurately known;
- correlations between forward model errors are difficult to quantify

in the retrieval algorithm we choose to use $\mathbf{S_m} = \mathbf{S_y}$. The entity of the forward model errors is evaluated by analyzing the behaviour of the χ^2 - test for the different microwindows, at the different altitudes. In particular, the obtained χ^2 - test is compared with its expected value as determined on the basis of the total error evaluated by the so called “Residuals and Error Correlation (= REC)" analysis (see *Piccolo et al. (2001)*).

Herewith we describe how the VCM of the observations $\mathbf{S_y}$ is derived.
Even if the points of the interferograms measured by MIPAS are sampled independently of each other (no correlation between the measurements), the spectral data are affected by correlation. The correlation arises from the data processing performed on the interferogram (e.g. apodisation).
For this reason the noise levels provided by Level 1B processing do not fully characterise the measurement errors and the computation of a complete VCM $\mathbf{S_y}$ of the spectrum $S(\sigma)$ is needed.

In Section 4.5.1 we describe the operations performed on the interferogram in order to obtain the apodised spectrum. On the basis of these operations, in Sect. 4.5.2 we describe how the variance covariance matrix $\mathbf{S_y}$ of the observations ise derived. Finally, in Sect. 4.5.3 the procedure used to invert $\mathbf{S_y}$ is described.

4.5.1 Operations performed on the interferogram to obtain the apodised spectrum

The standard MIPAS interferogram is a double-sided interferogram obtained with a nominal maximum optical path difference (MPD) of +/- 20 cm in the FR measurements and +/- 8 cm in the OR measurements. The apodised spectrum $\hat{S}(\sigma)$ is obtained by subsequently performing the following operations on the interferogram:

1. **Zero-filling**
   During Level 1B processing, in order to exploit the fast Fourier Transform algorithm, the number of points of the interferogram is made equal to a power of 2 by extending the interferogram with zeroes from the MPD to the Zero-Filled Path Difference (ZFPD).
   The measured interferogram is therefore equal to an interferogram with maximum path difference ZFPD, multiplied by a boxcar function *Π(d)* defined as:

$$\Pi^{MPD}(d)=\begin{cases}1 & \text{when } d\in[-\text{MPD},\text{MPD}]\\ 0 & \text{when } d\notin[-\text{MPD},\text{MPD}]\end{cases} \quad \text{(MPD = Max. Path Difference)} \qquad (4.5.2)$$

2. **Fourier Transformation (FT)**

Let us call $\mathbf{S}_{\mathbf{NAHR}}(\sigma)$ the spectrum obtained from the measured (and zero-filled) interferogram and $\mathbf{S}_{\mathbf{HR}}(\sigma)$ the spectrum that would have been obtained from the interferogram with maximum path difference ZFPD. $\mathbf{S}_{\mathbf{NAHR}}(\sigma)$, $\mathbf{S}_{\mathbf{HR}}(\sigma)$ and $\mathrm{FT}[\Pi^{MPD}(d)]$ are all given in the sampling grid $\Delta\sigma=\frac{1}{2\cdot ZFPD}$.

Since the FT of the product of two functions is equal to the convolution of the FT's of the two functions, we obtain:

$$\mathbf{S}_{\mathbf{NAHR}}(\sigma)=\mathbf{S}_{\mathbf{HR}}(\sigma)*\mathrm{FT}[\Pi^{MPD}(d)]. \qquad (4.5.3)$$

3. **Re-sampling at the fixed grid**

Since a pre-defined and constant grid is required by the ORM for its optimisations, the spectrum is re-sampled at a fixed grid $\Delta\sigma=0.025\,\mathrm{cm}^{-1}=\frac{1}{2\cdot D}$, with D equal to 20 cm ($\Delta\sigma=0.0625\,\mathrm{cm}^{-1}=\frac{1}{2\cdot D}$, with D equal to 8 cm for the OR measurements). The performed operation can be written as:

$$\mathbf{S}_{\mathbf{NA}}(\sigma)=\mathbf{S}_{\mathbf{NAHR}}*FT\left[\Pi^{ZFPD}(d)\right], \qquad (4.5.4)$$

where $\mathbf{S}_{\mathbf{NA}}(\sigma)$ is calculated at the fixed grid $\Delta\sigma=\frac{1}{2\cdot D}$.

In this case the operation (4.5.4) is not a classical convolution among quantities that are defined on the same grid (e.g. Eq. (4.5.3)), but is a re-sampling process which changes the grid spacing from $\frac{1}{2\cdot ZFPD}$ of $\mathbf{S}_{\mathbf{NAHR}}$ to $\frac{1}{2\cdot D}$ of $\mathbf{S}_{\mathbf{NA}}$.

This operation does not introduce correlation between the spectral points only if MPD ≥ D.
If MPD ≥ D the result of (4.5.4) is equal to the FT of a ±20 cm (±8 cm for OR) interferogram.
If MPD < D the result of (4.5.4) is equal to the zero-filling to 20 cm (8 cm for OR) path difference of an interferogram with path difference MPD, therefore the spectral points are correlated to each other.
The NESR values given in the Level 1B product are computed after this re-sampling step.

4. **Apodisation**

The apodised spectrum $\hat{\mathbf{S}}(\sigma)$ is obtained by convolving the spectrum $\mathbf{S}_{NA}(\sigma)$ with the apodisation function $\theta_{ap}(\sigma)$, sampled at $\Delta\sigma=\frac{1}{2\cdot D}$.

$$\hat{S}(\sigma)=S_{NA}(\sigma)*\theta_{ap}(\sigma) \qquad (4.5.5)$$

4.5.2 Computation of the VCM relating to a single microwindow

In the case of MIPAS data the microwindows are usually well separated and it is reasonable to assume as uncorrelated the spectral data points belonging to different microwindows. As a consequence, the variance covariance matrix of the spectrum $\mathbf{S}_y$ is a block-diagonal matrix with as many blocks as many microwindows are processed, and the dimension of each block is equal to the number of spectral points in the corresponding microwindow. We assume that different points of the microwindow are characterised by the same error, but different microwindows can have different errors. In this section we derive the relationship that applies to each block and for simplicity with $\mathbf{S}_y$ we refer to a single block rather than to the full VCM of the observations.

The correlation between different spectral points of the microwindow is due to the apodisation process and to the zero-filling that is present in the case of MPD < D.
If $\mathrm{MPD} \geq \mathrm{D}$, only the apodisation is a cause of correlation and the VCM $\mathbf{S}_y$ of the apodised spectrum $\hat{\mathbf{S}}(\sigma)$ can be computed from the VCM $\mathbf{S}_{NA}$ associated with $S_{NA}(\sigma)$, ($\mathbf{S_{NA}}$ is a diagonal matrix since the spectral points of $S_{NA}(\sigma)$ are uncorrelated) and from the Jacobian $\mathbf{J}$ of the transformation (4.5.5):

$$\mathbf{S}_y = \mathbf{J}\mathbf{S}_{\mathbf{NA}}\mathbf{J}^T = \mathbf{S}_{\mathbf{NA}}\mathbf{J}\mathbf{J}^T \tag{4.5.6}$$

In Eq. (4.5.6) the order of the operations has been changed because $\mathbf{S}_{NA}$ is a diagonal matrix and all the diagonal elements are equal. The diagonal values are equal to $(\mathrm{NESR})^2$, where NESR is the quantity calculated after operation 3 of Sect. 4.5.1.
The calculation of matrix $\mathbf{J}$ is straightforward. From the explicit expression of the convolution (4.5.5):

$$\hat{S}(\sigma_{\mathrm{i}}) = \sum_j S_{NA}(\sigma_{\mathrm{j}}) \cdot \theta_{ap}(\sigma_{\mathrm{i}} - \sigma_j) \tag{4.5.7}$$

it follows that the entry i,k of matrix $\mathbf{J}$ is equal to:

$$\mathbf{J}_{i,k} = \theta_{ap}(\sigma_i - \sigma_k) \tag{4.5.8}$$

and the variance covariance matrix $\mathbf{S}^{\mathbf{y}}$ can be computed as:

$$\left(\mathbf{S}_y\right)_{i,j} = \left(NESR\right)^2 \mathbf{J}_{i,k}\mathbf{J}^T_{k,j} = \left(NESR\right)^2 \cdot \sum_k \theta_{ap}(\sigma_{\mathrm{i}} - \sigma_k) \cdot \theta_{ap}(\sigma_j - \sigma_k)\,. \tag{4.5.9}$$

If $\mathrm{MPD} < \mathrm{D}$ also the effect of zero-filling must be taken into account. Furthermore, the mathematics is more difficult because zero-filling introduces a correlation between the spectral points of $\mathbf{S_{NA}}(\sigma)$ (Eq. (4.5.4)) and the measurement error of this spectrum is characterised by a VCM $\mathbf{S}_{NA}$, with off-diagonal elements different from zero.
The apodised spectrum $\hat{S}(\sigma)$ of a measurement made with MPD<D is given by:

$$\hat{S}(\sigma) = S_{NA}(\sigma) * \theta_{MPD}(\sigma) \tag{4.5.10}$$

where $\theta_{MPD}(\sigma)$ is the apodisation function that is used in the case of a zero-filled spectrum. In the interferogram domain the FT of $\theta_{MPD}(\sigma)$ is a function that applies the selected apodisation rule between zero and MPD and is zero-filled between MPD and D.
As in the case of Eq. (4.5.6), $\mathbf{S}_y$ is obtained from the following equation :

$$\mathbf{S}_y = \mathbf{J} \cdot \mathbf{S}_{\mathbf{NA}} \mathbf{J}^T \tag{4.5.11}$$

where in this case **J** is the Jacobian of the apodisation with $\theta_{MPD}(\sigma)$ and $\mathbf{S_{NA}}$ is the VCM of the zero filled spectrum and has off-diagonal elements different from zero. Therefore, we know the diagonal elements of this matrix, which are equal to the NESR calculated in Level 1B, but further calculations must be performed in order to determine the off-diagonal elements.

A few simple considerations allow us to overcome this difficulty.
The spectrum $S_{NA}(\sigma)$ measured with maximum path difference MPD can be expressed as a function of the spectrum $S_{NAD}(\sigma)$ measured with maximum path difference D :

$$S_{NA}(\sigma) = S_{NAD}(\sigma) * FT\left[\Pi^{MPD}(d)\right] \tag{4.5.12}$$

and $\mathbf{S_{NA}}$ can be computed as a function of $\mathbf{S_{NAD}}$ using the following expression:

$$\mathbf{S}_{\mathbf{NA}} = \mathbf{F}\mathbf{S}_{\mathbf{NAD}}\mathbf{F}^T, \tag{4.5.13}$$

where **F** is the Jacobian matrix associated with the transformation (4.5.12).
Since $\mathbf{S_{NAD}}$ is a diagonal matrix

$$\mathbf{S}_{\mathbf{NA}} = \mathbf{F} \cdot x \cdot \mathbf{I}\mathbf{F}^T = x\mathbf{F}\mathbf{F}^{\mathbf{T}}, \tag{4.5.14}$$

where $\boldsymbol{I}$ is the identity matrix and x is the value of each diagonal element of $\mathbf{S_{NAD}}$ (also in this case it is assumed that the spectral data in the same microwindow are affected by the same error).
From Eq. (4.5.14), the diagonal elements of $\mathbf{S_{NA}}$ are equal to:

$$\left(\mathbf{S}_{\mathbf{NA}}\right)_{ii} = \left| f(\sigma) \cdot x \right| ; \tag{4.5.15}$$

where $f(\sigma)$ is a "continuous representation" of the columns of the matrix **F**. Using the Parseval theorem we get:

$$\left| f(\sigma) \right|^2 = \frac{1}{D} \int_0^D \left[\Pi^{MPD}(d)\right] \cdot \left[\Pi^{MPD}(d')\right] dd' = \frac{MPD}{D}, \tag{4.5.16}$$

and since $\left(\mathbf{S}_{\mathbf{NA}}\right)_{ii} = \left(NESR\right)^2$, from Eq. (4.5.15) and Eq. (4.5.16) we obtain :

$$x = \frac{D}{MPD} \cdot \left(NESR\right)^2 \tag{4.5.17}$$

The result obtained with Eq. (4.5.17) implies that the measurement of the NESR, even if it does not fully determine $\mathbf{S_{NA}}$, can be used to fully determine $\mathbf{S_{NAD}}$.

Therefore, we can express $S(\sigma)$ as a function of $S_{NAD}(\sigma)$. From Eq. (4.5.10) and Eq. (4.5.12) we obtain:

$$S(\sigma) = S_{NAD}(\sigma) * FT\left[\Pi^{MPD}(d)\right] * \theta_{MPD}(\sigma) \quad (4.5.18)$$

and since from the definition of the apodisation function it follows that $FT\left[\Pi^{MPD}(d)\right] * \theta_{MPD}(\sigma) = \theta_{MPD}(\sigma)$, it results :

$$S(\sigma) = S_{NAD}(\sigma) * \theta_{MPD}(\sigma) \quad (4.5.19)$$

This expression is analogous to Eq. (4.5.5), where $S_{NA}(\sigma)$ has been replaced by $S_{NAD}(\sigma)$ and the apodisation function has been replaced with the apodisation function related to MPD. Using this expression the calculations of the VCM related to $S(\sigma)$ requires the following calculation:

$$\mathbf{S}_y = \mathbf{J}\mathbf{S}_{\mathbf{NAD}}\mathbf{J}^T = \mathbf{J} \cdot x \cdot \mathbf{I}\mathbf{J}^T = x\mathbf{J}\mathbf{J}^{\mathbf{T}} \quad (4.5.20)$$

and from Eq. (4.5.17) it follows that

$$\mathbf{S}_y = \frac{D}{MPD}(NESR)^2 \mathbf{J}\mathbf{J}^T \quad (4.5.21)$$

The result is similar to the one found for MPD ≥ D with the exception of the extra term $\frac{D}{MPD}$. Besides, since the apodisation function contains 0 values between MPD and D, $\mathbf{J} \cdot \mathbf{J}^T$ and $\mathbf{S_y}$ are singular matrices.

4.5.3 Computation of the inverse of the VCM

In the ORM the inverse of matrix $\mathbf{S_y}$ is required. If $\mathbf{S_y}$ is a block-diagonal matrix, also $(\mathbf{S_y})^{-1}$ is a block-diagonal matrix and is made of blocks equal to the inverse of the blocks of $\mathbf{S_y}$.
As stated earlier, when MPD < D the "ranks" of the blocks are smaller than their dimension. This fact would be evident in the case in which the VCM is calculated in a sufficiently broad spectral range. However, in the ORM, where microwindows are used and correlations are calculated in a limited spectral range, the truncations make the determinant different from zero even if the number of independent pieces of information is less than the dimension of the matrix and the singularity of the matrix is not always automatically detected. The problem can be solved by modifying the routine that inverts the VCM: the VCM is inverted with the Singular Value Decomposition method (see Section. 4.7) also when the determinant is different from zero and the smallest eigenvalues are set equal to 0. The number of the eigenvalues set to 0 is given by the number of dependent points in the spectrum ($(1-MPD/D)*n1$, where $n1$ is the dimension of the matrix (equal to the number of the sampling points of the microwindow included in the fit).
This issue is further complicated by the use of a selected set of spectral points for the retrieval (microwindows with masked points, see Appendix C). When a subset of points is used for the retrieval the blocks of $\mathbf{S_y}$ are made by a corresponding subset of lines and columns. By reducing the dimension of the block the ratio between the rank and the dimension of the block is altered. The selection of a fraction of eigenvalues provides an useful conservative criterion.

4.6 Calculation of the Jacobian matrix **K** *of the simulations*

The use of Gauss-Newton algorithm for the minimisation of the χ^2 function requires the computation of the Jacobian matrix **K** of the simulations. The element of indexes *i,j* of this matrix is defined by the following relationship:

$$K_{i,j} = \left.\frac{\partial F_i(x)}{\partial x_j}\right|_{x=\tilde{x}} \qquad (4.6.1)$$

where F_i is the spectrum simulated with the Forward Model, and x_j is the *j-th* component of the vector **x** containing the unknowns of the problem**.** The vector **x** of the unknown parameters may contain the following groups of the parameters:

- pressures at the tangent points,
- temperatures at tangent altitudes,
- VMR of one or more gases at tangent altitudes
- continuum at tangent altitudes, for the central frequencies of the microwindows used for the retrieval,
- instrumental continuum (i.e. additive term to the spectrum that is assumed as constant varying the observation geometry and function of the microwindow),

Notes regarding Version 8 of the ORM:

- ORM v.8 includes the so called *Multi-Target Retrieval* (MTR) functionality. Although not exploited in the standard Level 2 retrievals, this functionality allows the simultaneous retrieval of tangent pressure, temperature and VMR profiles of one or more atmospheric constituents. This functionality is particularly important for the retrieval of gases that contribute to the limb emission spectrum only with very weak features which, at the MIPAS spectral resolution, ovelap with lines of other gases that are also not retrievable with high precision. In this case, to minimize (and properly account for) the interference error, the best approach is the simultaneous retrieval of all the gases that contribute to the selected spectral region. This approach was used e.g. by *Valeri et al. 2016* to retrieve for the first time the Phosgene ($COCl_2$) vertical profile from MIPAS observations.
- The ORM v.8 includes the capability to retrievethe VMR of the HDO isotopologue. Since this is the only isotopologue retrieved in the standard MIPAS ESA Level 2 inversions, there is no specific algorithm implemented in the ORM v.8 to retrieve generic isotopic ratios or their deviation from the standard natural ratio assumed in the HITRAN spectroscopic database to scale the line intensities. In the ORM auxiliary data files, HDO is actually handled as a "separate" gas, with its own specific molecule code, line parameters and VMR profile different from those of the other H_2O isotopologues. Despite of that, like in HITRAN, also in the MIPAS spectroscopic database the HDO line intensities are scaled by the HDO natural isotopic abundance so that, whenever HDO is not retrieved, it is possible to use a single H_2O VMR profile in the forward model calculations. This choice implies that, internally, for the HDO retrieval the ORM still uses the H_2O VMR profile as initial guess (and a-priori, see Sect. 5.2) for HDO. After completion of the retrieval, however, the HDO profile is multiplied by the natural isotopic abundance assumed in the spectroscopic database and is reported in the output files with the correct units (ppmv).

The derivatives of the forward model are computed in correspondence of a vector $\tilde{\mathbf{x}}$ containing:

- the initial guess of the unknown parameters in the first iteration step,

- the new guess of the parameters in the subsequent iterations.

These derivatives can be computed either numerically or analytically. In general, the numerical approach requires an extra call to the forward model for the computation of each partial derivative, while in the analytical approach the calculation of the derivatives can be performed in parallel with the calculation of the spectrum.
Tests have shown that:

- the derivatives with respect to tangent pressure, VMR, continuum cross-sections, and instrumental continuum can be computed analytically using only minor approximations.
- the derivatives with respect to tangent temperature cannot computed analytically without introducing approximations that significantly degrade the accuracy.

The formulas to be used for the analytical calculation of the above derivatives are strictly linked to the mathematical optimisations used for the implementation of the atmospheric model into the program. These formulas are described in Sect. 6.7.

4.7 Generalised inverse

Even if a detailed description of the formulas needed for the calculation of the generalised inverse matrix can be found in *Kalman (1976)*, it is however useful to recall here a simple method that can be used for the computation of the generalised inverse of a symmetric matrix. This algorithm (the truncated singular value decomposition method) is used in the ORM to invert the matrices $\mathbf{S}_m$ and $(\mathbf{K}^T\mathbf{S}_m^{-1}\mathbf{K})$ appearing in equation (4.2.8). In the case in which these matrices are non-singular the method provides the exact inverse matrix.
Let's call **C** a symmetric matrix of dimension 'r'. It is possible to find a base of 'r' independent eigenvectors of **C.** If $\mathbf{S}_C$ is the matrix whose columns are the eigenvectors of **C**, matrix **C** can then be written in the form:

$$\mathbf{C} = \mathbf{S}_C \mathbf{w} \mathbf{S}_C^T \qquad (4.7.1)$$

where **w** is a diagonal matrix containing the eigenvalues of **C**. The inverse matrix of **C** is then:

$$\mathbf{C}^{-1} = \mathbf{S}_C \mathbf{w}^{-1} \mathbf{S}_C^T \qquad (4.7.2)$$

The appearance of singularities in **C** is detected by the presence of eigenvalues close to zero in **w**. In this case the singularities can be eliminated by imposing $1/w_i = 0$ whenever $w_i \approx 0$.
This procedure corresponds to the calculation of the generalised inverse matrix of **C**.

4.8 Variance-covariance matrix of tangent height corrections

In p,T retrieval the retrieved quantities are pressures at the tangent points and the temperatures corresponding to tangent pressures. In an atmosphere in hydrostatic equilibrium, after p,T retrieval is completed, it is always possible to derive from these two quantities an estimate of the differences between the tangent altitudes of two contiguous sweeps. Besides, if one of the tangent altitudes provided by engineering measurements is assumed as perfectly known, an estimate of all the tangent altitudes can be easily obtained. The differences between the tangent altitudes obtained from p,T

retrieval and the corresponding engineering estimates of the tangent altitudes constitute the so called vector of 'tangent heights corrections'. Purpose of this section is to define the algorithm for the calculation of the VCM of this vector.
Let's assume that the analysed scan consists of N_{SW} sweeps and that the tangent altitude $z(N_{SW})$ of the lowest sweep is perfectly known. The corrections δz_i to the engineering tangent altitudes are defined as:

$$\delta z_i = z_i^{RET} - z_i^{ENG} \tag{4.8.1}$$

where z_i^{RET} are the tangent altitudes derived from p,T retrieval and z_i^{ENG} the engineering estimates of the tangent altitudes; the index i ranges from 1 to N_{SW}-1. It is important to appreciate that the error on δz_i that is given in its VCM, is not intended as the error on the difference contained in equation (4.8.1), which is complicated by the fact that both estimates of the tangent altitude are affected by an error and the two errors are not independent. The error on $\delta \mathbf{z}$ is intended as the error which should be attributed to the retrieved tangent altitude when this quantity is reconstructed by adding the correction $\delta \mathbf{z}$ to the reference levels provided by the engineering tangent altitudes.
By using hydrostatic equilibrium law and the tangent altitude of the lowest sweep, z_i^{RET} (i = 1, …, N_{SW}-1) can be expressed as:

$$z_i^{RET} = z(N_{SW}) + \sum_{j=i+1}^{N_{SW}} \frac{T_j + T_{j-1}}{2K_M} \cdot \log\left(\frac{P_j}{P_{j-1}}\right) \tag{4.8.2}$$

where, as usual, T_j and P_j are respectively temperature and pressure at tangent altitude z_j^{RET} and K^M=M/g with M = air mass and g = acceleration of gravity.
Therefore, the tangent altitude corrections can be expressed as a function of T_j and P_j by substituting equation (4.8.2) in (4.8.1):

$$\delta z_i = \sum_{j=i+1}^{N_{SW}} \frac{T_j + T_{j-1}}{2K^M} \cdot \log\left(\frac{P_j}{P_{j-1}}\right) - \Delta z_j^{ENG} \qquad i = 1,\ldots, N^{SW} - 1 \tag{4.8.3}$$

where Δz_i^{ENG} are defined as:

$$\Delta z_i^{ENG} = z_{j-1}^{ENG} - z_j^{ENG} \qquad j = 2,\ldots, N^{SW} \tag{4.8.4}$$

Now, equation (4.8.3) allows the evaluation of the variance-covariance matrix $\mathbf{S}_{HC}$ of the heights corrections δz_i starting from the variance-covariance matrix ($\mathbf{S}_x$) of the retrieved values of pressure and temperature (see Eq. (4.2.11) in Sect. 4.2.2, this matrix is directly provided by the retrieval algorithm). The transformation which links $\mathbf{S}_{HC}$ and $\mathbf{S}_x$ is:

$$\mathbf{S}_{HC} = \mathbf{K}_D \mathbf{S}_x \mathbf{K}_D^T \tag{4.8.5}$$

where $\mathbf{K}_D$ is the jacobian matrix connecting δz_i with T_i and P_i. The elements of $\mathbf{K}_D$ are the derivatives:

$$\mathbf{K}_D(i,j) = \frac{\partial(\delta z_i)}{\partial P_j} \qquad \text{with } i = 1, \ldots, N_{SW}-1 \text{ and } j = 1, \ldots, N_{SW}$$

and (4.8.6)

$$\mathbf{K}_D(i,N_{SW}+j) = \frac{\partial(\delta z_i)}{\partial T_j} \qquad \text{with } i = 1, \ldots, N_{SW}-1 \text{ and } j = 1, \ldots, N_{SW}$$

these expressions can be easily evaluated by deriving Eq. (4.8.3) with respect to pressure and temperature. We obtain:

$$\frac{\partial(\delta z_i)}{\partial P_h} = \sum_{j=i+1}^{N_{sw}} \frac{T_j + T_{j-1}}{2K} \cdot \left(\frac{\delta_{h,j}}{P_j} + \frac{\delta_{h,j-1}}{P_{j-1}} \right) \text{ with } i = 1, \ldots, N_{SW}-1 \text{ and } h = 1, \ldots, N_{SW}$$

and (4.8.7)

$$\frac{\partial(\delta z_i)}{\partial T_h} = \sum_{j=i+1}^{N_{sw}} \frac{1}{2K} \cdot \left(\delta_{j,h} + \delta_{j-1,h}\right) \cdot \log\left(\frac{P_j}{P_{j-1}} \right) \text{ with } i = 1, \ldots, N_{SW}-1 \text{ and } h = 1, \ldots, N_{SW}$$

Summarising, the steps to be carried-out for the calculation of the variance-covariance matrix $\mathbf{S}_{HC}$ are:

- calculation of the jacobian matrix $\mathbf{K}_D$ by using equations (4.8.7),
- transformation of the variance-covariance matrix $\mathbf{S}_x$ of the retrieved pressures and temperatures, by using equation (4.8.5).

4.9 Tangent heights correction based on ECMWF data

MIPAS limb emission measurements are very sensitive to pressure at the tangent point. For this reason, tangent pressures are retrieved by the Level 2 processor with a precision reaching a few percents. The retrieved pressures and temperatures are fed onto the hydrostatic equilibrium equation to derive tangent height increments with a precision better than 100 m. Despite this relatively high precision of the retrieved tangent height increments, the absolute values of tangent heights remain uncertain, due to the intrinsic lack of sensitivity of the limb measurements to the geometrical altitude of the tangent points, when pressure is considered an independent variable. At each pT retrieval iteration, tangent heights are re-calculated by adding the tangent height increments to the lowest tangent height of the scan, which is assumed to be known from engineering pointing data. The absolute accuracy of engineering pointing data, however, can be as poor as 1 km, according to the specifications (see Appendix A).
To improve the accuracy of the absolute tangent heights of each MIPAS scan, we apply to the retrieved tangent altitudes a common vertical shift, calculated on the basis of the nearest ECMWF profiles matching in space and time the considered MIPAS scan. The vertical shift is calculated as follows: we consider the retrieved tangent pressures and altitudes of the three lowest sweeps of the processed scan. Using log(p) interpolation, we find the three ECMWF altitudes that correspond to the retrieved tangent pressures of the lowest three sweeps. We compute the average difference between these three altitudes and the three lowest retrieved tangent heights. We finally shift all the tangent heights of the scan by adding to them this average difference.
Validations against correlative independent measurements have confirmed that this a-posteriori correction of the altitude scale of MIPAS profiles is very effective in reducing the discrepancies between MIPAS and correlative measurements. As an example, Fig. 4.9.1 (courtesy of Daan Hubert, BIRA-IASB) shows the median bias between MIPAS retrieved profile altitudes and altitudes obtained from co-located radiosonde measurements for matching pressures. Top plots refer to the Full

Resolution (FR) MIPAS measurements, bottom plots to the Optimized Resolution (OR) measurements. Plots from left to right refer to different latitude bands as displayed in the plot's key. Different line colors refer to different Level 1 and Level 2 processor versions: L1v5-L2v6 (light brown), L1v7-L2v7 (dark blue), L1v7-L2v8 (light blue), L1v8-L2v8 (dark brown), L1v8-L2v7 (orange). Due to interface problems at the ESA data processing center, the Level 2 v.6 had no access to ECMWF data therefore, in this case, it was not possible to apply any altitude correction to the MIPAS retrieved profiles. As we can see from the figure, for this processing version the altitude bias is significantly greater than for all other processing versions. This proves the real effectiveness of the implemented tangent height correction scheme.

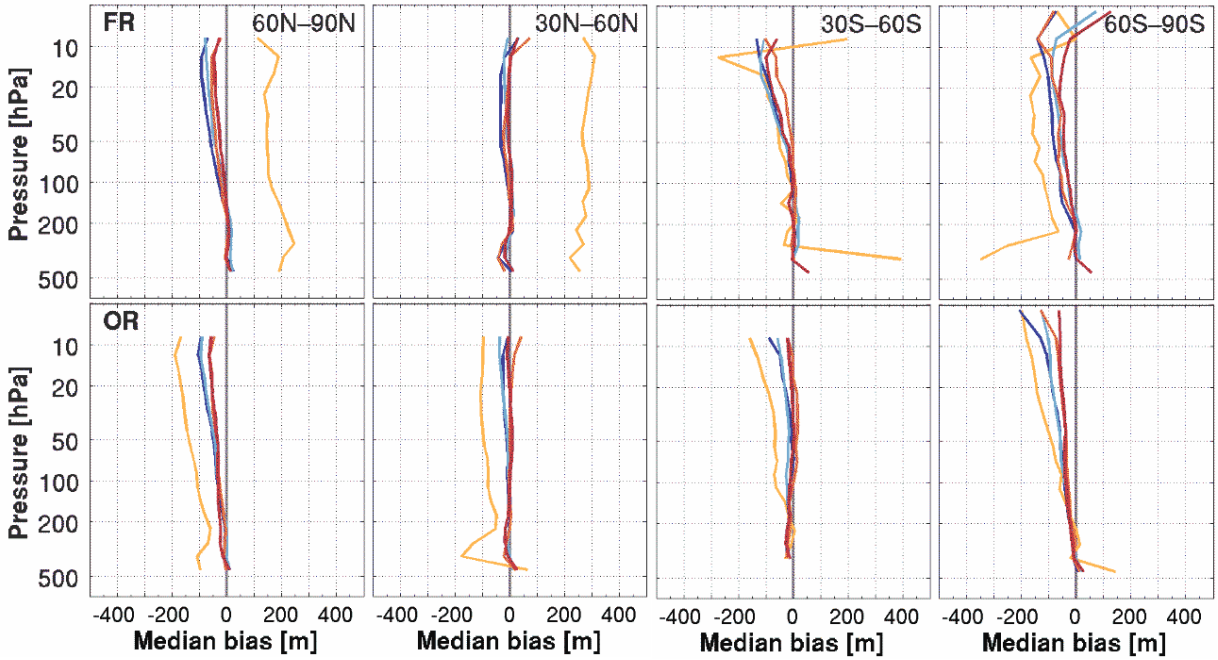

Figure 4.9.1: Median differences between MIPAS Level 2 retrieved altitudes and altitudes from radiosonde correlative measurements for matching pressures. Top plots refer to FR measurements, bottom plots to OR. Plots from left to right refer to different latitude bands as displayed in the plot's key. Different line colors refer to different Level 1 and Level 2 processor versions: L1v5-L2v6 (light brown), L1v7-L2v7 (dark blue), L1v7-L2v8 (light blue), L1v8-L2v8 (dark brown), L1v8-L2v7 (orange). Courtesy of Daan Hubert (BIRA - IASB).

5 - Scientific aspects and physical optimisations

In this section the baselines for the choice of the implementation of specific physical aspects and optimisations into the code are discussed. This discussion includes the following items:

- explanation of the physical effects
- possible physical models for the description of these effects
- options for the implementation into the code
- optimisations: improved algorithms, simplifications, items to be neglected
- choices for the implementation
- accuracy of baselines

The discussed aspects are:

1. Retrieval grid: retrieval of the unknowns at fixed levels or at tangent altitudes
2. Use of a-priori information
3. Latitudinal variability of atmospheric parameters
4. Model of the earth and calculation of the gravity
5. Ray tracing: refraction model and determination of the optical path
6. Line shape
7. Line mixing
8. Pressure shift
9. Non local thermodynamic equilibrium (NLTE)
10. Self broadening
11. Continuum: instrumental, near, far
12. Interpolation of the profiles

5.1 Choice between retrieval of profiles at fixed levels and at tangent altitude levels

In the case of the onion peeling method, the retrieved values of VMR can only be determined at the pressure levels that correspond to the tangent altitude of the limb scanning sequence. In the case of global fit this constraint does not exist and other discrete levels can be used. Since in Level 3 data processing global maps on pressure surfaces are produced, an interesting possibility offered by global fit is that of using fixed pressure levels which will in general be different from the tangent altitude levels.

5.1.1 Retrieval at tangent altitude and interpolation between retrieved values

If the pressure levels at which the retrieval is performed are the ones identified by the observation geometries of the limb scanning sequence they may not correspond to those needed by the user. In this case an interpolation can be applied and, as it is shown in *Carli (1995)*, the equations that fully characterise the interpolated values of the profiles assess that, even if a reduced statistic error applies to the profile at the interpolated altitude levels, the vertical resolution of the measurement is degraded. Numerical tests have shown that between two retrieved values the measurement error has a minimum while the width of the averaging kernel (see e.g. *Rodgers (1976)*) has a maximum (i.e. the interpolation changes the trade-off between vertical resolution and precision in favour of the latter). Interpolation of retrieved values provides therefore a variable trade-off between precision and vertical resolution of the

measurement. Alternative interpolation schemes to be applied to retrieved profiles have been studied in *Carli et al., (2001)*. One of the methods proposed in this reference is discussed in Sect. 5.13.

5.1.2 Retrieval at fixed levels

If the data utilisation requires VMR at fixed levels (for instance in level 3 data processing global maps on pressure surfaces are produced) an alternative could be that of retrieving the VMR directly at the required fixed levels. The quality of the retrieval performed at fixed levels should be assessed with appropriate tests, but it is reasonable to expect that in general it provides larger noise and a more uniform vertical resolution.

5.1.3 Discussion of the problem

The basic problem that is behind the different trade-off between precision and vertical resolution of the profile retrieved with the two approaches can be explained by the Nyquist theorem. This theorem states that in order to measure a periodic variation of a distribution, the distribution must be sampled with steps at least as small as half the period of the variation. If the maxima and the minima of the variation coincide with the sampling points (detection of the cosine variation) a sampling step equal to half of the period is sufficient to detect the signal. A sampling step equal to a quarter of the period is needed in order to detect a variation with any phase (detection of both the cosine and the sine components).
According to the Nyquist theorem, we have that:

- the vertical resolution of the retrieved profiles coincides (if no a-priori information and/or external constraints are explicitly used in the inversion) with the vertical sampling step of the sounding if the retrieval is performed at tangent altitudes levels
- the vertical resolution of the retrieved profiles cannot be equal to the vertical resolution of the sounding if the retrieval is performed at intermediate levels.

Therefore, if the offset introduced by the pointing system, between wanted and implemented tangent altitudes causes a sounding of the atmosphere at tangent altitudes located in between the fixed levels required by the user, it is impossible to obtain at the fixed levels the maximum vertical resolution. This result, which is based on the implicit assumption that the weighting functions of limb sounding observations peak at the tangent altitudes, may have a partial exception if the difference between weighting functions at different frequencies and in different microwindows provides some information at intermediate altitudes. However, the exploitation of this second order information is bound to cause a major increase of the measurement error.
The choice is therefore between:

1. retrieval at tangent altitude levels followed by interpolation for determination of VMR at required levels: this procedure makes the best use of the data when no interpolation is used. If interpolation is used, the vertical resolution of the measurement depends upon the offset between retrieved and interpolated points. Up to a factor of two of loss in vertical resolution can be encountered.
2. retrieval at fixed pressure levels: this option has not been adequately tested, it is expected to provide retrievals at roughly (T dependence) constant vertical resolution, but the noise depends upon the offset between wanted and implemented tangent altitudes. A very large increase of noise can be encountered and it is not easy to quantify this increase.

The first option is the one with fewer risks. The second option is simpler from the conceptual point of view. The two options imply a different implementation of level 2 data analysis and a significant

compromise in scientific requirements, but from the code point of view there is no strong reasons in favour of any of the two.

5.1.4 Conclusions

The following strategy has been assumed for the development of Level 2 scientific code:

- for the level 2 retrieval algorithm we have adopted the option of the retrieval at tangent altitudes levels eventually followed by interpolation. The reason for this choice is that at the time of the code development we could not afford the unknowns of the other option.
- Some flexibility is maintained in the code in order not to prevent the implementation of the alternative approach in subsequent versions, in case it is recommended by retrieval studies.

The trade-off between vertical resolution and precision and the alternative of retrieving the profiles either at tangent altitude levels or at fixed (user-defined) levels have been fully addressed in a quantitative study carried-out in a parallel ESA contract (12055/96/NL/CN). We therefore refer to the final report of that study for a quantitative assessment of the topics described in the present section. In any case, no explicit recommendation for a retrieval at fixed levels emerged from the mentioned study.

5.2 Use of a-priori information

The use of information provided by sources different from the spectroscopic measurements can increase the overall information content (equal to retrieval information plus extra information) and improve the quality of the retrieved profiles. This possibility is source of both, improvements and concern because, if on one hand it can lead to a positive result in the case of marginal precision in the retrieval, on the other hand it can become a cosmetic exercise which hides serious systematic errors. These two aspects of external information will be discussed in the next two sections.

5.2.1 - Precision improvement

The exploitation of external information is worthwhile only if it leads to a significant precision improvement. In order to understand the entity of the improvement, the mathematics of the combination of information is herewith briefly recalled.
It is well known that if two independent measurements x_1 and x_2 exist of a scalar quantity x, the two measurements can be combined by way of their r.m.s. errors σ_1 and σ_2 leading to the new estimate:

$$q_c = (\sigma_1^{-2} + \sigma_2^{-2})^{-1}(\sigma_1^{-2} x_1 + \sigma_2^{-2} x_2) \qquad (5.2.1)$$

with an error:

$$\sigma_c = \left(\sigma_1^{-2} + \sigma_2^{-2}\right)^{-1/2} \qquad (5.2.2)$$

We know that in this case the error of the new estimate:

- is reduced by a factor $1/\sqrt{2}$ when the two measurements have the same error,
- is practically equal to the error of the best measurement when a large difference exists between the two errors.

In practice, combining information from different measurements brings no advantage when the measurements have different quality.
A similar error combination can be made in the case in which the measured quantity is a vector **x**. The weighted combination $\boldsymbol{x}_c$ of the two measurements $\boldsymbol{x}_1$ and $\boldsymbol{x}_2$ having respectively the variance-covariance matrices $\mathbf{S}_{x1}$ and $\mathbf{S}_{x2}$ is equal to:

$$\mathbf{x}_C = \left(\mathbf{S}_{x1}^{-1} + \mathbf{S}_{x2}^{-1}\right)^{-1}\left(\mathbf{S}_{x1}^{-1}\cdot\mathbf{x}_1 + \mathbf{S}_{x2}^{-1}\cdot\mathbf{x}_2\right) \qquad (5.2.3)$$

and has a variance-covariance matrix equal to

$$\mathbf{S}_{xC} = \left(\mathbf{S}_{x1}^{-1} + \mathbf{S}_{x2}^{-1}\right)^{-1} \qquad (5.2.4)$$

The similarity of respectively expressions (5.2.1), (5.2.2) and (5.2.3), (5.2.4) may suggest that also similar properties apply, and it is not worthwhile to combine two measurements if their errors are very different.
In our case this would imply that if the external information is better than the retrieved information we do not need the limb scanning measurements and if the external information is worse than the retrieved information we do not need to waste efforts combining the two. However, the situation is not so simple in the case of measurements of vectors and the considerations made for scalar quantities do not fully apply.
Limb scanning observations often provide very good measurements with low errors at some altitudes, and undetermined measurements with large errors at other altitudes. An approximate estimate, which may be available from either statistical studies or models, of course does not directly add information where good measurements have been retrieved, but can reduce significantly the errors where the retrieved measurements are undetermined. Since a correlation exists between measurements at different altitudes, the reduction of the errors at some altitudes may lead to a reduction of all the errors. This explains why in the case of combination of vectors the errors may be reduced more than what is expected on the basis of the quadratic combination.
In *Carlotti et al.* (1995) some numerical tests were performed showing that a significant improvement is possible by using a-priori knowledge such as that which can be obtained from either the previous measurement or statistical seasonal and geographical maps.
The use of external information can, therefore, be very profitable and should be seriously considered as part of the retrieval strategy.

5.2.2 - Systematic errors

A concern about the combination of the retrieved information with an a-priori estimate of the profile is that whenever the same a-priori information is used for several profiles, the error budget of each profile contains both a random and a systematic component (the first due to the measurement and the second due to the constant a-priori information).
Usually it is a good rule to list separately random and systematic errors in order to avoid mistakes in the subsequent operations. In fact in the case of averages random errors are reduced and systematic errors remain constant, while in the case of differences, systematic errors cancel and random errors increase. If we want to maintain this separation between random and systematic errors it is necessary, therefore, to make retrievals without a-priori information (our primary output) and combine externally provided profiles with the retrieved profiles only optionally.

The different approach of using a-priori information routinely, during the retrieval iterations, can be adopted when the a-priori information has a random character.

5.2.3 - Hydrostatic equilibrium and LOS Engineering information

In the case of p, T retrieval an external information is also provided by the hydrostatic equilibrium. This information is a relationship between the unknowns and another measurement (provided by the engineering data) rather than a constant a-priori estimate and implies therefore different choices.
Hydrostatic equilibrium is a condition that applies to an ideal atmosphere which is perfectly stratified. The integrated form of the equation that describes this condition is:

$$p_n = p_0 \exp\left(-\frac{M}{R} g \sum_{i=0}^{n} \frac{1}{T_i} \Delta z_i \right) \qquad (5.2.5)$$

where the notations are:

p_n pressure at a given altitude,
p_o pressure at the reference altitude,
M average molecular weight of the atmosphere,
R universal gas constant,
T_i temperature of the atmospheric layer i,
Δz_i thickness of the atmospheric layer i.

Now, since equation (5.2.5) is a relationship between T, p_n / p_0 and Δz_i increments, the measurements of pressure and temperature at tangent altitude obtained from the spectroscopic observations, can be used to get an estimate of the differences Δz_i between the tangent altitudes of the sweeps in the same limb-scanning sequence. Another estimate of the differences between tangent altitudes is provided by the engineering measurements. The two estimates are then combined using equation (5.2.3) and the variance covariance matrix of the new estimate is computed using (5.2.4). The variance covariance matrix related to the engineering pointing that is needed for the above operations is an input of p, T retrieval program. The mathematics required by this operation is discussed with further details in Sect. 4.2.6.
Note that in this approach, only the differences between tangent altitudes and not the absolute pointing altitudes are improved by the retrieval process. In fact, when pressure is a fitted quantity, the sensitivity of radiative transfer to the tangent altitude of the measurement is very weak and it is not possible to retrieve any of the tangent altitudes of the limb-scanning sequence.

Baselines:

Engineering LOS data is routinely used in p,T retrieval by exploiting the constraint provided by hydrostatic equilibrium, as explained in the above section.

The ORM version 8 includes the possibility to perform the inversions using also the Optimal Estimation (or the Maximum A-Posteriori) method (*Rodgers, 2000*). With a user selectable switch, it is possible to enable the use of a-prori estimates and error covariance matrices for selected sets of retrieval parameters. In practice this option is used only for the retrieval of the VMR of gases that contribute to MIPAS radiances the with very weak spectral features as compared to the measurement noise. As

already mentioned in Sect. 4.6, HDO is treated as a separate gas, independent of the other H2O isotopologues, and is retrieved using optimal estimation.

5.3 Latitudinal variability

5.3.1 Angular spread of the limb measurements

Here we will examine the extent of the angular spread of the beam of a limb scanning observation with respect to the earth centre. Exact computation gives for this value

$$\vartheta_{as} = 2\arccos\left(\frac{R_e + z_g}{R_e + z}\right) \tag{5.3.1}$$

where R_e is the earth radius (assumed spherical for simplicity), z_g is the tangent height and z is the height for which the angle should be calculated. For a tangent height of 10 km and an atmospheric boundary of 100 km we get $\vartheta_{as} = 19°$.

Deaspite this large spread, we note that most of the signal reaching the instrument actually originates from the lower layers, close to the tangent point. Figure 5.3.1 shows which gas column percentage (in the horizontal axis) is located around the tangent point, winthin the angular spread indicaed in the vertical axis. The integrated columns were computed for tangent altitudes of 10 km and 17 km, for a gas with constant VMR. We can see that more than 90% of the emitting gas column is concentrated within +/- 4° about the tangent point.

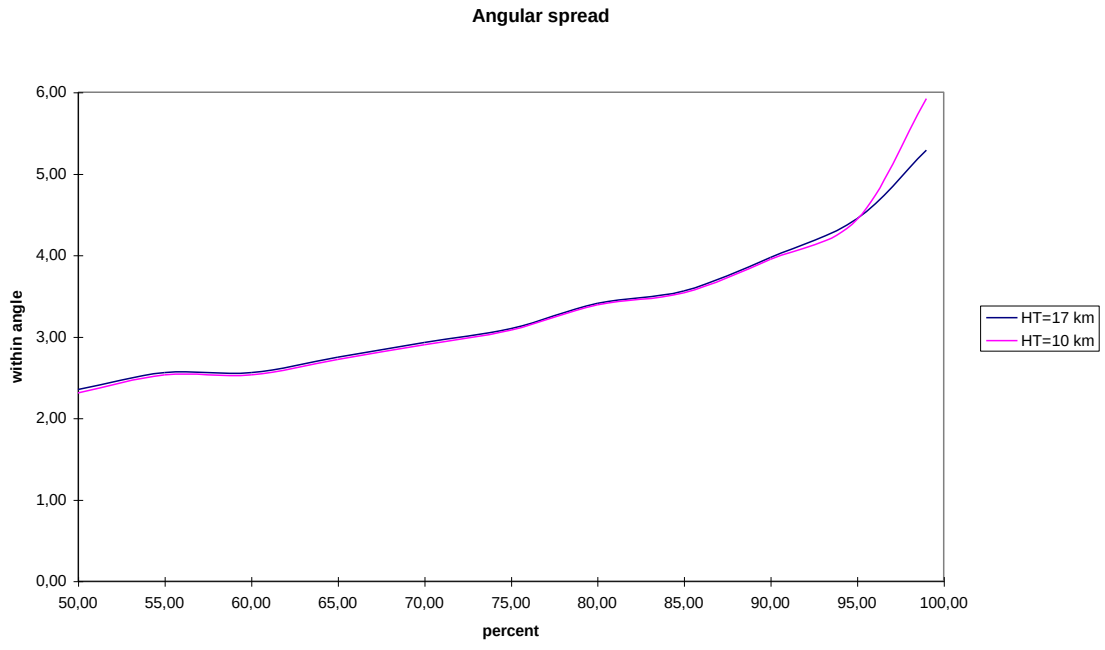

Figure 5.3.1: Angle [°] at the earth centre over the percentage of the integrated column for two different tangent altitudes (HT in the plot's key).

5.3.2 Latitudinal temperature gradients

Figure 5.3.2 shows climatological temperature differences (vertical axis) obtained for latitudinal distances of 15°, as a function of altitude (horizontal axis), for various latitudes over the Northern hemisphere (different line colors). Data from the COSPAR International Atmosphere Reference (1986).

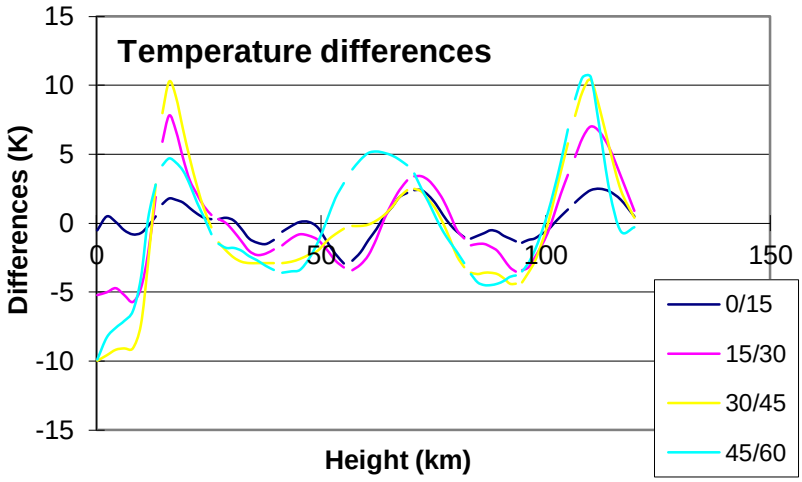

Figure 5.3.2: Temperature differences as a function of the altitude between latitudes separated by 15°.

We can see that maximal latitudinal temperature gradients are of the order of 0.6-0.7 K/deg. This results in differences of about 2-3 K along the LOS where the main contribution to the emitted intensity originates. Instantaneous latitudinal variations can be larger than these climatological differences, but taking into consideration the large amount of memory and computation time which are necessary to simulate horizontal gradients, the baseline of the ORM, up to version 7 (NRT code), has been to perform retrievals of individual limb-scan sequences for which horizontal homogeneity is assumed.

5.3.3 Modeling the latitudinal variability with a horizontal gradient

During the activities aiming at the characterization of the quality of MIPAS Level 2 products, the horizontal homogeneity assumption made in the ORM up to v.7 was found (Kiefer et al., 2010) to be the cause of a systematic difference in the average profiles, in the same latitude bands, when these are calculated separately from measurements acquired in the ascending (AX) or descending (DX) parts of the orbits. Being of the order of the noise error of the individual profiles, this systematic effect is evident only when comparing averages of statistically significant sets of profiles.
The systematic difference between AX and DX profiles arises from to the fact that the MIPAS line of sight points rearward, so that when the tangent point is at a middle latitude south, for instance, the satellite is closer to the south pole in the descending part of the orbit, and closer to the equator in the ascending part. As a consequence, scans with tangent points at the same latitude sample differently the latitudinal variation of the atmosphere depending on whether they are acquired in the AX or in the DX parts of the orbit. The horizontal homogeneity assumption prevents from taking properly into account this feature of MIPAS observations and the retrieval introduces a systematic compensation effect.
For long time the MIPAS Quality Working Group has been discussing about the most effective strategy to implement a satisfactory model for the horizontal variability of the atmosphere in the ORM, always keeping in mind the tradeoff between accuracy improvements and development costs. Extensive tests carried-out at ISAC (Castelli et al. 2014, 2016) showed that modelling the horizontal variability of the atmosphere with a user supplied horizontal gradient (HG) for temperature and VMR reduces

significantly the systematic AX-DX differences. Of course this is true only if the HGs provided in input to the code are sufficiently accurate. Tests have shown that horizontal gradients inferred either from a previous retrieval based on the horizontal homogeneity assumption, or from the ECMWF analysis can adequately serve the objective. The possibility to model HGs was finally implemented in the ORM version 8. This functionality of modelling the HGs implied modifications in several parts of the algorithm. In particular, the ray-tracing routine (see Sect. 5.5) and the parts for the calculation of the Curtis-Godson (CG) integrals were completely rewritten. The calculation of the derivatives and the radiative transfer were also heavily modified. In particular, the new radiative transfer algorithm does not exploit any longer neither the spherical symmetry hypothesis nor the secant law approximation (see Sect.s 6.2 and 6.4). Of course, along with a more accurate model, these choices imply also much heavier calculations.

With a selectable switch, the ORM v.8 models the horizontal variability of pressure, temperature and gases VMR with a height-dependent horizontal gradient that may have different values before and after the tangent point of each limb measurement. Horizontal gradients are not retrieval parameters, they are assumed as known and are read from input files. In the ORM v.8 it is possible to use horizontal gradients inferred from:

1. The ECMWF database (only for p, T, H2O and O3)
2. Previous ORM processing obtained with the horizontal homogeneity assumption
3. Climatology (i.e. from the IG2 climatological database)

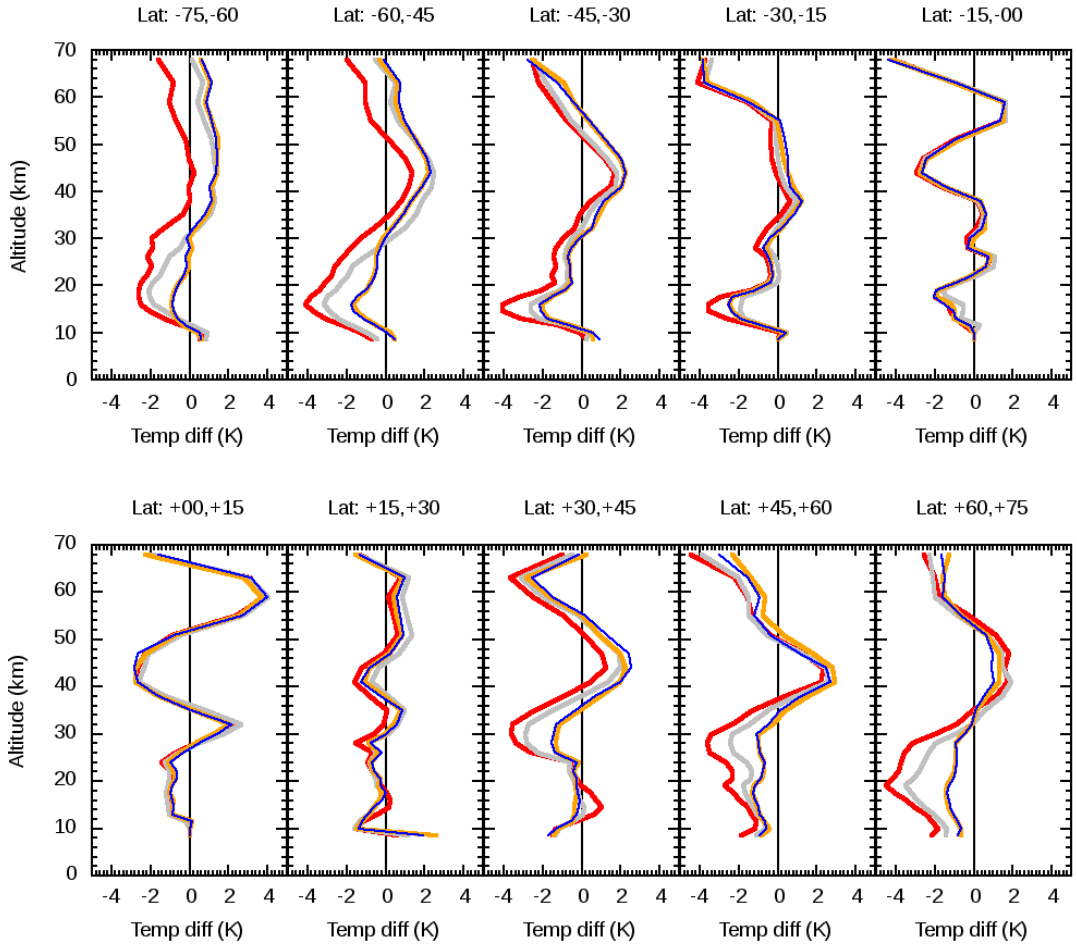

Figure 5.3.3: Temperature AX-DX average differences for various latitude bands (see key on top of each plot) as a function of altitude. Different sources are used for Temperature HG. Red: no HG used, grey: HG from IG2, blue: HG estimated from previous processing with horizontal homogeneity assumption, gold: HG form ECMWF.

As an example, Figure 5.3.3 illustrates the results of a test attempting to estimate the accuracy of each of the above HG sources on the basis of their effectiveness in reducing the AX-DX differences of the retrieved Temperature. The figure shows the Temperature AX-DX average differences, as a function of altitude. Each panel refers to a latitude band as specified by the legend on top. The red curves refer to the AX-DX differences obtained in the case of horizontal homogeneity assumption, i.e. in this case the ORM v8 mimics the ORM v6 processor by forcing to zero the temperature HGs. Note that the red curve shows AX-DX differences as large as −2.5 K around 20 km in the latitude band from 45 to 60N. The AX-DX differences generally decrease when a non-zero HG is used. However, compared to the HGs derived from ECMWF or a previous processing, the HGs derived from the IG2 climatology are less effective in reducing the AX-DX differences. HGs inferred from ECMWF or a previous processing produce very similar results.

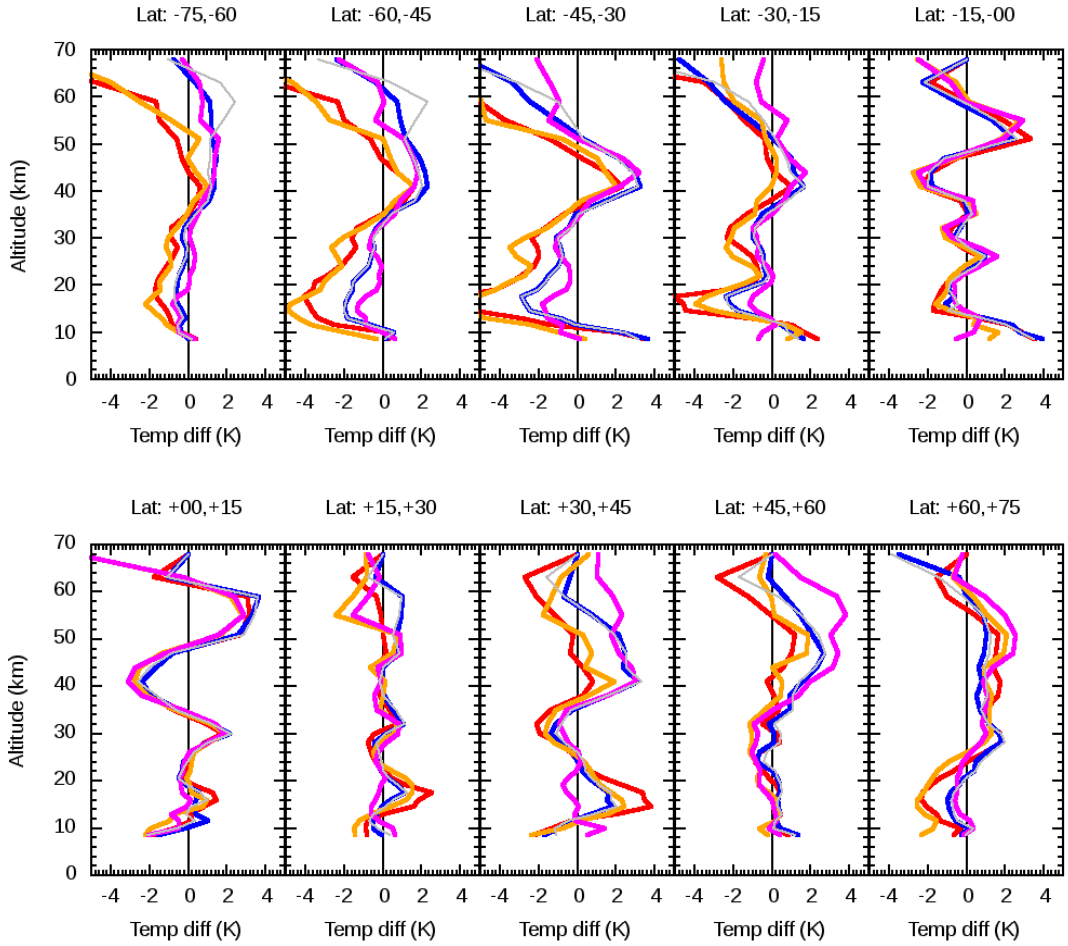

Figure 5.3.4: Temperature AX-DX differences for KOPRAFIT and ORM v8. Red: ORM v8 forcing to zero all HGs; blue: ORM v8 modelling only the Temperature HG as inferred from ECMWF. Grey: ORM v8 modeling Temperature, Pressure and (H2O, O3) VMR HGs as inferred from ECMWF. Brown: KOPRAFIT forcing to zero all HGs; magenta: KOPRAFIT modelling the Temperature HG as inferred from ECMWF.

For validation purposes, the effect of the HG model on AX-DX differences was also compared to what is achieved by the KOPRAFIT code developed at KIT (Karlsruhe, DE) for MIPAS data analysis. Figure 5.3.4 shows an example of results obtained by averaging ORM v8 and KOPRAFIT AX-DX differences of temperature profiles retrieved from the same set of MIPAS measurements considered in the work of Kefer et al., (2010). The Figure adopts the following keys. Red curve: ORM v8 forcing to zero all HGs; blue: ORM v8 modelling the Temperature HG from ECMWF. Brown: KOPRAFIT forcing to zero all

HGs; pink: KOPRAFIT modelling the Temperature HG from ECMWF. From the figure it is evident that both KOPRAFIT and the ORM v8 achieve very similar AX-DX differences both when the Temperature HG is modelled and when the atmosphere is assumed horizontally homogeneous.

Details of implementation of the HG model in the ORM v.8 are described in *Sgheri and Ridolfi (2018)*. The results of validation, and assessment tests are presented in *Ridolfi et al. (2017)*.

5.4 Earth model and gravity

5.4.1 Earth model

For the earth shape the simplified WGS84 model has been adopted. This model simulates the earth as an ellipsoid with the half-major axis a = 6378.137 km and the half-minor axis b = 6356.752 km. From the WGS84 model, also the local radius of curvature is derived.

5.4.2 Gravity

For the calculation of the gravity as a function of altitude and latitude a formula taken from *Clarmann (1986)* has been adopted. The acceleration of gravity at the sea level (identified by the WGS84 ellipsoid), as a function of geodetic latitude Φ can be computed using the following empirical formula which includes the centrifugal effect:

$$g_0 = 9.80616 \cdot [1 - 0.0026373 \cdot \cos(2\Phi) + 0.0000059 \cdot \cos^2(2\Phi)] \qquad (5.4.1)$$

Since the centrifugal component of g_0 has a different dependence on the altitude as compared to the gravitational component, it is then necessary to separate the two components in order to properly insert in g_0 the dependence on the altitude. Let us define:

$$g_g = g_0 + \omega^2 \frac{f^2}{R^e} \cos^2\Phi_s \qquad (5.4.2)$$

where g_g is the gravitational component and does not contain the centrifugal effect; ω is the angular speed of the earth and is equal to:

$$\omega = \frac{2\pi}{86400\,\text{sec./day}} / 1.002737904 \qquad (5.4.3)$$

the factor 1.002737904 is the star time rotation factor which takes into account the motion of the earth along the orbit. Furthermore, the meaning of R_e and f is explained in Fig. 5.3 and they are computed using the following formulas:

$$f = \frac{a}{\sqrt{1 - \left(1 - \frac{b^2}{a^2}\right) sen^2\Phi_s}} \qquad (5.4.4)$$

$$R_e = \sqrt{f^2 \cos^2 \Phi + \left(\frac{b^2}{a^2} f \cdot sen\Phi_s \right)^2} \qquad (5.4.5)$$

where *a* and *b* are respectively the equatorial and the polar radii of the Earth.

The dependence on the altitude is then included in *g*:

$$g = g_g \left(\frac{R_e}{R_e + z} \right)^2 - \omega^2 f \left(\frac{f + z}{R_e} \right) \cos^2 \Phi_s \qquad (5.4.4)$$

In the above equation, *z* is the altitude of the considered point with respect to the sea level.
The results provided by equation (5.4.4) have been compared with the values of the gravity provided by other models (see e.g. *List (1963), Stern (1960), Defense (1987)*): the observed relative differences are always smaller than $2*10^{-4}$.

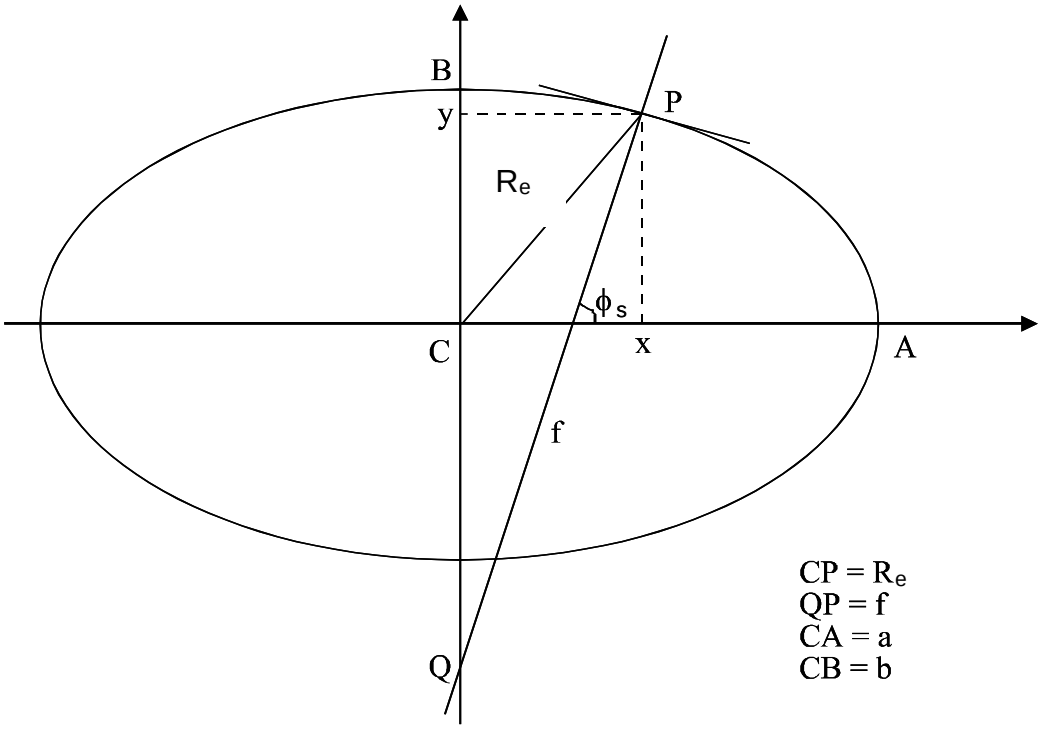

Fig. 5.3: Earth model

5.5 Ray tracing and atmospheric refraction

In the ORM versions older than v8, the atmosphere is modelled with concentrical spherical shells assumed homogeneous in composition and physical state. Within this assumption, the ray tracing is computed by applying Snell's law at the boundaries of homogeneous shells. In the ORM v8 the atmospheric composition and physical state are allowed to change as a function of both altitude and polar coordinate (i.e. horizontally), therefore the ray-tracing has been updated to allow also for this new modelling capability. Various ray-tracing methods were considered for implementation in the ORM version 8. In *Ridolfi and Sgheri (2014)*, these methods are reviewed and evaluated with respect to their accuracy and computational demands. Here we summarize the results of the study.

The propagation path of electromagnetic rays through an inhomogeneous medium is governed by the eikonal equation (Born and Wolf, 1975):

$$|\nabla\phi(\boldsymbol{x})|^2 = n^2(\boldsymbol{x}) \tag{5.5.1}$$

where $\boldsymbol{x}$ is the position vector, $n(\boldsymbol{x})$ the refractive index and $\phi(\boldsymbol{x})$ is the so called *eikonal function*. This equation can be derived directly from the first-order Maxwell equations or from the second-order wave equations for either the electric or the magnetic field. The only simplifying assumption used in this derivation is that $n(\boldsymbol{x})$ varies slowly with respect to the wavelength of the electromagnetic field. Of course, for the propagation of mid-infrared radiation in the Earth's atmosphere, this hypothesis is verified with extremely high accuracy. The surfaces $\phi(\boldsymbol{x}) = constant$ are the geometrical wave fronts. Therefore, the ray direction is parallel to $\nabla\phi(\boldsymbol{x})$. Let $\mathbf{p}(s)$ be the ray path, parametrized with the arc parameter s. We can write

$$\frac{d\mathbf{p}(s)}{ds} = \frac{\nabla\phi(\mathbf{p}(s))}{|\nabla\phi(\mathbf{p}(s))|} \tag{5.5.2}$$

After some algebraic manipulation, using Eq. (5.5.1) we get the differential form of the light rays equation (Born and Wolf, 1975):

$$\frac{d}{ds}\left(n(\mathbf{p}(s))\frac{d(\mathbf{p}(s))}{ds}\right) = \nabla n(\mathbf{p}(s)) \tag{5.5.3}$$

This is a vectorial second-order differential equation that permits one to derive the full ray path across an inhomogeneous medium, if $n(\boldsymbol{x})$ and the boundary conditions are known. From this equation, several ray-tracing methods can be derived with different tradeoffs between accuracy and computational speed. In *Ridolfi and Sgheri (2014)*, the following three ray-tracing methods are compared and assessed:

- direct numerical solution of Eq. (5.5.3)
- tangential displacement method (Hase and Hoepfner, 1999),
- iterative Snell's law (Thayer 1967, Hobiger et al. 2008),

In Thayer's implementation of Snell's law, the atmosphere is assumed horizontally homogeneous. This implementation is one of the fastest ray-tracing methods, however, if the horizontal variability of the atmosphere is taken into account, this method is not adequate. For horizontally varying atmosphere, the level lines of $n(\boldsymbol{x})$ do not coincide with the altitude levels. Thus, in the Thayer implementation, the calculation of the refraction angle with Snell's law is based on a wrong hypothesis. From test calculations we found that in several synthetic but realistic atmospheric conditions, with strong horizontal gradients of pressure and temperature, the method produces a wrong ray path, partly following Earth's curvature. In Hobiger et al. (2008), a refined approach of Thayer's method is

proposed, removing the horizontal homogeneity assumption at the expense of significantly increased computational complexity.
The tangential displacement method (TD) is an iterative approach for the solution of the eikonal equation, using an approximation to avoid the calculation of the second derivatives of **p**(*s*). This is the method implemented in the KOPRA retrieval code developed at the Karlsruhe Institute of Technology (KIT, Germany).

To test the direct numerical solution of the eikonal equation we implemented a multi-step predictor-corrector method (referred to as EIK) using the two-step Adams-Bashforth formula for the predictor and the BDF2 formula for the corrector (Isaacson, 1994). The shape of the ray path, however, suggests that the method can be further optimized using an adaptive step length based on the second derivatives of **p**(*s*) that are linked to the local ray of curvature. These derivatives are easily obtained from the numerical solution of the eikonal equation. Thus, we also implemented this adaptive method (referred to as AEIK) while still maintaining the property that in each atmospheric layer the step is fixed. This is an efficient choice, considering also the need of implementation of the Curtis-Godson (CG) integrals for the calculation of the radiative transfer in a horizontally varying atmosphere. In fact, since the curvature of the ray path and the atmospheric variability of the quantities to be integrated are relatively small, it is possible to a priori estimate the step size for the numerical calculation of the CG integrals within a prescribed accuracy. With this approach the same set of nodes can be used for the calculation of all CG integrals, and the iterative refinement of the integration step size can be avoided. While all the considered methods can be applied to a three-dimensional ray tracing, our implementation is limited to the two-dimensional as the ORM assumes all MIPAS limb measurements to lie in the orbit plane.
Figure 5.5.1 shows the tradeoff between accuracy and computing time for the different methods described, for various step lengths. The accuracy of each method (vertical axis) is evaluated as the average of the absolute differences between real and computed tangent heights for a set of 12 orbits of measurements acquired in 2010 (see *Ridolfi and Sgheri, 2014*). In the case of the AEIK method, the values reported in the figure are the initial step lengths, which are then adapted by the method itself. For sufficiently small step lengths, all the three considered methods are very accurate. The AEIK method is, however, the most efficient. For this reason, the AEIK method was chosen for implementation in the ORM version 8.

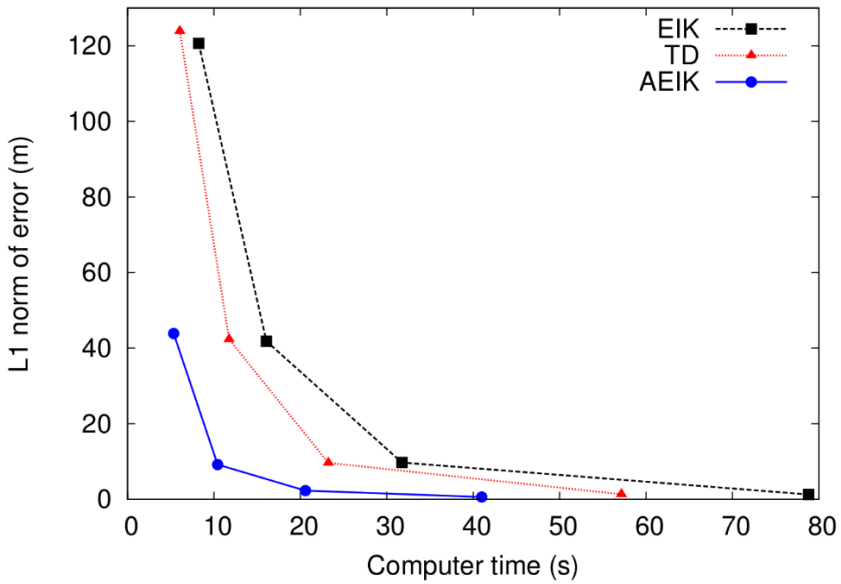

Figure 5.5.1: Efficiency of the tested ray-tracing methods, for step sizes of 0.1, 0.25, 0.5 and 1.0 km. From *Ridolfi and Sgheri, (2014)*.

5.5.1 Refraction model

In the study of *Ridolfi and Sgheri (2014)*, three refraction models of the air are reviewed and evaluated. Namely:

- the Barrel–Sears formula (*Barrel and Sears, 1939*),
- the simplified Edlén formula (*Edlén, 1966*),
- the Ciddor formula (*Ciddor, 1996*).

The Barrel–Sears empirical formula has been used for long time in atmospheric infrared applications. The version we implemented for testing purposes is:

$$(n-1)\times 10^6 = \left(77.48 + \frac{0.44}{\lambda^2} + \frac{0.007}{\lambda^4}\right)\frac{p}{T} - \left(12.79 - \frac{0.14}{\lambda^2}\right)\frac{p_w}{T} \qquad (5.5.4)$$

where p is the total air pressure expressed in hPa, T is the temperature in Kelvin, λ the wavelength in μm and p_w is the water vapor partial pressure in hPa.

The simplified Edlén's formula is the model implemented in the ORM code up to version 7. The formula is:

$$n - 1 = c_0 \cdot \frac{T_0}{p_0} \cdot \frac{p}{T} \qquad (5.5.5)$$

with the constants p_0 = 1013.25 hPa, T_0 = 288.16 K and c_0 = 0.000272632. This formula clearly does not model the dependence of the refraction on the wavelength and the water vapor amount.

Ciddor's formula models the refractive index as a function of wavelength, pressure, temperature, water vapor and carbon dioxide content. The formula was originally tested with experimental data extending only up to 1.7 μm; however, the work of *Mathar (2004)* suggests that its accuracy should be on the order of 10^{-6} also up to 25 μm, i.e., over the whole spectral region covered by MIPAS observations (4.1-14.9 μm). We implemented Ciddor's formula following the original paper of *Ciddor, (1996)*.

The differences implied by the three considered refraction models in the calculation of the tangent heights of the limb measurements is actually very small as compared to the accuracy required (of the order of 50 – 100 m). Test computations show that Edlén's and Ciddor's models are in very good agreement, producing tangent heights that, on average, differ by less than 30 cm. The Barrel Sears model produces tangent heights differing by less than 2.5 m as compared to those calculated using the Ciddor's formula. According to these results, there is no strong preference for the implementation of one specific refraction model in the ORM. As a baseline for implementation in the ORM Version 8 the Ciddor formula was chosen, as it is considered the most accurate by *Young, (2011)*. As a backup option, should the water and / or CO_2 profiles be unavailable, the ORM v.8 uses Edlén's formula.

5.6 Line shape modeling

The line shape function which has to be modelled appropriately inside the forward model is the Voigt profile (equation 4.4.15), equal to the convolution of the Doppler profile caused by the velocity of the molecules and the Lorentz profile induced by collisions. While the Doppler function is the correct description of the physical effect of Doppler shift, the Lorentz profile is an approximation that is valid if:

- the spectral region under consideration is not far from the line centre and
- the distance from other lines of the molecule is so large that the line can be considered as isolated

The first assumption fails if we try to model lines far away from the centre. Two important examples for this are the sub-Lorentzian shape of the line wings of CO_2, or the super- and sub-Lorentzian behaviour of H_2O. These effects are normally modelled by introducing a (experimentally determined) χ-factor into the line-wing description (see 5.6.3).
The second assumption causes major problems in the modelling of Q-branches since the lines are very close to each other and molecular collisions lead to an intensity transfer between the transitions. This effect is called line-mixing (see also 5.7).

5.6.1 Numerical calculation of the Voigt profile

Since the convolution integral of the Voigt profile cannot be evaluated in an analytical form it has to be calculated numerically. In order to fulfil this task several algorithms were developed and compared (e.g. Schreier, 1992) with regard to speed and accuracy, especially for the application in line-by-line models. Due to the recommendations of the latter intercomparison and our own tests regarding computation time of different approaches (see Table 5.1) it was decided to use the algorithm described by Humlicek (1982). This routine calculates a rational approximation (with a relative accuracy of 10^{-4}) of the complex probability function:

$$w^H(\breve{z}) = \mathrm{e}^{-\breve{z}^2}\left(1+\frac{2i}{\sqrt{\pi}}\int_0^{\breve{z}}\mathrm{e}^{t^2}\,\mathrm{d}t\right) = K_w(x,y) + iL_w(x,y) \qquad (5.6.1)$$

with:

$$\breve{z} = x + iy$$

$K_w(x,y)$ is the convolution integral of the Voigt function from equation (4.4.15).

Method	Relative run time
Humlicek (Humlicek, 1982)	1
AFGL (Clough et al., 1981)	1.2
Drayson (Drayson, 1976)	3.0

Table 5.1: Run time comparison between different approaches for the calculation of the Voigt lineshape.

As a baseline Humlicek (1982) has been implemented in the scientific code. A more sophisticated and optimised version of the Humlicek algorithm has been developed at IMK by M.Kuntz (priv. com.). However, the algorithm currently implemented in the scientific code will not be upgraded because, as it will be shown in Sect. 6.11, the final baseline of MIPAS Level 2 processor for operational retrievals is to compute cross-sections using compressed Look-Up Tables (LUTs).

5.6.2 Approximation of the Voigt profile by the Lorentz function

Since the calculation of the Voigt function is much more time consuming than the Lorentz function it is reasonable to use the Voigt shape only near the line centre where the differences between both are relatively large. Outside this region the Lorentz line shape can be used. The criterion that can be used for the application of the different functions is the relative error as a function of the distance from the centre in multiples of the Doppler half width α^D. The maximum relative errors are:

Distance from the line centre	Relative error (Lorentz-Voigt)/ Voigt
10 α^D	-1.5%
20 α^D	-0.37%
30 α^D	-0.17%
40 α^D	-0.10%
50 α^D	-0.06%

Table 5.2: The maximum ($y \to 0$ in eq. 4.4.15) relative error between the Voigt and the Lorentz function as a function of the difference from the line centre.

Besides, test calculations using the $30\alpha^D$ boundary for 6 selected pT microwindows showed maximum differences in the order of NESR/120. In these cases the time saving was 60% with respect to the calculation with the Voigt-profile.
The baseline is to use the Voigt profile only within 30 Doppler half-widths from the line centre. A less conservative transition can be considered if further computing time saving is found to be necessary.

5.6.3 χ-factors in the case of CO_2 and H_2O

In order to describe the sub-Lorentzian behaviour of the CO_2 lines χ-factors were experimentally determined e.g. by Cousin et al. (1985) for the CO_2 ν_3 band head at 4.3 μm. These factors start from unity at the line centre and remain 1 until 0.5-5 cm^{-1} distance (temperature dependent). Afterwards they decay exponentially.
The χ-factor for H_2O represents the super-Lorentzian behaviour of water vapour until some 100 cm^{-1} from the line centre and the sub-Lorentzian shape beyond this (Clough et al., 1989).
Since the χ-factors are equal to 1 up to some wavenumbers from the line centre, we can disregard them inside one microwindow. On the other hand the factors are considered for those lines which contribute as near continuum (see Sect. 5.11.2) to the radiation inside the microwindow.

5.7 Line-mixing

Line mixing, known also as line interference, line coupling, collision narrowing, Q-branch collapse, corresponds to the deviation of the measured line shape from the Lorentzian function (generally in regions with dense rotational structures, but effects in microwindows of transparency in vibration-rotation bands have been observed as well).

For practical calculations the suggested line shape (Rosenkranz, 1975) is:

$$A(\sigma,\sigma_l)=\frac{1}{\pi}\frac{\alpha_l^L+(\sigma-\sigma_l)pY_l}{(\sigma-\sigma_l+\mathrm{Im}\{\Gamma_{ll}\})^2+\alpha_l^{L\,2}} \tag{5.7.1}$$

with the first order coupling coefficient:

$$Y_l=2\sum_{l'(l'\neq l)}\frac{d_{l'}}{d_l}\cdot\frac{\Gamma_{l'l}}{\sigma_l-\sigma_{l'}} \tag{5.7.2}$$

$\mathbf{\Gamma}$ is the (frequency dependent) relaxation matrix, with diagonal elements determining the shape of uncoupled lines ($\mathrm{Re}\{\Gamma_{ll}\}=\alpha_l^L$, the Lorentz half widths) and the lineshifts ($-\mathrm{Im}\{\Gamma_{ll}\}$), and off-diagonal elements responsible for non additive effects (line mixing) when the lines overlap, and d_l is the reduced matrix of the dipole moment.

The Rosenkranz expression for the line shape is easily convoluted with the Doppler function. The modified Voigt function resulting from this convolution may be written in terms of the real ($K_w(x,y)$) and imaginary parts ($L_w(x,y)$) of the complex error function $w(z)$ which are calculated by the Humlicek algorithm (equation 5.6.1):

$$A_l^{V_{LM}}(\sigma-\sigma_l)=\sqrt{\frac{\ln 2}{\pi}}\frac{1}{\alpha_l^D}\left[K_w(x_l,y_l)+pY_lL_w(x_l,y_l)\right] \tag{5.7.3}$$

The baseline for Level 2 processor up to IPF version 5.0 has been not to use Q-branches where line-mixing is known to have strong effects. These spectral regions were avoided with an appropriate choice of the microwindows, so that line mixing does not need to be simulated. Starting from Level 2 processor IPF version 6, the line-mixing model of *Niro et al., (2007)* has been implemented in the algorithm that computes off-line the cross-section lookup tables (see Appendix D).

5.8 Pressure shift

Beside the line mixing effect, equation (5.7.1) contains the pressure shift in the form of the term $-\mathrm{Im}\{\Gamma_{ll}\}$which is proportional to the atmospheric pressure p. Since at the time of the ORM development pressure shift data were available only for CH_4 and for CO_2 above 2300 cm^{-1} (in the HITRAN96 data base) pressure shift was not coded in the forward model within the ORM. Pressure-shift is however modelled in the calculation of cross-section LUTs. Therefore, when LUTs are enabled, pressure-shift is correctly modelled by the forward model internal to the ORM.

5.9 Implementation of Non-LTE effects

The recommendation arising from the final report of Non-LTE study (Bologna, January 23, 1996) is that no inclusion of externally provided vibrational temperatures for target transitions is needed in operational processing. The impact of Non-LTE effects in p, T and VMR retrievals is reduced by using an appropriate selection of microwindows. The capability of handling NLTE is therefore not implemented in the OFM / ORM.

5.10 Self broadening

The Lorentz half width from equation (4.6.12) includes both, foreign $\alpha^{L_0^f}$ and self broadened $\alpha^{L_0^s}$ components:

$$\alpha^{L_0,i} = (1 - x^{VMR})\alpha^{L_0^f,i} + x^{VMR}\alpha^{L_0^s,i} \qquad (5.10.1)$$

With the volume mixing ratio x^{VMR}.

The relative error which is done when neglecting the self broadening is $x^{\mathrm{VMR}}\left(\alpha^{L_0^s,i}/\alpha^{L_0^f,i} - 1\right)$. Table 5.3 gives the maximum errors of the half width when assuming maximum values for x^{VMR} and maximum values for the quotient of self and foreign broadened half widths.

Gas	**Max.** $\alpha^{L_0^s,i}/\alpha^{L_0^f,i}$	**Max.** x^{VMR} **(8-50 km) [ppmv]**	**Max. error [%]**
CO_2	1.3	360	0.011
O_3	1.3	7	0.0002
H_2O	10 5 (average)	700 (tropical) 200 (mid-latitude)	0.7 0.08 (average/mid-lat.)
CH_4	1.3	1.7	0.00005
N_2O	not in HITRAN92	-	-
HNO_3	not in HITRAN92	-	-

Table 5.3: Maximum errors in the Lorentz half width when neglecting the self-broadening. Data was taken from HITRAN92 considering the entire range 685-2410 cm^{-1}

From Table 5.3 it is evident, that the self-broadening is negligible for all target species except water vapour in the tropical troposphere where maximum errors of about 0.7% can occur. However, this maximum error corresponds (through the Lorentz line shape formulation) directly to a pressure error of 0.7% which is one third of our acceptance criteria for approximations (2%, see chapter 3). Therefore our baseline is to disregard the self-broadening in all cases. Self broadening is modelled in the algorithm that computes cross-section LUTs. Therefore, when LUTs are enabled, self-broadening is correctly modelled by the forward model internal to the ORM.

5.11 Continuum

Three different effects contribute as a continuum to the spectral emission in a given microwindow:

- the instrumental continuum
- the near continuum
- the far continuum

First we discuss these effects and their origin, then we discuss how they can be simulated on the light of the objectives of this study. For their simulation by the forward model it is necessary to distinguish between the self standing forward model and the model included in the retrieval code.

5.11.1 Instrumental continuum

This continuum contribution is caused by the instrument itself. Its effect on the spectrum is a pure additive offset. The reasons for an instrumental continuum are manifold - e.g. self emission of the instrument, scattering of light into the instrument, or 3rd order non-linearity of the detectors. These distortions are corrected during the calibration in the Level 1b data processing but specifications indicate that the residual instrumental continuum averaged over the spectral range of the microwindow can be larger than the measurement noise. Therefore, the retrieval must be able to model the remaining radiometric errors. The simulation of the instrumental continuum can be performed by adding a wavenumber dependent offset to the spectrum.
The baselines are:

- for the self-standing forward model to disregard this effect since this program should only simulate atmospheric contributions.
- for the retrieval to assume that the instrumental offset does not vary with changing limb scan angles and fit for each microwindow only one instrumental continuum offset value.

5.11.2 Near continuum

This contribution to the intensity inside a microwindow is caused by nearby emission lines of atmospheric gases. Therefore, the simulation of this effect has to be performed during the calculation of the absorption cross sections. The different possibilities for its calculation are:

1. explicit calculation of the wings of the lines at each fine-grid point inside the microwindow (see 5.6).
2. calculation only at three grid points inside the microwindow and parabolic interpolation in between

For the simulation of the near continuum the ORM uses a switch stored in the MW-specific spectroscopic database files. These files include, for each spectral line, a parameter indicating whether the line is to be calculated explicitly at each spectral grid point in the MW (option 1) or can be calculated only at three spectral grid points and interpolated at the remaining grid points. Baseline is to use option 2. The same option is used for both self standing and retrieval forward model.

5.11.3 Far continuum

This term includes all continuum-like contributions which are not included in the previous two definitions. These are e.g. the line wings of lines farther than 25 cm^{-1} from the current wavenumber (the most important contribution here is from H_2O), the pressure broadened bands of O_2 at 1550 cm^{-1}

and N_2 at 2350 cm^{-1} and the absorption by aerosols. For this continuum we have to distinguish between the self standing forward model and the forward model implemented into the retrieval code.

Self standing forward model:

The self standing forward model must produce realistic simulations of the atmospheric spectra that include the continuum. We decided to use the same continuum as in FASCOD (Clough et al., 1989). The water continuum is described in Clough et al. (1989). Herein the continuum cross section $k^{cont_{H_2O}}(\sigma)$ is given by the sum of the far line wings using the Van Vleck and Huber line shape function which is modified in order to fit the experimental data of Burch and Alt (1984):

$$k^{cont_{H_2O}}(\sigma) = \sigma \tanh\left(\frac{hc\sigma}{2K_B T}\right) \sum_{l(ines)} \frac{S_l}{\sigma_l \tanh\left(hc\sigma_l / 2K_B T\right)} \left[f(\sigma,\sigma_l)\chi_{H_2O}(\sigma,\sigma_l) + f(-\sigma,\sigma_l)\chi_{H_2O}(-\sigma,\sigma_l) \right] \quad (5.11.1)$$

where:

$$f(\pm\sigma,\sigma_l) = \frac{1}{\pi} \frac{\alpha_l^L}{\alpha_l^{L\,2} + (\sigma \pm \sigma_l)^2} \qquad \text{if} \quad |\sigma \pm \sigma_l| \geq 25\,\text{cm}^{-1} \quad (5.11.2)$$

$$f(\pm\sigma,\sigma_l) = \frac{1}{\pi} \frac{\alpha_l^L}{\alpha_l^{L\,2} + 25^2} \qquad \text{if} \quad |\sigma \pm \sigma_l| \leq 25\,\text{cm}^{-1} \quad (5.11.3)$$

and $\chi_{H_2O}(\sigma,\sigma_l)$ is the χ-factors of water.

For the implementation into the forward model the following equation is used:

$$k^{cont_{H_2O}}(\sigma) = \sigma \tanh\left(\frac{hc\sigma}{2k^B T}\right) \frac{\eta}{\eta^0} \left(\chi_{H_2O} C_{0s}(\sigma,T) + \left(1 - x_{H_2O}\right) C_{0f}(\sigma,T) \right) \quad (5.11.4)$$

$C_{0s}(\sigma,T)$ and $C_{0f}(\sigma,T)$ are the continuum absorption parameters for the self and the foreign broadening at the reference number density η_0. η is the actual air density. To determine the temperature dependence of the self broadening values, exponential interpolation between the tabulated parameters $C_{0s}(\sigma,260\,\text{K})$ and $C_{0s}(\sigma,296\text{K})$ is performed. For the foreign broadening $C_{0f}(\sigma,296\text{K})$ is used for all temperatures. The interpolation in frequency is performed linearly.

This continuum description includes only contributions of lines farther than 25 cm^{-1} from the line centre. Since the self standing forward model will use the spectroscopic database which uses various selection criteria for the lines, not all water lines within 25 cm^{-1} may be considered.

However, tests have shown that the error due to this fact is less than 0.175×NESR (and in most cases much less than this). Because this is presumably smaller than the absolute accuracy of the continuum model and because the self-standing forward model is not required to describe the continuum with very high accuracy, our baseline is to use selected water lines from the spectroscopic database. If higher accuracy is needed, the missing water lines can be added to the data-base.

The N_2 continuum is parameterised, temperature independently, every 5 cm^{-1} between 2020 and 2800 cm^{-1} for a reference number density η_0. In order to calculate it for the actual pressure and temperature it has to be multiplied by the ratio η/η_0, where η is the actual number density, and linearly interpolated to the wavenumber. For a details on the implemented N_2 continuum model, please refer to Lafferty at al., (1996).

The O_2 continuum is given in the form of three parameters (one strength and two for the temperature correction) from 1395-1760 cm^{-1}. For a detailed description of the adopted model of O_2 continuum, please refer to the paper of Thibault et al., (1997).

Forward model in the retrieval:

The forward model in the retrieval code simulates the far-continuum using a MW- and altitude-dependent cross-section $K_{\mathrm{MW}}(z)$. The transmission of each atmospheric layer ownig to the gases is multiplied by $\xi_{\mathrm{MW}}(z) = \exp\left(-K_{\mathrm{MW}}(z) \cdot C_{AIR}(z)\right)$ where $C_{AIR}(z)$ is the total air column of the atmospheric layer at altitude z. A profile $\xi_{\mathrm{MW}}(z)$ is retreived for each MW, in the altitude range where the MW is used, possibly limited to the top altitude bound for continuum retrieval, that is supplied by the user in the settings file (tipycally 30 km). In order to limit the number of retrieved parameters / profiles, the retrieval algorithm offers the possibility to apply some constraints to the retrieved $\xi_{\mathrm{MW}}(z)$ profiles.
For each microwindow and each altitude, the frequency range $\Delta\nu$ is defined in which the continuum is expected to vary linearly with frequency. This frequency range is used to establish the constraints between retrieved continuum profiles. Particularly, if the distance between the centers of two (or more) selected MWs is less than a fraction f of $\Delta\nu$, the MWs are considered to be in 'tight contiguity' and they share the same retrieved continuum profile $\xi_{\mathrm{MW}}(z)$. If a set of MWs is located in a frequency interval whose width is less than $\Delta\nu$, continuum profiles $\xi_{\mathrm{MW}}(z)$ are retrieved for the MWs at the edges of the set and continuum is obtained via linear interpolation for the MWs in between. The MWs within this type of set are said in 'loose contiguity'.

The most recent versions of the algorithm for automated selection of spectral microwindows (MWMAKE, see Appendix C and Bennett et al., 1999) use the fitted atmospheric continuum parameters to compensate for various systematic error sources that introduce in the spectrum a continuum-like effect. This baseline implies that currently, the fitted "continuum" parameters have lost their physical meaning. Therefore, while in principle in the ORM it is still possible to apply the above mentioned constraints, in routine retrievals these are not applied. Continuum constraints are disabled by setting to a very small value the continuum linearity range $\Delta\nu$.

Note that, in the first versions of the MIPAS Level 2 processor (up to Version 5.0) the baseline was to retrieve vertical profiles of continuum cross-sections $K_{\mathrm{MW}}(z)$. Starting from Version 6.0, the baseline has changed to the retrieval of $\xi_{\mathrm{MW}}(z)$ profiles. According to the results of the studies of *Ridolfi and Sgheri, (2013)*, this new baseline makes the retrieval better conditioned and improves the stability.

5.12 Interpolation of the profiles in the forward / retrieval model

Since both initial guess and retrieved profiles are often represented on a grid much coarser (≈ 3km) than the grid used for the discretization of the atmosphere (≈ 1km, for the radiative transfer calculation), a set of interpolation rules must be established for the various types of profiles.
Pressure and temperature profiles are always constrained to fulfil the hydrostatic equilibrium equation. Tests have shown that, using any of the atmospheric standard models, neglecting the temperature gradient leads to negligible errors when layers thinner than 6 km are adopted and the temperature in the middle of the layer is used as the representative temperature of the layer.
When the altitude is the independent variable, it is common to consider the temperature and the VMR profiles as varying linearly with altitude, and pressure as varying accordingly to the hydrostatic

equilibrium law (i.e. exponentially with the altitude if the temperature is assumed locally constant for the calculation of pressure).
Now, since in our case the independent variable is pressure, the most appropriate interpolation rule is linear interpolation for both temperature and VMR profiles in log(P). The baseline is therefore to use type of interpolation for temperature and VMR profiles whenever an interpolation is required.
Regarding continuum cross-section profiles: whenever an interpolation is required, since the continuum emission behaves as the square of pressure (Clough et al., 1989), and since the fitted continuum cross-section profiles are multiplied by the air column (proportional to pressure) in order to obtain continuum emission, it is then reasonable to interpolate continuum profiles linearly in pressure.

5.13 Interpolation of the "retrieved" profiles to a user-defined grid

5.13.1 Description of the problem

The baseline of the Level 2 scientific processor is to retrieve the target profiles in correspondence of the tangent pressures. However, the users of MIPAS products may need to resample the retrieved profiles to a user-defined set of pressures. The problem arises therefore of providing a recommended interpolation scheme consistent with the Level 2 algorithm assumptions.
The first possibility is to recommend the use of the same set of interpolation rules used in the retrieval processor (see Sect. 5.12). However, considering that Level 2 profiles have been derived from limb-scanning measurements, the a-posteriori interpolation process should generate profiles that, when provided in input to the forward model, reproduce the simulated spectra calculated in the retrieval at convergence. Therefore, considering that the simulated limb-radiances strongly depend on the total column amounts above the tangent point, the interpolation scheme should conserve the total column. In other words, the column calculated for the interpolated points should be equal, within some pre-defined tolerance, to the column obtained with the original data profile.
We recall that the vertical column of a gas, above a particular altitude *rz*1 is defined as

$$Col = Const \int_{rz1}^{rulatm} x_{gas}^{VMR} \frac{p(z)}{T(z)} dz \qquad (5.13.1)$$

where *rulatm* is the altitude of the upper boundary of the atmosphere and x_{gas}^{VMR}, *p(z)* and *T(z)* are the gas VMR, pressure and temperature respectively.
The quantities x_{gas}^{VMR}, *p(z)* and *T(z)* are measured for a discrete altitude grid, thus, in order to have a realistic result we must calculate the total column as the sum of partial columns between the altitudes of this grid. In turn these partial columns can be calculated interpolating the pressure, temperature and VMR profiles between the two edge altitudes: linear interpolation is used for Temperature and VMR, and exponential interpolation for the pressure.
Therefore, the problem of the interpolation of the VMR profiles becomes one of finding an appropriate transformation of the VMR profile that fulfils the constraint of an unchanged vertical column.

5.13.2 Strategy

The strategy adopted consists of constructing a new grid of VMR points and to impose a one-to-one correspondence of partial columns with the original profile. By finding the VMR values that satisfy this condition, a profile is identified at the new grid points. The latter will be different of the one obtained with a classical interpolation rule.

A 'classical' interpolation law is defined in order to identify from the discrete output of the ORM a continuous representation of the atmosphere. For each value of the independent variable (pressure), the corresponding altitude and temperature can be obtained by means of hydrostatic equilibrium equation, assuming a linear dependence of temperature on altitude. In turn, the VMR values at each user-defined altitude can be obtained by linear interpolation between the two nearest retrieved values.
On the basis of this continuous representation, partial columns and total columns can be defined with respect to both the retrieval grid and the user defined grid in the following way:

1. First partial columns are calculated on the retrieval-grid
2. Then the VMR values are calculated at the user-defined grid using linear interpolation with the altitude.
3. Then the partial columns at the retrieval-grid are calculated following a spline that joins the user-defined grid points only.
4. We then vary the VMR values at the user-defined grid until the difference between the partial columns of the new profile and of the original profile are minimum. By definition, the resulting profile has the property of keeping unmodified the vertical column.

The variation of the VMR values on the user-defined grid are calculated using a non-linear least-squares fitting procedure. The quantities to be fitted are the partial columns on the retrieval grid. The parameters to be fitted are the VMR values at the pressure levels of the user-defined grid. The fitting method is the Gauss-Newton method: if $\Delta_{\mathbf{XV}}$ is a vector containing the difference between the observed partial columns and the calculated partial columns, then the correction $\Delta_{\mathbf{CV}}$ to be applied to the values of the VMR at the user-grid to minimise this difference is given by:

$$\Delta_{\mathbf{CV}} = \mathbf{G}_{\mathbf{V}} \Delta_{\mathbf{XV}} \tag{5.13.2}$$

where $\mathbf{G}_{\mathbf{V}} = \left(\mathbf{K}_{\mathbf{v}}^{T}\mathbf{S}_{\mathbf{col}}^{-1}\mathbf{K}_{\mathbf{v}}\right)^{-1}\mathbf{K}_{\mathbf{v}}^{T}\mathbf{S}_{\mathbf{col}}^{-1}$ and $\mathbf{K}_{\mathrm{v}}$ is the Jacobian matrix and $\mathbf{S}_{\mathbf{col}}$ is the Variance Covariance Matrix (VCM) of the measured columns.
Since the values of the partial columns are numbers that change by several orders of magnitude from the highest altitude to the lowest, instead of fitting their values we fit the logarithm of their values. So $\mathbf{S}_{\mathbf{col}}$ becomes the VCM of the logarithm of the partial columns $\mathbf{S}_{\log(\mathrm{col})}$.
An output of the retrieval code is the VCM of the measured columns *col(i)* at the various tangent altitudes *i*. To get the VCM of the logarithm of the columns we apply the following transformation:

$$\left(\mathbf{S}_{\log(\mathrm{col})}\right)_{i,j} = \frac{\left(\mathbf{S}_{\mathrm{col}}\right)_{i,j}}{col(i) * col(j)} \tag{5.13.3}$$

The errors associated with the solution of the fit are given by the square roots of the diagonal elements of the VCM of the solution (**S**) given by:

$$\mathbf{S} = \left(\mathbf{K}_{\mathbf{v}}^{T}\mathbf{S}_{\log(\mathrm{col})}^{-1}\mathbf{K}_{\mathbf{v}}\right)^{-1} \tag{5.13.4}$$

After solving equation (5.13.2), the VMR profile on the user-defined grid will be given by the new vector $\mathbf{x}^{\mathbf{VMR}\mathrm{int}}$:

$$\mathbf{x}^{\mathbf{VMR}\mathrm{int}} = \mathbf{x}^{\mathbf{VMR}\mathrm{linint}} + \Delta_{\mathbf{CV}} \tag{5.13.5}$$

The fitting procedure is repeated until the sum of the squares of the differences between the new columns and the measured ones doesn't change of more than 1%. In the ORM code the retrieved profile above the highest fitted altitude is obtained by scaling the initial-guess profile of the same quantity used for the highest fitted point. The same procedure has to be applied to the interpolated points above the highest fitted altitude or to the highest point of the user-defined grid if it happens to be below the highest fitted altitude.
The errors associated with the new VMR values are characterised by the variance-covariance matrix **S** provided by equation (5.13.4).

5.14 Optimized algorithm for construction of initial guess profiles and gradients

The scientific version of this function was implemented only in the ORM v.8. Earlier ORM versions had no access to operational data from the European Centre for Medium-range Weather Forecast (ECMWF), therefore this function was only implemented in the so called "framework" module of the industrial Level 2 processor. Furthermore, the construction of the initial guess profiles requires knowledge of the profiles retrieved from the "previous scan" in the orbit and, at the beginning of the development, the ORM had the capability of handling only individual scans.

For the analysis of a given limb scan of measurements, the ORM needs the vertical profiles and horizontal gradients of the following quantities:

1. Pressure and temperature,
2. VMR of retrieved and non-retrieved (or assumed) gases contributing to the MWs used in the retrievals to be performed.
3. Continuum vertical profiles for the microwindows used in the retrievals to be performed.

The profiles can be used in the different retrievals either as a first guess of the profiles that are going to be retrieved or as assumed profiles of the atmospheric model (profiles of interfering species and p,T profiles in the case of VMR retrievals). Horizontal gradients are assumed (not retrieved) in the forward model computations.

5.14.1 Initial guess pressure, temperature and VMR profiles, and their horizontal gradients

The ORM v.8 builds the initial guess / assumed profiles and horizontal gradients of Pressure, Temperature and VMR on the basis of input files. These files are built by the ORM pre-processing stage, starting from the following sources:

- IG2: the IG2 climatological profile database (*Remedios et al., 2007*)
- ORM: profile retrieved by the ORM from the current scan being processed, e.g. pT and H2O profiles already retrieved from the current scan
- ADJ: profiles retrieved by the ORM from the scan adjacent to the current scan.
- NET: profiles retrieved by the ORM in a previous processing of the current orbit of measurements.
- ECM: ECMWF profiles (p, T, H_2O and O_3 profiles) obtained by inerpolationg to time and geo-location of the current scan the ECMWF analysis profiles.

In the ORM, the above profile sources are prioritized according to a list provided by the user in the settings file. Intial profiles and gradients are then computed by the ORM pre-processing module for each scan, using first the highest priority sources available, then eventually extending them in altitude,

with profiles and horizontal gradients from lower priority sources, so as to cover the whole 0 – 120 km vertical range that is adopted for the IG2 profiles.
From the ORM settings file it is possible to require the profiles arising from a specific gas retrieval not to contribute to building the initial guess / assumed profiles for the subsequent retrievals. This option is especially useful for gas profiles retrieved with extremely low signal to noise ratio, large error bars and, possibly, large oscillations. Test retrievals have shown that in these cases the use of IG2 climatological profiles as initial guess makes the retrieval generally more stable and improves the quality of the results. Full details of the algorithm employed by the ORM v.8 to build initial guess / assumed profiles are described in *Sgheri, (2017*).

5.14.2 Initial guess continuum profiles

The initial guess continuum profiles used by the retrieval algorithm are purely climatological profiles. Retrieved continuum profiles are not considered for the generation of the initial guess as they suffer of very large uncertainties (and also because retrieved continuum parameters, being used also to compensate for continuum-like error sources, may be very different from scan to scan).
Climatological continuum profiles are generated on the basis of a simple algorithm that, starting from given profiles of pressure, temperature and water vapor, calculates profiles of water vapor cross-sections in correspondence of the central frequencies of the considered microwindows. Water vapor continuum cross-sections are calculated using the CKD v.2.4 model (Clough, (1989)). The continuum of other species like CO_2, N_2, O_2, aerosols etc. is not considered in this algorithm because we have found that in the presence of large uncertainties on the continuum emission, it is by far preferred to use initial guess profiles that underestimate the real continuum. In fact, an overestimated initial guess continuum easily leads to a very opaque atmosphere in which the line of sight may not be able to penetrate. In these conditions the fitting procedure may be unable to recover the correct continuum emission.

5.15 Profiles regularization

In the nominal observation mode adopted after January 2005, a MIPAS limb-scan consists of 27 spectra that look at tangent altitudes from 7 to 72 km, with 1.5 km steps from 7 to 22 km, 2 km steps from 22 to 32 km, 3 km steps from 32 to 47 km, 4 km steps from 47 to 63 km and 4.5 km steps from 63 to 72 km. The signal measured by the instrument is obtained with an instantaneous field of view (IFOV) equal to 3x30 km^2 (vertical height times across-track width). Since the step of the measurement grid is for some altitudes smaller than the vertical IFOV, contiguous limb scanning views have overlapping IFOVs. This situation, combined with the choice of using a retrieval grid that matches the measurement grid, determines an ill-conditioning of the inversion and the need for a regularization in order to avoid instabilities in the retrieved profiles. The ORM adopts a Tikhonov-Twomey regularization scheme (Tikhonov, 1963), whose strength can be established (depending on the features of the retrieved profile) using two alternative approaches: the error consistency (EC) method of Ceccherini, (2005), or the Iterative Variable Strength (IVS) method proposed by *Ridolfi and Sgheri, (2009)*. These two methods are herewith briefly described.

5.15.1 The error consistency (EC) method

The Tikhonov regularized solution of the retrieval problem can be obtained by minimizing the following cost function (see e. g. Rodgers (2000)):

$$f(\mathbf{x}) = (\mathbf{y} - \mathbf{F}(\mathbf{x}))^T (\mathbf{S}_y)^{-1} (\mathbf{y} - \mathbf{F}(\mathbf{x})) + \lambda_R (\mathbf{x} - \mathbf{x}_a)^T \mathbf{R} (\mathbf{x} - \mathbf{x}_a) \quad (5.15.1)$$

where $\mathbf{x}$ is the vector representing the profile to be determined, $\mathbf{y}$ is the measurement vector, $\mathbf{S}_y$ is the VCM describing the errors of $\mathbf{y}$, $\mathbf{F}(\mathbf{x})$ is the forward model, λ_R is a positive parameter characterizing the strength of the regularization, $\mathbf{x}_a$ is an a priori estimate of the state vector and $\mathbf{R}$ is a regularization matrix. The cost function f($\mathbf{x}$) contains two terms: the first term is the ``chi-square'' that measures how well the forward model calculated in $\mathbf{x}$ is able to reproduce the measurements within their errors, and the second term measures how well the retrieved profile follows some feature of $\mathbf{x}_a$ determined by the regularization matrix. In our case, where $\mathbf{R}=\mathbf{L_1}^T\mathbf{L_1}$ with $\mathbf{L_1}$ equal to the discrete first derivative operator, the vertical increments of the retrieved profile are constrained to follow those of $\mathbf{x}_a$. If $\mathbf{x}_a$ is a smooth profile, the $\mathbf{L_1}$ operator provides a smoothing of the retrieved profile while reducing the negative correlations between vertically adjacent values introduced by the fact that contiguous limb views have overlapping IFOVs.
The minimum of f($\mathbf{x}$) may be searched iteratively using the Gauss-Newton method, that provides the following expression of $\mathbf{x}$ at each iteration:

$$\mathbf{x} = \left(\mathbf{S}_{\hat{\mathbf{x}}}^{-1} + \lambda_R \mathbf{R}\right)^{-1} \left(\mathbf{S}_{\hat{\mathbf{x}}}^{-1} \cdot \hat{\mathbf{x}} + \lambda_R \mathbf{R} \mathbf{x}_a\right) \quad (5.15.2)$$

where $\hat{\mathbf{x}}$ is the non-regularized state vector, i.e. the solution obtained when only the first term of f($\mathbf{x}$) is minimized and $\mathbf{S}_{\hat{\mathbf{x}}}$, is its VCM. This is an unconventional expression of the solution that will be useful for the subsequent considerations and that can be reduced to the conventional expression recalling that:

$$\hat{\mathbf{x}} = \hat{\mathbf{x}}_0 + \left(\mathbf{K}^T \mathbf{S}_y^{-1} \mathbf{K}\right)^{-1} \mathbf{K}^T \mathbf{S}_y^{-1} (\mathbf{y} - \mathbf{F}(\hat{\mathbf{x}}_0)) \quad (5.15.3)$$

$$\mathbf{S}_{\hat{\mathbf{x}}} = \left(\mathbf{K}^T \mathbf{S}_y^{-1} \mathbf{K}\right)^{-1} \quad (5.15.4)$$

$\hat{\mathbf{x}}_0$ being the initial guess of the iteration and $\mathbf{K}$ the Jacobian matrix of $\mathbf{F}(\mathbf{x})$ calculated in $\hat{\mathbf{x}}_0$.
The solution of Eq. (5.15.2) is characterized by the following averaging kernel matrix (AKM) (Rodgers, 2000):

$$\mathbf{A}_{\mathbf{x}}^{AKM} = \left(\mathbf{S}_{\hat{\mathbf{x}}}^{-1} + \lambda_R \mathbf{R}\right)^{-1} \mathbf{S}_{\hat{\mathbf{x}}}^{-1} \quad (5.15.5)$$

and by the following VCM:

$$\mathbf{S}_{\mathbf{x}} = \left(\mathbf{S}_{\hat{\mathbf{x}}}^{-1} + \lambda_R \mathbf{R}\right)^{-1} \mathbf{S}_{\hat{\mathbf{x}}}^{-1} \left(\mathbf{S}_{\hat{\mathbf{x}}}^{-1} + \lambda_R \mathbf{R}\right)^{-1}. \quad (5.15.6)$$

To determine the regularization strength, the EC method (Ceccherini, 2005) can be applied. It is based on the requirement that the difference between the regularized and the non-regularized profiles weighted with the inverse of the VCM of the regularized profile must be equal to the number n^R of points of the profile:

$$(\mathbf{x} - \hat{\mathbf{x}})^T \mathbf{S}_x^{-1} (\mathbf{x} - \hat{\mathbf{x}}) = n_R \,. \quad (5.15.7)$$

A simplified interpretation of Eq. (5.15.7) is obtained in the case that $\mathbf{S_x}$ is a diagonal matrix (even if this never occurs for atmospheric profiles retrieved from remote sensing measurements). In this case the differences between the regularized and the non-regularized profiles must be on average equal to the errors of the regularized profile (measured by the square root of the diagonal elements of $\mathbf{S_x}$).
Substituting in Eq. (5.15.7) $\mathbf{x}$ from Eq. (5.15.2) and $\mathbf{S_x}$ from Eq. (5.15.6), with straightforward calculations the following value for λ_R is obtained:

$$\lambda_R = \sqrt{\frac{n_R}{(\mathbf{x}_a - \hat{\mathbf{x}})^T \mathbf{R}\mathbf{S}^{\hat{\mathbf{x}}}\mathbf{R}(\mathbf{x}_a - \hat{\mathbf{x}})}}. \qquad (5.15.8)$$

In Eq. (5.15.8) the $\mathbf{S}_{\hat{\mathbf{x}}}$, which measures the random errors due to the mapping of random radiometric noise into the retrieved profile, is used instead of the VCM of the total retrieval errors. In this way the error components due to forward model errors are neglected in the regularization process. This choice is based on the consideration that these components are usually characterized by a positive correlation between values contiguous in altitude, and therefore, the regularization does not need to account for them.
The application of this method to the MIPAS retrieval code has to take into account the following considerations. The Gauss-Newton iterative method is successful only in the case of a sufficiently weak non-linearity of the forward model. In the case of strong non-linearities some iterations of the iterative method can lead to an increase rather than to a decrease of the residuals. For this reason in the ORM a modification of the Gauss-Newton method, the Levenberg-Marquardt technique (Levenberg, 1944; Marquardt, 1963), is used. This latter modifies Eqs. (5.15.3) and (5.15.4) into:

$$\hat{\mathbf{x}} = \hat{\mathbf{x}}_0 + \left(\mathbf{K}^T\mathbf{S}_y^{-1}\mathbf{K} + \alpha_{reg}\mathbf{M}\right)^{-1}\mathbf{K}^T\mathbf{S}_y^{-1}\left(\mathbf{y} - \mathbf{F}(\hat{\mathbf{x}}_0)\right) \qquad (5.15.9)$$

$$\mathbf{S}_{\hat{\mathbf{x}}} = \left(\mathbf{K}^T\mathbf{S}_y^{-1}\mathbf{K} + \alpha_{reg}\mathbf{M}\right)^{-1}\mathbf{K}^T\mathbf{S}_y^{-1}\mathbf{K}\left(\mathbf{K}^T\mathbf{S}_y^{-1}\mathbf{K} + \alpha_{reg}\mathbf{M}\right)^{-1} \qquad (5.15.10)$$

where $\mathbf{M}$ is a matrix that in the ORM is diagonal, with the diagonal elements equal to those of the matrix $\mathbf{K}^T\mathbf{S}_y^{-1}\mathbf{K}$ and α_{reg} is a parameter that, during the retrieval iterations, is increased or decreased depending on whether the chi-square function increases or decreases while the atmospheric state is upgraded from $\hat{\mathbf{x}}_0$ to $\hat{\mathbf{x}}$ only when the chi-square function decreases**.** Accordingly, the AKM is not an identity matrix, as in the pure Gauss-Newton approach, but it is equal to:

$$\mathbf{A}_{\hat{\mathbf{x}}}^{AKM} = \left(\mathbf{K}^T\mathbf{S}_y^{-1}\mathbf{K} + \alpha_{reg}\mathbf{M}\right)^{-1}\mathbf{K}^T\mathbf{S}_y^{-1}\mathbf{K} \qquad (5.15.11)$$

Some tests on MIPAS measurements have confirmed that, because of the high non-linearity of the problem, the pure Gauss-Newton iteration often produces an increased chi-square value. The Levenberg-Marquardt method is needed to determine the minimum of the chi-square, and this need is not abated by the use of the Tikhonov regularization. For this reason we decided to use both the Levenberg-Marquardt method and the Tikhonov regularization.

Recalling that the objective of the Levenberg-Marquardt method is to reach the minimum of the chi-square and the objective of the Tikhonov regularization is to limit the oscillations of the retrieved profile, it is convenient to exploit Eq. (5.15.2) which calculates the regularized profile from the non-regularized one and to perform the two operations sequentially. First the chi-square function is minimized using the Levenberg-Marquardt method by means of the iterative application of Eq.

(5.15.9), secondly, when convergence has been reached, an a-posteriori regularization defined by Eq. (5.15.2), with $\hat{\mathbf{x}}$ and $\mathbf{S}_{\hat{\mathbf{x}}}$ given by the Eqs. (5.15.9-5.15.10) at the last iteration of the minimization process, is applied. This procedure is different from the commonly used procedure that performs the regularization at each iteration step. The two procedures produce similar performances in terms of vertical resolution and retrieval errors and the adopted strategy has the advantage of lighter calculations that is important for operational retrievals.

The strength of the regularization can be determined by means of the EC method using Eq. (5.15.8). The VCM of the regularized profile is given by Eq. (5.15.6) and the AKM is obtained by calculating the derivative of $\mathbf{x}$ (provided by Eq. (5.15.2)) with respect to the atmospheric true state, taking into account that the derivative of $\hat{\mathbf{x}}$ with respect to the atmospheric true state is (by definition) $\mathbf{A}_{\hat{\mathbf{x}}}^{AKM}$:

$$\mathbf{A}_{x}^{AKM} = \left(\mathbf{S}_{\hat{\mathbf{x}}}^{-1} + \lambda_R \mathbf{R}\right)^{-1} \mathbf{S}_{\hat{\mathbf{x}}}^{-1} \mathbf{A}_{\hat{\mathbf{x}}}^{AKM} \tag{5.15.12}$$

where $\mathbf{A}_{\hat{\mathbf{x}}}^{AKM}$ is provided by Eq. (5.15.11) calculated at the last iteration of the minimization process.
The methods described so far have a limitation in the case of H_2O whose VMR values change several order of magnitude within a single profile. In fact in this case the procedure regularizes the profile only in the altitude regions where the VMR is large (because in this region the absolute error is the largest), and does not regularize the profile where the VMR is small. This problem can be overcome considering the logarithm of the profile in the place of the profile, in this case the regularization method uses the relative errors (instead of the absolute errors) to choose where to regularise the profile. Since the relative errors are expected to be more constant along the profile, a more uniform regularisation is expected.
In this case the regularisation must be applied to the profile of the logarithm of water vapour VMR. When the cost function of equation (5.15.1) is defined for the logarithm of the profile, solution (5.15.2) becomes:

$$\log(\mathbf{x}) = \left(\mathbf{S}_{\log(\hat{\mathbf{x}})}^{-1} + \lambda_R \mathbf{R}\right)^{-1} \left[\mathbf{S}_{\log(\hat{\mathbf{x}})}^{-1} \log(\hat{\mathbf{x}}) + \lambda_R \mathbf{R} \log(\mathbf{x}_a)\right] \tag{5.15.13}$$

where:

$$\left(\mathbf{S}_{\log(\hat{\mathbf{x}})}\right)_{i,j} = \frac{\left(\mathbf{S}_{\hat{\mathbf{x}}}\right)_{i,j}}{\hat{x}_i \hat{x}_j} \tag{5.15.14}$$

From Eq. (5.15.13) it follows that:

$$\mathbf{S}_{\log(\mathbf{x})} = \left[\left(\mathbf{S}_{\log(\hat{\mathbf{x}})}^{-1} + \lambda_R \mathbf{R}\right)^{-1} \mathbf{S}_{\log(\hat{\mathbf{x}})}^{-1} \left(\mathbf{S}_{\log(\hat{\mathbf{x}})}^{-1} + \lambda_R \mathbf{R}\right)^{-1}\right] \tag{5.15.15}$$

The regularised profile is obtained by means of the exponential function:

$$\mathbf{x} = \exp(\log(\mathbf{x})) = \exp\left[\left(\mathbf{S}_{\log(\hat{\mathbf{x}})}^{-1} + \lambda_R \mathbf{R}\right)^{-1} \left[\mathbf{S}_{\log(\hat{\mathbf{x}})}^{-1} \log(\hat{\mathbf{x}}) + \lambda_R \mathbf{R} \log(\mathbf{x}_a)\right]\right] \tag{5.15.16}$$

and is characterized by the following VCM and AKM:

$$\left(\mathbf{S}^{\mathbf{x}}\right)_{i,j} = \left[\left(\mathbf{S}_{\log(\hat{\mathbf{x}})}^{-1} + \lambda_R \mathbf{R}\right)^{-1} \mathbf{S}_{\log(\hat{\mathbf{x}})}^{-1} \left(\mathbf{S}_{\log(\hat{\mathbf{x}})}^{-1} + \lambda_R \mathbf{R}\right)^{-1}\right]_{i,j} x_i x_j \tag{5.15.17}$$

$$\mathbf{A}_{\mathbf{x}}^{AKM} = \mathbf{C}\mathbf{A}_{\hat{\mathbf{x}}}^{AKM} \tag{5.15.18}$$

where **C** is defined by:

$$(\mathbf{C})_{i,j} = \left[\left(\mathbf{S}_{\log(\hat{\mathbf{x}})}^{-1} + \lambda_R \mathbf{R}\right)^{-1} \mathbf{S}_{\log(\hat{\mathbf{x}})}^{-1}\right]_{i,j} \frac{x_i}{\hat{x}_j} \tag{5.15.19}$$

The value of the regularization parameter λ_R can be determined applying the EC method to the logarithm of the profile:

$$\left(\log(\mathbf{x}) - \log(\hat{\mathbf{x}})\right)^T \mathbf{S}_{\log(\mathbf{x})}^{-1} \left(\log(\mathbf{x}) - \log(\hat{\mathbf{x}})\right) = n_R \tag{5.15.20}$$

Substituting the equations (5.15.13) and (5.15.15) in equation (5.15.20) we find an analytical solution for the regularization parameter λ_R :

$$\lambda_R = \sqrt{\frac{n_R}{\left(\log(\mathbf{x}_a) - \log(\hat{\mathbf{x}})\right)^T \mathbf{R}\mathbf{S}_{\log(\hat{\mathbf{x}})}\mathbf{R}\left(\log(\mathbf{x}_a) - \log(\hat{\mathbf{x}})\right)}} \tag{5.15.21}$$

Remark: application to real data of the method presented above, in which the logarithm of the H_2O VMR is regularized with the EC approach, has been found to be critical. The criticality arises from the large error bars (< 100%) that sometimes are encountered, in localized altitude ranges (just above the tropopause), in the H_2O profiles. In fact, too large error bars imply the failure of the linearity hypothesis used above, for the calculation of the VCM of the logarithm of the VMR profile. For this reason H_2O profile regularization has been disabled in the ESA IPF version 6.0 retrievals. The IPF/ML2PP version 7 implements a more sophisticated approach for the selection of the regularization strength, the so called "Iterative Variable Strength" (IVS) method.

5.15.2 The Iterative Variable Strength (IVS) regularization method

Due to the above mentioned problems with the EC regularization method, in *Ridolfi and Sgheri, (2009)* we proposed the VS (variable strength) regularization scheme, a self-adapting and altitude-dependent approach that detects whether the actual observations contain information about small-scale profile features, and determines the strength of the regularization accordingly. While representing an optimal solution, this method has two drawbacks. First, the method relies on an external minimization routine that needs to be carefully tuned to obtain optimal performances. Second, the computational requirements of the method, and specifically of the optimization routine, lead to an increase of the retrieval time of more than 20%. This extra computing load was considered unacceptable by ESA for the MIPAS ground processor. For this reason we explored the possibility to simplify the VS method, with the aim of reducing its computational cost while preserving the good performances. Therefore we proposed the IVS (iterative variable strength) method, an alternative to the VS scheme. The IVS, while based on the same rationale of the VS, does not use any minimization routine, so that the implementation is easier and the additional computational effort required amounts only to about 1.5% of the total retrieval time.

Tikhonov regularization is often used to improve the conditioning of atmospheric profile inversion. Smoother profiles are obtained by penalizing the oscillating solutions in the inversion formula. Let $\mathbf{y} = \mathbf{f}(\mathbf{x})$ be the forward problem, where $\mathbf{y}$ is the m-dimensional vector of the observations with error covariance matrix $\mathbf{S}_y$, $\mathbf{f}$ is the forward model, function of the n-dimensional atmospheric state vector $\mathbf{x}$, whose components represent the unknown profile at altitudes $z = z_j$, $j = 1, \ldots, n$. The Tikhonov solution is the state vector $\mathbf{x}_t$ minimizing the following cost function:

$$\xi^2 = \left(\mathbf{y}-\mathbf{f}(\mathbf{x})\right)^T \mathbf{S}_y^{-1}\left(\mathbf{y}-\mathbf{f}(\mathbf{x})\right) + \left(\mathbf{x}_s-\mathbf{x}\right)^T \mathbf{L}^T \Lambda \mathbf{L}\left(\mathbf{x}_s-\mathbf{x}\right) \quad (5.16.1)$$

The first term of the right side of (5.16.1) is referred to as χ^2 and represents the cost function minimized in the least-squares (LS) approach. The vector $\mathbf{x}_s$ is an a-priori estimate of the solution. Since it is usually not easy to have reliable a-priori estimates of the solution we always take $\mathbf{x}_s = 0$, $\mathbf{L}$ is a h x n matrix operator, usually approximating a linear combination of the i-th order vertical derivatives ($i = 0, 1, 2$). The h x h matrix Λ is diagonal, positive semi-definite and drives the strength of the regularization. Note that normally $h < n$. The standard scalar Tikhonov regularization is obtained when $\Lambda = \lambda \mathbf{I}$. Several methods may be used to select the regularization strength through the amplitude of Λ. The IVS method determines a profile of Λ as the result of an optimization process. In the ORM v.8 we apply the regularization a-prsteriori after the convergence of the minimization sequence. As reported in *Ceccherini et al. (2007)* and in *Ridolfi and Sgheri (2009)*, this choice improves the convergence rate. In other words, we first find the minimum of the χ^2 using the Levenberg-Marquardt (LM) approach:

$$\mathbf{x}_{k+1} = \mathbf{x}_k + \left(\mathbf{K}^T\mathbf{S}_y^{-1}\mathbf{K} + \alpha \cdot \mathrm{diag}[\mathbf{K}^T\mathbf{S}_y^{-1}\mathbf{K}]\right)^{-1} \cdot \left[\mathbf{K}^T\mathbf{S}_y^{-1}\left(\mathbf{y}-\mathbf{f}(\mathbf{x}_k)\right)\right] \quad (5.16.2)$$

Let k be the iteration count at convergence, thus $\mathbf{x}_{OE} = \mathbf{x}_{k+1}$ is the unregularized solution. Let $\mathbf{A}_{OE}$ be the averaging kernel of $\mathbf{x}_{OE}$ and $\mathbf{S}_{OE}$ its measurement error covariance matrix. Within the ORM $\mathbf{A}_{OE}$ and $\mathbf{S}_{OE}$ can be calculated with alternative algorithms of different sophistication as explained in *Ceccherini et al.(2007)* and *Ceccherini and Ridolfi (2010)*. The theory explained hereafter does not depend on the method used to infer $\mathbf{A}_{OE}$ and $\mathbf{S}_{OE}$. We can compute the last iterate as the minimizer of (5.16.1) that includes also the regularization term. Thus the regularized solution $\mathbf{x}_\Lambda$ is given by:

$$\mathbf{x}_\Lambda = \mathbf{x}_k + \left(\mathbf{K}^T\mathbf{S}_y^{-1}\mathbf{K} + \alpha \cdot \mathrm{diag}[\mathbf{K}^T\mathbf{S}_y^{-1}\mathbf{K}] + \mathbf{L}^T\Lambda\mathbf{L}\right)^{-1} \cdot \left[\mathbf{K}^T\mathbf{S}_y^{-1}\left(\mathbf{y}-\mathbf{f}(\mathbf{x}_k)\right) - \mathbf{L}^T\Lambda\mathbf{L}\mathbf{x}_k\right] \quad (5.16.3)$$

If we set:

$$\mathbf{D} = \left(\mathbf{K}^T\mathbf{S}_y^{-1}\mathbf{K} + \alpha \cdot \mathrm{diag}[\mathbf{K}^T\mathbf{S}_y^{-1}\mathbf{K}] + \mathbf{L}^T\Lambda\mathbf{L}\right)^{-1} \cdot \left(\mathbf{K}^T\mathbf{S}_y^{-1}\mathbf{K} + \alpha \cdot \mathrm{diag}[\mathbf{K}^T\mathbf{S}_y^{-1}\mathbf{K}]\right) \quad (5.16.4)$$

Then, after a few algebraic manipulations and using (5.16.2), (5.16.3) can be re-written as:

$$\mathbf{x}_\Lambda = \mathbf{D}\mathbf{x}_{OE} \quad (5.16.5)$$

the averaging kernel $\mathbf{A}_\Lambda$ and the covariance matrix $\mathbf{S}_\Lambda$ of $\mathbf{x}_\Lambda$ can be written as:

$$\mathbf{A}_\Lambda = \mathbf{D}\mathbf{A}_{OE} \quad (5.16.6)$$

$$\mathbf{S}_\Lambda = \mathbf{D}\mathbf{S}_{OE}\mathbf{D}^T \quad (5.16.7)$$

To determine the regularization strength Λ the IVS method proceeds as follows. We define a Λ -profile $\lambda(z)$ on a vertical grid so fine that we can consider it a continuous function. We start with a large $\lambda^{(0)}(z) = \lambda_{MAX}$ constant profile and decrease it iteratively until the following requirements are fullled:

$$\left(\mathbf{x}_{\Lambda}^{(l)}-\mathbf{x}_{OE}\right)^{T}\mathbf{S}_{OE}^{-1}\left(\mathbf{x}_{\Lambda}^{(l)}-\mathbf{x}_{OE}\right)\le w_e n \tag{5.16.8}$$

$$v_j\left(\mathbf{x}_{\Lambda}^{(l)}\right)\le w_r\cdot\Delta z_j \qquad \text{with } j = 1, ..., n \tag{5.16.9}$$

Where l is the iteration count, $\mathbf{x}_{\Lambda}^{(l)}$ is the regularized solution calculated from (5.16.5) using $\Lambda_{jj}=\lambda^{(l)}(\tilde{z}_j)$ for j=1, ..., h. $v_j\left(\mathbf{x}_{\Lambda}^{(l)}\right)$ is the vertical resolution calculated at altitude z_j, as the FWHM of the averaging kernels (5.16.6). Condition (5.16.8) ensures that, on average, the regularized profile lays within a fraction w_e of the error bars of the unregularized profile. Condition (5.16.9) guarantees that at any altitude z_j in the retrieval range the vertical resolution is kept smaller than a multiple factor w_r of the vertical step Δz_j of the retrieval grid. w_e and w_r are user-selectable parameters. Fix a threshold λ_{MIN}. Let $J\subset\{1,...,n\}$ the set of indeces of the altitudes z_j for which $\lambda^{(0)}(z_j)>\lambda_{MIN}$ and:

$$\left|\left(\mathbf{x}_{\Lambda}^{(l)}\right)_j-\left(\mathbf{x}_{OE}\right)_j\right|>w_e\cdot\sqrt{\left(S_{OE}\right)_{jj}} \text{ or} \tag{5.16.10}$$

$$v_j\left(\mathbf{x}_{\Lambda}^{(l)}\right)>w_r\cdot\Delta z_j \tag{5.16.11}$$

If the requirements (5.16.8) and (5.16.9) are not met J is not empty and we decrease $\lambda^{(l)}(z)$. The decreased profile $\lambda^{(l+1)}(z)$ is calculated as:

$$\lambda^{(l+1)}(z)=\left[\prod_{j\in J}T\left(z-z_j,\delta_j^{-},\delta_j^{+}\right)\right]\cdot\lambda^{(l)}(z). \tag{5.16.12}$$

Where T is the triangular shaped function defined as:

$$T\left(z-z_j,\delta_j^{-},\delta_j^{+}\right)=\begin{cases}1 & \text{if } z<\delta^{-} \text{ or } z>\delta^{+},\\ r+\dfrac{1-r}{\delta^{-}}|z| & \text{if } \delta^{-}\le z\le 0,\\ r+\dfrac{1-r}{\delta^{+}}|z| & \text{if } 0\le z\le\delta^{+},\end{cases} \tag{5.16.13}$$

and $0 < r < 1$, $\delta^{+},\delta^{-}>0$ are constants. Note that $\lambda^{(l+1)}(z)<\lambda^{(l+1)}(z)$ if and only if $z\in\left(z_j-\delta_j^{-},z_j+\delta_j^{+}\right)$ for some $j\in J$. The parameter r drives the speed of the attenuation of the Λ-profile, in our implementation we used r = 0.99. Furthermore we set $\delta_j^{-}=z_{j-3}-z_j$, $\delta_j^{+}=z_j-z_{j+3}$ on the basis of the following considerations. The $\mathbf{x}_{\Lambda}$ profile is obtained from $\mathbf{x}_{OE}$ via the formula (5.16.5). For any standard choice of $\mathbf{L}$, $\mathbf{L}^T\Lambda\mathbf{L}$ is at most a pentadiagonal matrix. In our case we use $\mathbf{L}=\mathbf{L}_2$ (the discrete second derivative operator), therefore $\mathbf{L}^T\Lambda\mathbf{L}$ is pentadiagonal. Moreover the

matrix $\mathbf{K}^T\mathbf{S}_y^{-1}\mathbf{K}$ tends to be diagonally dominant, therefore the influence of Λ_{jj} is mostly localized in the altitude range $z_j \in \left(z_j - 3\Delta z_j, z_j + 3\Delta z_j\right)$.

With its self-adaptability and altitude-dependence, also in the difficult cases of profiles rapidly varying with altitude, the IVS method ensures the strongest possible regularization permitted by the parameter w_e, without degrading the vertical resolution beyond a pre-defined bound w_r. Tests of the performance of developed method and further implementation details are provided in *Ridolfi and Sgheri (2011)* and in *Ridolfi and Sgheri (2011b)*.

5.16 Cloud filtering

Scattering and absorption of radiation by clouds is not modelled by the ORM (all versions). For this reason, to preserve the quality of retrieved profiles also in the presence of clouds, measurements affected by clouds are filtered out before Level 2 processing. This filtering is done by checking a so called *Cloud Index* (CI) against a threshold value. An ideal cloud index should be sensitive only to the presence of clouds in the line of sight of the instrument, while it should be mostly independent on the tangent height of the measurement and on the atmospheric state, in terms of temperature and gas vertical distributions.

In MIPAS Level 2 processing, the CI is defined, for each measured limb emission spectrum, as the ratio between the integrated radiance in two spectral intervals with different characteristics. The first interval, 788-796 cm^{-1}, is dominated by carbon dioxide emission and weak ozone emissions. The second interval, 832-834 cm^{-1}, is dominated by aerosol and cloud emissions, some weak ozone and CFC11 emission lines, and is relatively insensitive to temperature. The CI value, therefore, should depend weakly on the tangent height of the limb measurements and is expected to become smaller in the presence of a cloud in the line of sight of the instrument. Compared to the clear sky case, the CI reduction is expected to be directly linked to the cloud optical thickness: the greater the cloud optical thickness the greater will be the observed CI reduction. Unfortunately, the real behaviour of the defined CI is not ideal because, also in clear-sky conditions, the CI values show a dependence on altitude and atmospheric state. Figure 5.16.1 shows the actual CI profiles (thin lines with coloured symbols) obtained from the measurements of MIPAS orbit 33153 acquired on 3 July 2008.

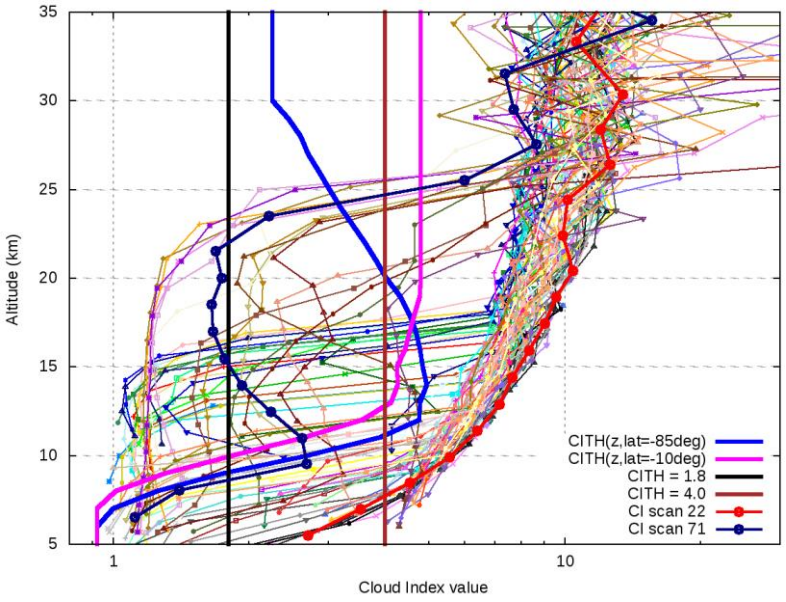

Figure 5.16.1: Cloud Index profiles (lines with symbols) for MIPAS measurements acquired during the ENVISAT orbit 33153 from 7 July 2008. Thick solid lines show some threshold values used for cloud detection (see the text).

The bulk of clustered CI profiles shown in Fig. 5.16.1 corresponds to clear-sky conditions. Particularly, the thick red line with symbols represents the CI profile of scan 22 that apparently corresponds to clear-sky, and is going down to 6 km tangent height. The thick (dark) blue line with symbols represents the CI profile of scan 71 acquired at Antarctic latitudes. This CI profile shows a marked reduction already at 23 km tangent height, corresponding to a Polar Stratospheric Cloud (PSC) entering the FOV of the instrument. In general, we see that the CI values change significantly with the tangent height of the measurements. Moreover, above 25 or 30 km, the measurement noise has a significant impact on the cloud index calculation. These features make it hard to detect clouds by comparing the CI with a single threshold independent of altitude.
The thick vertical black line shown in Fig. 5.16.1 represents the (height independent) CI-threshold of 1.8 used for cloud detection in MIPAS Level 2 processings up to Version 7. With this choice, several sweeps affected by high-clouds (namely PSCs) are classified as clear-sky and used in the retrievals, causing outliers in the retrieved VMR profiles, especially of H_2O, NO_2 and N_2O_5. In a first attempt we tried to solve the problem by using the more conservative CI-threshold of 4 (thick vertical brown line in Fig. 5.16.1), already adopted at KIT (Karlsruhe) for the scientific KOPRAFIT retrievals. This choice mostly solves the problem of undetected high clouds, however, many clear sky measurements with tangent heights below 10 km are erroneously flagged as cloudy. In the ORM version 8, altitude- and latitude- dependent CI-threshold profiles are employed. The used CI-threshold profiles are obtained multiplying by 0.8 the profiles established by Reinhold Spang in the so called “MIPAS clouds” study (ESA contract no. 400011677/16/NL/LvH, lead by the Forschungszentrum Juelich GmbH). Figure 5.16.1 shows two specific CI-threshold profiles used by the ORM v.8 at the two latitudes of 85°S (thick blue line) and 10°S (thick magenta line). As we can see, these altitude- and latitude- dependent CI-thresholds permit to avoid high-clouds and, at the same time, do not represent a too conservative filter for the lowest measurements of the MIPAS scan.

6 - Mathematical Optimisations

In this section we describe the different mathematical optimisations implemented in the optimised forward-retrieval model (OFM/ORM): in particular, the advantages and disadvantages of the different options are reviewed and the preferred option is identified.
The parameters defining the different optimisations, like parameters dealing with layering, have been determined on the basis of intercomparisons with the RFM.

These are the guidelines used in the search for possible mathematical optimisations:

- Research of feasibility of performing analytically integrals and derivatives.
- When this is not possible, in case of numerical integrals, minimisation of the number of the intervals over which complex expression are evaluated.
- In case of very time consuming calculations, study of feasibility of using pre-tabulated data and interpolation schemes.
- Research and exploitation of the symmetries that can reduce the number of calculations.
- Study of the possibility of storing quantities that are used more than once.

Whenever possible, for each of the implemented optimisations we identify:

- physical aspect
- different options for modelling it
- selected choice
- reason for choice
- how the optimisation is implemented into the program
- performed validations

Since the calculation of the synthetic spectra and of their Jacobian matrix used in the LM algorithm are by far the most time consuming parts of the retrieval code, the optimisations concern mainly the forward model and its interfaces with the retrieval module.

6.1 Radiative Transfer integral and use of Curtis-Godson mean values

Forward model consists essentially of the calculation of Radiative Transfer integral (eq. (4.4.5)), a curvilinear integral along the line of sight. Optimising the forward model means to optimise the calculation of this integral. An analytical expression of absorption cross-sections as a function of pressure and temperature is not available, so the integral must be solved numerically, using a discretisation, i.e. by calculating the individual elementary contributions and summing them up. This implies that atmosphere has to be segmented or “discretized”. Two main optimisations can be implemented:

- the first refers to the type of segmentation: since spectra corresponding to different lines of sight have to be calculated, a segmentation that can be used to simulate all the limb views of a scan avoids to repeat several times the same calculations;
- the second refers to the length of the segments and consequently to the number of segments to be considered: the coarser is the segmentation the faster is the forward model.

In this section we describe two different methods for building the segmentation, as well as different possibilities to calculate the contribution of individual segments (or paths) to the whole integral.

Integration variable
If the arc parameter *s*, i.e. the co-ordinate along the line of sight, is used as integration variable, the optical path is subdivided into intervals of equal length, so that the jump in altitude, at each increment of *s* decreases when approaching the tangent point: in this way the atmosphere is sampled with greater detail near the tangent point, from where most of the signal originates. The disadvantage of this method is that a different segmentation is necessary for each limb view, thus the results from one limb view cannot be used for the others.
On the contrary, if the altitude *z* is used as integration variable, the atmosphere can be divided in a pre-defined number of layers, that are valid for the calculation of all limb views. This layering can be critical near the tangent altitude if the layering is not sufficiently fine, but it has an important advantage: the same layering can be used for the calculation of all limb views of the scan, allowing to save a great amount of calculations if the atmosphere is assumed horizontally homogeneous. As it will be clear from the following sections, this characteristic looses its importance when the layers are not considered homogeneous and a latitudinal gradient is introduced. Despite of this loss, for continuity with the earlier ORM versions, also the ORM v.8 adopts a vertical layering of the atmosphere.
The atmosphere is subdivided in a set of layers, whose thickness is defined according to the criteria discussed in section 6.1.1.

Layers versus levels in the discretisation of the unknown profiles
The unknown profiles (temperature and VMR) must be represented by discrete values corresponding to a finite set of altitudes. The altitude distribution that corresponds to these discrete values can be obtained either with the *layer approach* (the profile is constant between contiguous altitudes) or with the *level approach* (the profile changes linearly between contiguous altitudes). The level approach has been chosen as baseline for OFM / ORM algorithms: the reason for this choice is simply that, from the physics point of view, continuous profiles are always considered more realistic than step-like profiles.

Planarity of MIPAS observations and polar angle
In the ORM v.8, all MIPAS measured limb scans of a given orbit are assumed to lay in the orbit plane. This is not exactly true in the Polar regions where the instrument pointing azimuth angle is usually slightly steered from the rear-looking direction to the side-looking direction, in order to cover higher latitudes that otherwise would not be covered due to the orbit inclination. In the studies related to the GEOFIT development (Carlotti et al, 2001), however, this assumption was proven to introduce negligibly small inaccuracies. The planarity hypothesis permits to use a 2-dimensional ray-tracing instead of a 3-dimensional one, thus each point of the instrument line of sight is identified by only two coordinates: its altitude *z* (or equivalently its distance *r* from the Earth's center) and the polar angle θ, measured starting from the tangent point of the considered sweep.

Calculation of the transmission of each path in a layer
In order to compute the radiative transfer integral, the transmission of each path within the layers must be computed. Two options have been analysed for this purpose.

The first option consists in using interpolated cross-sections from the values computed at the boundaries of the layer: this method requires layers thinner than 1km, because of the critical dependence of cross-sections on temperature and pressure. With this method, analytical calculation of the radiative transfer integral is possible only in the absence of refraction. Using the refraction model illustrated in Sect. 5.5 prevents the analytical integration and makes this approach much less attractive.

The second option consists in the calculation of path transmission by computing the cross-sections at some values of pressure and temperature representative of the layer. These quantities can be either the mean pressure and temperature of the layer, or the Curtis-Godson (CG) equivalent values. These latter allow using a coarser atmospheric layering as they are gas-density weighted averages computed along the ray path within each layer. Namely, the CG Equivalent pressures and temperatures are given by:

$$p^{e}_{m,l,g} = \frac{\int_{z_{l-1}}^{z_l} p(z,\theta)\cdot x_m^{VMR}(z,\theta)\cdot\eta\left(p(z,\theta),T(z,\theta)\right)\cdot\frac{ds_g}{dz}\cdot dz}{\int_{z_{l-1}}^{z_l} x_m^{VMR}(z,\theta)\cdot\eta\left(p(z,\theta),T(z,\theta)\right)\cdot\frac{ds_g}{dz}\cdot dz}, \qquad (6.1.1)$$

$$T^{e}_{m,l,g} = \frac{\int_{z_{l-1}}^{z_l} T(z,\theta)\cdot x_m^{VMR}(z,\theta)\cdot\eta\left(p(z,\theta),T(z,\theta)\right)\cdot\frac{ds_g}{dz}\cdot dz}{\int_{z_{l-1}}^{z_l} x_m^{VMR}(z,\theta)\cdot\eta\left(p(z,\theta),T(z,\theta)\right)\cdot\frac{ds_g}{dz}\cdot dz} \qquad (6.1.2)$$

Where: z is the altitude, z_l and z_{l-1} are the heights of the layer boundaries, θ is the polar angle, $x_m^{VMR}(z,\theta)$ is the VMR of the m-th gas, s_g is the line of sight dependent on geometry, $\eta\left(p(z,\theta),T(z,\theta)\right)$ is the air number density. The normalisation factor of these expressions is the gas column $C_{m,l,g}$ for the considered path:

$$C_{m,l,g} = \int_{z_{l-1}}^{z_l} x_m^{VMR}(z,\theta)\cdot\eta\left(p(z,\theta),T(z,\theta)\right)\cdot\frac{ds_g}{dz}\cdot dz\,. \qquad (6.1.3)$$

Integrals (6.1.1), (6.1.2), (6.1.3) are solved taking into account refraction, that impacts the term ds_g/dz (see section 5.5). We have verified that, as expected, using CG pressures and temperatures, instead of mean values, allows for a coarser stratification of the atmosphere. A complication of this method is that, in principle, the CG equivalent pressures and temperatures are specific for each gas and each ray-path within the layers. In particular, their dependence on the gas (that is useful when calculating the analytical derivatives with respect to the VMR) implies that cross-sections for all the gases need to be stored into the computer RAM memory (see Sect. 6.2.2), thus requiring a large amount of memory. On the contrary, the use of mean temperature and pressure, that do not depend neither on the molecules nor on the geometry, requires a finer layering and consequently more computing time.

We have to underline that the calculation of CG equivalent pressures and temperatures, as well as gas columns, is not a time consuming part of forward model calculation, and no optimisation effort is worthwhile.

Using equivalent pressure and temperature, the transmission τ of the path l relating to the limb geometry g, due to all the gases, is given by:

$$\tau_{\sigma,l,g} = \exp\left(-\sum_m \int_{z_{l-1}}^{z_l} k_\sigma\left(p(z,\theta),T(z,\theta)\right)\cdot x_m^{VMR}(z,\theta)\cdot\eta\left(p(z,\theta),T(z,\theta)\right)\cdot\frac{ds_g}{dz}\cdot dz \right) \approx$$

$$\approx \exp\left(-\sum_m k_{\sigma,l,g}\left(p_{l,g}^e,T_{l,g}^e\right)\cdot \int_{z_{l-1}}^{z_l} x_m^{VMR}(z,\theta)\cdot\eta\left(p(z,\theta),T(z,\theta)\right)\cdot\frac{ds_g}{dz}\cdot dz \right) = \quad (6.1.4)$$

$$= \exp\left(-\sum_m k_{\sigma,l,g}\left(p_{l,g}^e,T_{l,g}^e\right)\cdot C_{m,l,g} \right)$$

Using this result, expression (4.4.5) can be rewritten as:

$$S_{\sigma,g} = \sum_{l=1}^{N} B_\sigma\left(T_{l,g}^{e\,\mathrm{main}}(z)\right)\cdot\left(1-\tau_{\sigma,l,g}\right)\cdot\prod_{j=1}^{l-1}\tau_{\sigma,j,g} \quad (6.1.5)$$

N represents the number of paths defined by the intersection of the line of sight with the levels used for atmospheric layering. N is equal to twice the number of layers minus one. The source function B_σ, that has to be calculated for each frequency of the considered microwindow and each layer, does not depend on the gas, while the equivalent temperature of the layer is gas-dependent.

If the retrieval of a single gas VMR or of Temperature is carried-out, we can assume each selected microwindow as characterised mainly by emission lines of the gas being retrieved or of CO_2 in the case of Temperature retrieval. Non-retrieved gases may be assumed to contribute very little to the total spectrum of the MWs. Therefore, we choose to calculate the source function at the CG temperature of the main (retrieved) gas contributing to the spectrum in the considered microwindows.
If the VMR profiles of several gases are retrieved simultaneously or, if pT retrieval is simoultaneous with the retrieval of one or more gases, several gases may contribute significantly to the spectrum of each considered MW in the retrieval. In this case the ORM v.8 offers two alternative possibilities selectable via a setting parameter:

1. Calculation of the Planck function at the CG temperature of air (obtained assuming a constant VMR in Eq. 6.1.2), or
2. Calculation of the Planck function at a temperature obtained as the weighted average of the CG temperatures of the gases contributing to the spectrum in the considered MWs. The weights being provided by the inverse of the VMRs of the individual gases.

Currently, ESA Level 2 processings do not exploit the Multi-Target Retrieval functionality of the ORM v.8. For this reason, no tests have been carried-out so far to decide which of the two approaches 1. or 2. is the most accurate.

6.1.1 Layering of the atmosphere

On the basis of the above choices, the atmosphere is modelled using layers whose boundaries are marked by levels at fixed pressure. Within the levels the temperature and the VMR profiles are assumed to vary linearly with the altitude, while the behaviour of pressure profile is assumed exponential with altitude. Pressure and temperature profiles obey to the hydrostatic equilibrium law. Either altitude or pressure can be considered the independent variable at this stage, provided that we use the correct interpolation rules for dependent variables. While setting-up the layering of the atmosphere the chosen independent variable is the altitude; this is because the visual inspection of the generated levels is easier. The algorithm which builds the levels proceeds as follows:

- Step 1:
  A set of levels corresponding to the tangent altitudes of the spectra we want to simulate is set-up; radiative transfer calculation is indeed simpler if the tangent altitudes are at the boundary of one layer. Since we want to take into account the FOV effect using interpolation of the spectra in the altitude domain (see Sect. 6.6), not only the spectra whose tangent altitudes correspond to measurements have to be simulated, but 'extra' spectra are needed as well. In the case of p,T retrieval, the simulated spectra are the ones corresponding to the measurements, plus one extra spectrum located below the lowest measurement and one extra spectrum located above the highest measurement. The distance between the tangent altitude of each extra spectrum and the tangent altitude of the nearby measurement is kept equal to half of the FOV width.
  Tests have shown that the explained set of simulations does not allow performing an accurate interpolation of the spectra when the VMR of the main gas of the retrieval has a large gradient as at low altitudes in the case of H_2O, (see Sect. 6.6). In these cases further intermediate simulations are included in the set.

- Step 2:
  Each couple of adjacent levels generated at step 1 is considered. We check whether, moving from one level to the other, the following two conditions are satisfied:

  1. the variation of the temperature is below a fixed threshold. Two different thresholds are used depending on the altitude of the first considered level, a more conservative threshold is used at low altitudes.
  2. The variation of the Voigt half-width of a reference line is below a fixed threshold.

  If both these conditions are satisfied then we consider the next couple of levels generated at step 1 and redo checks 1 and 2. If one or both the above conditions are not satisfied, then we insert new evenly-spaced levels within the couple of considered levels, until conditions 1 and 2 are satisfied for all the new sub-levels.

  After this step is completed, it turns out that the altitude range in which the tangent altitudes of the simulated geometries lie, is sub-divided into layers of suitable thickness, whose boundaries are marked by the levels.

- Step 3:
  Above the tangent altitude of the highest simulated spectrum a set of levels is determined which divide the atmosphere into layers for the radiative transfer calculation.
  Starting from the tangent altitude of the highest simulated spectrum,
  $^{(*)}$ a user-defined guess increment Δz is used to build next level, then, conditions 1. and 2. (used at the previous step) are checked and:
  $\Rightarrow$ if the two conditions are both satisfied then the guess level is accepted and the algorithm proceeds to $^{(*)}$
  $\Rightarrow$ else, the guess increment Δz is reduced using an appropriate factor and the conditions 1. and 2. are checked again.
  It is clear that after this procedure the maximum allowed thickness of the layers is equal to the initial value of Δz that is controlled by the user.
  The new levels are added to those obtained in step 2.

  The user-defined parameters that control the layering of the atmosphere are subject of tuning: because of the speed requirements, in operational conditions, the parameters that allow a more coarse layering without significantly affecting the accuracy of the computed spectra have to be

adopted. Tests have been carried-out using some microwindows involved in p,T retrieval. The results are shown in Table 6.1; the spectra computed using layerings 2 and 3 have been compared with spectra obtained using a really conservative layering (reference layering 1). It turns out that layering 2 represents a suitable compromise between accuracy and number of levels.

	Layering 1 (reference)	Layering 2	Layering 3
Low altitude T threshold (K)	1.5 K	5 K	25
Hig altitude T threshold (K)	5 K	15 K	35
Altitude where the threshold is changed (km)	56	56	56
Max. HW-variation	1.05	1.5	2.5
Max. thickness of the layers (km)	10	10	10
N. of obtained levels	146	42	22
Max. difference		NESR / 5	NESR/0.6
Average difference		NESR / 60	NESR/17

Table 6.1: Tuning of the parameters used for the layering of the atmosphere. The tests have been performed considering 7 microwindows of p,T retrieval. The upper limit of the atmosphere has been set equal to 100 km.

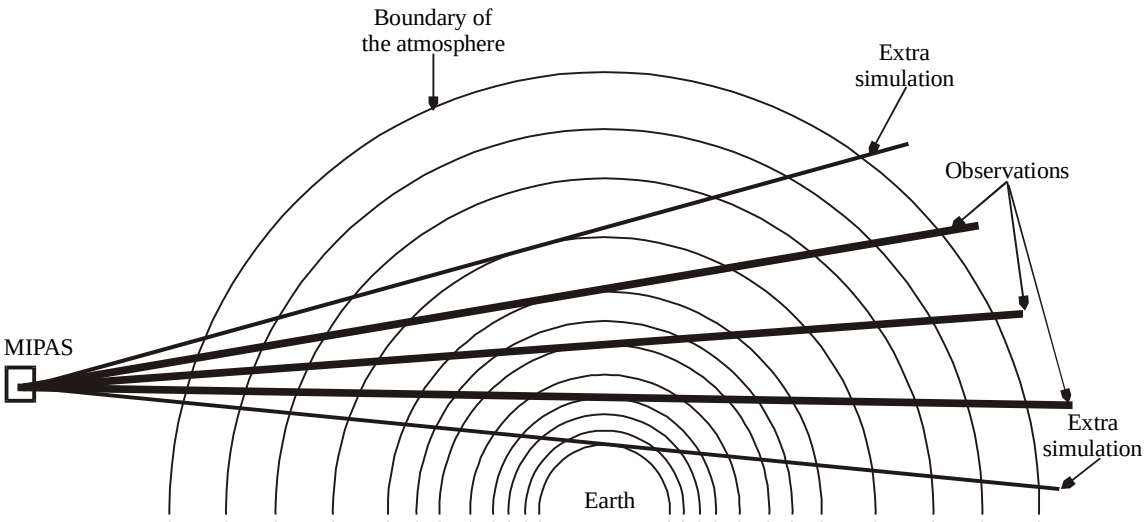

Figure 6.1: Sketch of the layering of the atmosphere.

6.2 Secant law approximation for the calculation of Curtis-Godson quantities and definition of paths (not used in the ORM v.8)

Secant law approximation consists in the calculation of CG quantities as if the layer was flat and the line of sight a straight line. In this case the secant law applies and the same values of p^e and T^e are obtained independently of the angle between the line of sight and the vertical direction.
In Fig. 6.2 the percent deviation of p^e and T^e from the values calculated in the case of vertical penetration are reported. These tests were done for ozone using a standard atmosphere, 3 km and 1 km thick layers and tangent altitude of 8 km. No significant changes occur at different tangent altitudes.

Secant law approximation causes only very small errors at all altitudes, except for the tangent layer and the layer above. According to this result, it is sufficient to calculate the values of p^e and T^e for all the layers of the lowest limb view, and only for the lowest layers of all the other limb views. If we associate a *path* with each combination of layer and geometry of the complete limb-scanning sequence, we can say that the values of p^e and T^e do not have to be calculated for all the different paths. Figure 6.3 shows a scheme of the paths for which $p^e$and T^e are to be calculated. The atmospheric levels used for the simulations are represented by the columns of the table, while the rowss of the table represent the limb views to be simulated. The grey cells represent all the possible paths. The grey cells marked with either 'X' or 'x' are the paths for which a customised calculation of equivalent pressure and temperature is needed. In the following these particular p^e - T^e couples will be called 'Implemented Atmospheric Pressures and Temperatures', IAPTs. For the paths corresponding to the grey cells without either 'X' or 'x', values of the top row are used.
The number of extra-paths to be calculated for each limb view is an input parameter of the retrieval program, but the current baseline is to re-compute only the IAPTs relative to the tangent layer. Tests have shown that this is a good approximation, since the tangent layer is significantly thinner than the value of 3 km explored in the test of Fig. 6.2 (b).

Up to Version 7 of the ORM the use of IAPTs was a crucial optimisation, not only because less equivalent pressures and temperatures had to be calculated (the calculation of CG quantities themselves is not time consuming), but mainly because less cross-sections (corresponding to the p^e,T^e pairs) had to be calculated (see Table 6.2) and stored. The saving in number of calculations was significant: without using secant law approximation, the number of p^e,T^e pairs for which cross-sections have to be calculated, that is the number of total paths, is given by half of the product of the number of the layers (about 40) in each geometry times the number of geometries used for the simulations (18), that is 360 paths; on the contrary, the number of the IAPTs is given by the number of paths for the lowest geometry (about 40) plus the number of extra-paths (about 2) times the number of remaining geometries (17), that is about 74.

Note that, since the lines of sight of different limb views intersect a given layer for different values of the polar coordinate θ, the secant law approximation makes sense only if the atmospheric layers are assumed homogeneous, i.e. if pressure, temperature and VMR profiles do not depend on the polar coordinate θ. In the ORM v.8, these profiles are modelled using also an horizontal gradient, therefore they are dependent on θ, and the secant law could not be exploited.

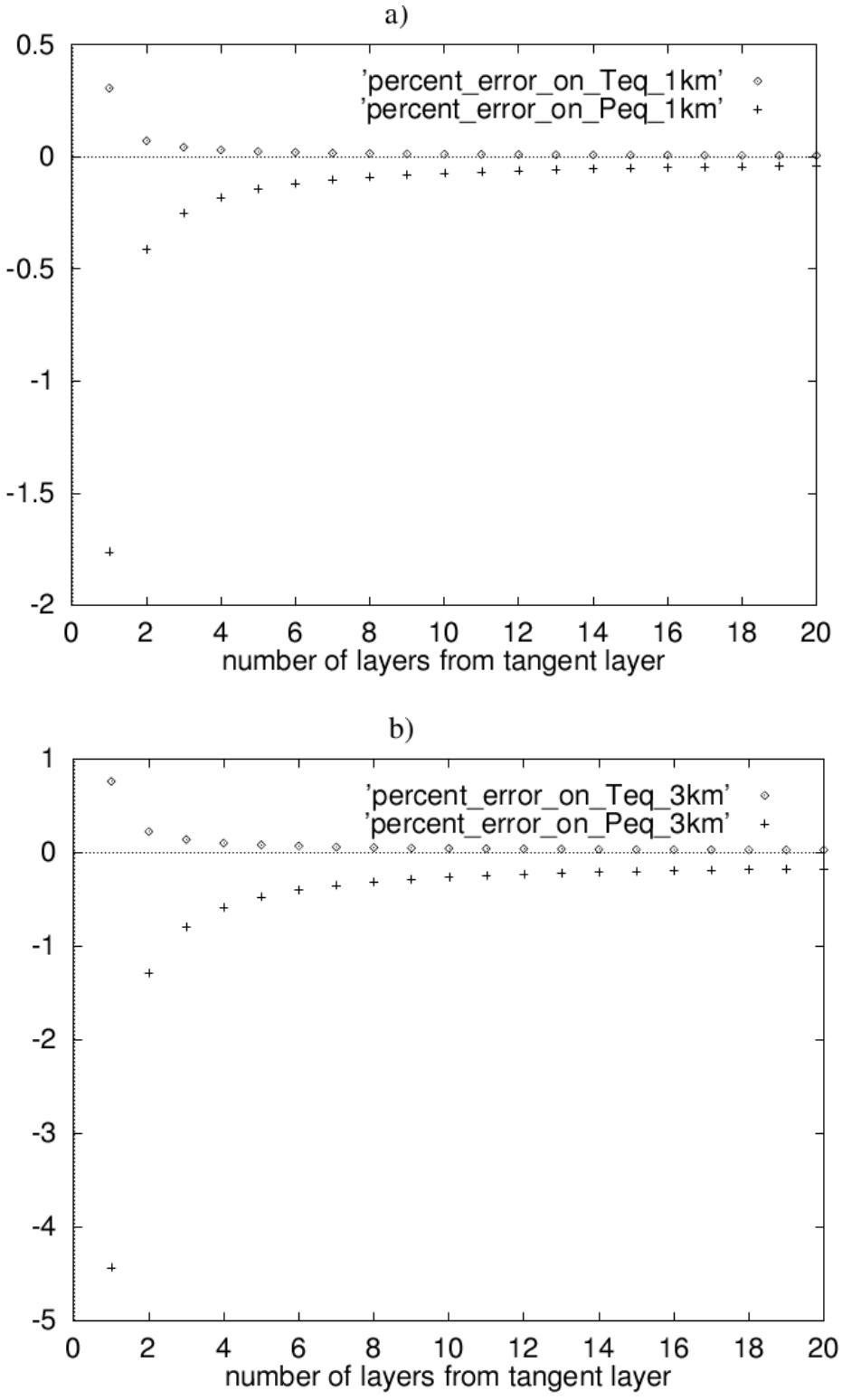

Fig. 6.2 The percentage deviation of equivalent temperature (squares) and equivalent pressure (crosses) from that in the case of vertical penetration are reported for the different layers, starting from the tangent layer. a) Layers thickness is about 1 km; b) Layers thickness is about 3 km. Test performed for a tangent altitude of 8 km.

Fig.6.3 **TABLE of PATHS**

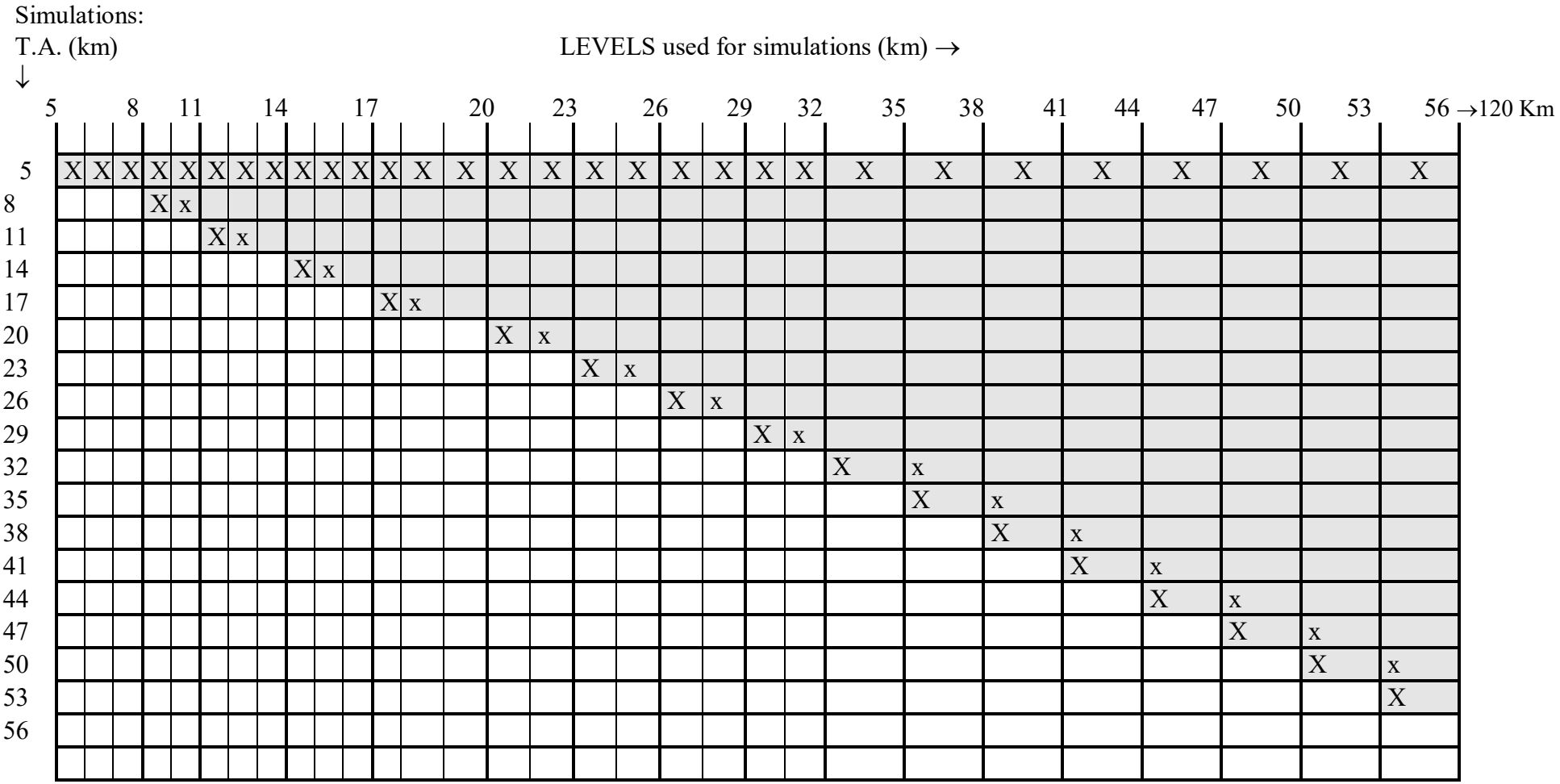

6.2.2 Sequence of the operations

ORM Versions up to 7

The fact that only a limited number of layers for each geometry need a customised calculation of equivalent pressure and temperature was the basis of the structure of the optimised forward model included in the ORM up to Version 7. After setting-up the layering of the atmosphere (see section 6.1) the matrix of the IAPT numbers wass built. This matrix associates with each path a number that refers to the corresponding IAPT.

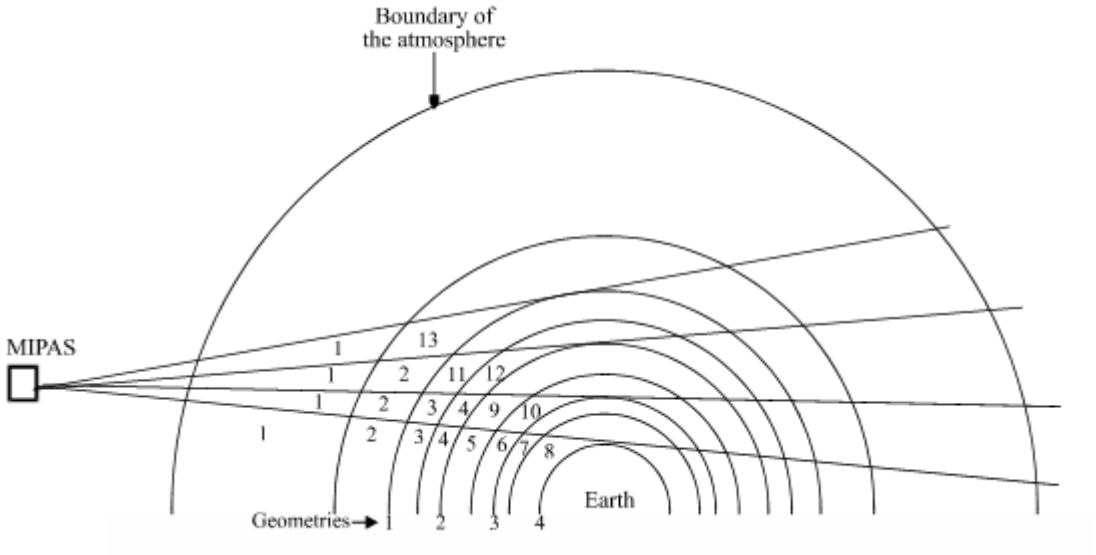

Fig. 6.4 Example of the association of the appropriate IAPT to each path.

We start from the line of sight to which the lowest tangent altitude corresponds and a progressive IAPT number is associated to each layer. For all the other geometries a new IAPT number is assigned to the tangent layer and in some cases to others layers above it, all the other layers have the same IAPT number as the lowest geometry. The matrix below refers to the example of figure 6.4:

$$\begin{pmatrix} 13 & & & & & & & \\ 1 & 2 & 1 & 1 & 2 & & & \\ 1 & 2 & 3 & 4 & 9 & 10 & & \\ 1 & 2 & 3 & 4 & 5 & 6 & 7 & 8 \end{pmatrix}$$

At this point the calculation of ray-tracing is performed and all the IAPTs are computed, while the gas columns are calculated for all the paths. For each of the selected microwindows the computation of the cross-sections is performed for the different IAPTs (some possible optimisations are discussed in section 6.3, 6.8, 6.9, 6.10). The spectra of all the limb scan are calculated accounting for the contribution of all the layers (see Sect. 6.4). Finally, the convolution of the spectrum with the apodised instrument line-shape (AILS), and the convolution with the function that describes FOV is performed (see Sect. 6.6).

ORM Version 8

In the ORM Version 8 the secant law approximation is not applied, therefore CG equivalent quantities and absorption cross-sections of the gases are computed for all the paths identified by the intersection of

the lines of sight of all the limb views with the atmospheric layers. The sequence of operations remains the same as for the earlier ORM versions.

6.3 Interpolation of cross sections for different geometries

We have explained in the previous section that the equivalent temperature and pressure of each layer remain nearly constant for the different geometries of a limb scan. As was shown in Figure 6.2 the differences become larger the closer we are to the tangent layer and are the largest for the tangent layer itself. The absorption cross sections do not need to be calculated for all paths, but only for the IAPTs (see Sect. 6.2).
After calculating the absorption cross sections for all the IAPTs of the lowest geometry of the limb scan, in order to calculate the cross sections for the different IAPTs of the other geometries we have to distinguish between two kinds of IAPTs, either the IAPTs corresponding to the paths indicated with 'X' in Figure 6.3, or the IAPTs corresponding to the paths indicated with 'x'.

1. IAPTs corresponding to paths with 'x': the cross sections can be interpolated (in pressure) between the cross sections of the lowest geometry.
2. IAPTs corresponding to paths with 'X' in geometries different from the lowest one: new calculation of the absorption cross sections for the equivalent temperature and pressure of the new path is done.

We performed calculations in order to test the feasibility of case 1. Since the Lorentz line wings are in first approximation proportional to the pressure we used this parameter for the interpolation value (i.e. we interpolated the cross sections of the lowest layer to the equivalent pressure of the new path). We decided to use linear interpolation. Tests with higher order interpolation gave often better results but failed in those cases where there was an inversion of the absorption cross section profile with altitude.
In these tests the maximum differences of the cross sections between recalculation and linear interpolation was 2% for the tangent layer, 0.3% for the layer above the tangent layer and 0.1% for the second layer above the tangent layer (layer thickness 3 km). The reason for this decreasing errors results obviously from the fact that the secant law approximation becomes more and more valid when moving away from the tangent layer.
Table 6.2 shows the results of test calculations which were performed using 6 microwindows for p-T retrieval. It is obvious that no recalculations of the cross sections for the tangent layer (1st column) or interpolation for the tangent layer (2nd column) results in maximum errors larger than NESR/5. Recalculation of the tangent layer (3rd column) leads to acceptable maximum errors of NESR/21 and recalculation of the tangent and interpolation of the layer above the tangent layer to NESR/70. As a baseline we recalculate the absorption cross sections only for the tangent layer. Since the code is structured in order to be very flexible in handling these three different cases higher accuracy can be obtained only by changing one input parameter.

Note that this optimization of cross-section interpolation is useful only if cross-sections are computed with the line-by-line approach. When the use of cross-section LookUp-Tables (LUTs) is enabled (see Sect. 6.11), the individual cross-setions are all obtained by interpolation in the p,T domain, within pre-tabulated cross-section values.

no. of recalculations 'X'	0	0	1	1	2
no. of interpolations 'x'	0	1	0	1	0
max. difference	NESR/0.9	NESR/4.4	NESR/21	NESR/70	NESR/70
average difference	NESR/3.7	NESR/20	NESR/79	NESR/ 114	NESR/ 330

Table 6.2: Maximum and average differences in NESR fraction, between a reference simulation and simulations made with different methods of cross-sections calculation for the geometries above the lowest one for 6 selected p-T microwindows.

6.4 Calculation of the spectrum: spherical symmetries (not used in the ORM v.8)

The use of the altitude as the integration variable and the layering of the atmosphere that results from this choice, together with the hypothesis of homogeneity of the atmosphere with latitude, allows to exploit some symmetries and reduce the number of computations.
In fact, the line of sight crosses each layer twice, in a symmetrical position with respect to tangent layer. The symmetry derives from the fact that the atmospheric layers are spherical, and dependence on latitude is neglected (section 5.3).
The two contributions of the same layer to the total intensity reaching the observer are characterised by the same emission, but different transmissions.
Since the cross-sections for all the layers have been previously calculated, while the first contribution is calculated, also the second one is taken in account.
So, instead of calculating the integral for all the altitude intervals in which the line of sight intersects the different layers, that are twice the number of layers, it is possible to calculate the integral only for all the layers.
Expression (6.1.5) is modified into the following expression:

$$S_{\sigma,g} = \sum_{l=1}^{L_l} B_\sigma\left(T_l^e\right)\cdot\left(1-\tau_{\sigma,l,g}\right)\cdot\left(1+\tau_{\sigma,l,g}\cdot\prod_{j=l+1}^{L_l}\tau_{\sigma,j,g}^2\right)\cdot\prod_{j=1}^{l-1}\tau_{\sigma,j,g}\ , \qquad (6.4.1)$$

with $\prod_{j}^{j-1}\tau_{\sigma,j,g} \equiv 1$.

L_l is the total number of the layers (in order to maintain the symmetry, the tangent layer is also divided into two parts, symmetrical with respect to tangent point).

In the ORM v.8, the symmetry of the radiative transfer about the tangent point of the limb views is broken due to the existence of horizontal gradients of pressure, temperature and gases VMR. For this reason, in the ORM v.8 the radiative transfer is computed directly using Eq. (6.1.5).

6.5 Use of interpolation for the calculation of Planck function

In order to save computing time, for the calculation of the Planck function B(σ,T) a linear interpolation is used in between the values of this function computed at the edges of the microwindow (MW). The expression for B(σ,T) is given in Eq. (4.4.2). To quantify the error implied by this approximation we carried out the following test. We divided the 500 – 2500 cm^{-1} spectral interval into 5 cm^{-1} sub-intervals, emulating possible MWs that could be used for MIPAS retrievals. For each of these MWs we computed, on a 0.1 cm^{-1} fine grid, the Planck function B(σ,T) with two methods: a) using Eq. (4.4.2) at every frequency grid point and, b) using linear interpolation (in wavenumber) within the values of B(σ,T) computed by Eq. (4.4.2) at the edge wavenumbers of the MW. Figure 6.5 shows, for each of the mentioned MWs, the maximum of the absolute differences between the calculations a) and b). The results of Fig. 6.5 refer to typical (250 K) and extreme (180 and 300 K) temperature values that may be encountered in the atmosphere. As we can see, in the MIPAS wavenumber range the absolute error due to the linear interpolation of the Planck function is always smaller than 0.2 nW / (cm^2 sr cm^{-1}), i.e more than one order of magnitude smaller than the measurement NESR (that is always greater than 4.2 nW / (cm^2 sr cm^{-1})).
While this approximation does not imply a noticeable accuracy degradation, there is a relevant saving in CPU time due to the avoided computation of some thousands of exponential functions (one for each fine frequency grid point) for each microwindow. A test on the simulation of a 0.25 cm^{-1} wide microwindow containing 74 transitions led to a global run time saving of about 10% in the calculation of the limb emission radiance.

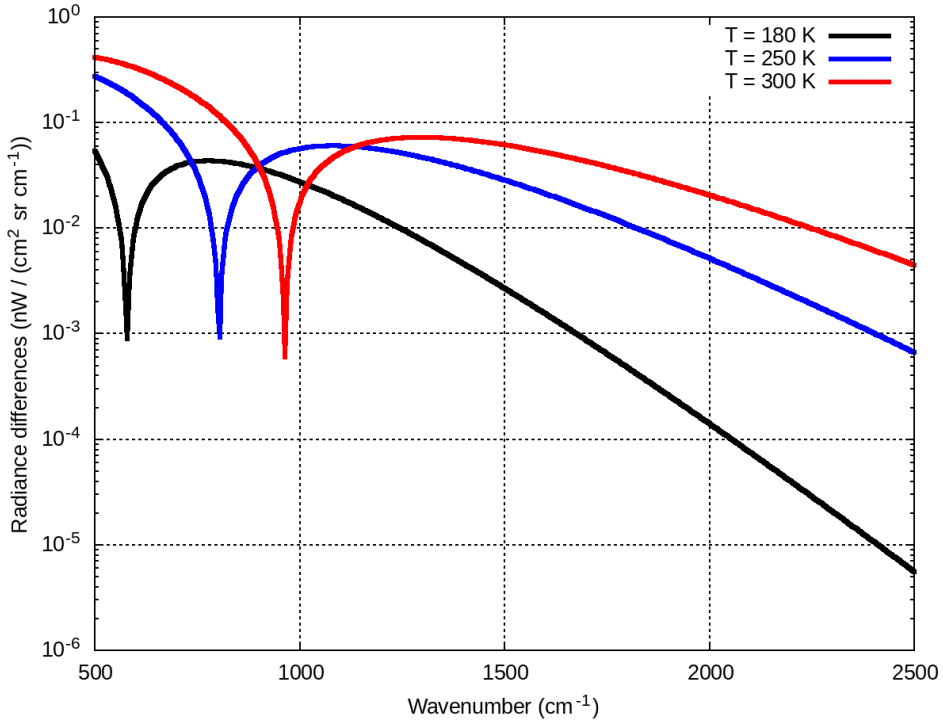

Fig. 6.5: Maximal absolute differences between the direct calculation of the Planck function and its linearly interpolated value within 5 cm^{-1} MWs. These differences are negligible if compared to the NESR, whose values range from 30 nW/(cm^2 sr cm^{-1}) in the region around 800 cm^{-1} to 4.2 nW/(cm^2 sr cm^{-1}) around 2000 cm^{-1}.

6.6 Finite instrument field of view.

The problem of finite field of view is a consequence of the fact that:

- the input diaphragm of the interferometer has non-zero angular size;
- light from an extended source crosses it;
- this source is characterised by a vertical exponential energy distribution.

These factors have two main effects: a modification in the ILS and a modification in the 'effective' tangent altitude of the spectrum.
The change of the ILS in the specific case of MIPAS rectangular aperture, with a vertical exponential energy distribution across it, have been analysed by L. Debouille and G. Roland (1995): they found that the use of a rectangular aperture creates a small asymmetry in the ILS, but even the strongest exponential energy distribution across the field of view does not significantly modify the ILS with respect to that calculated in the case of homogenous source.
The other effect is that the exponential distribution introduces a non-negligible difference between the geometrical tangent altitude, defined by the centre of the input diaphragm, and the 'spectral tangent height', that is the position, along the vertical scale, of the mean emitted signal.
Delbouille and Roland (1995) found that corrections (dependent on the molecule) up to nearly 1 km have to be applied to tangent altitude when the rate of change of the emission is of the order of a factor three per kilometre.
We have verified that, at least at low tangent altitudes, neglecting the field of view effect implies an error in the spectrum larger than NESR.
The antenna pattern of the field of view provided by ESA was initially represented by a spread in the altitude domain *FOV(z)*, independent on the tangent height of the considered sweep, and with the shape of a trapezium with the greater base of about 4 km and the smaller base of about 3 km. Ground characterization measurements on the MIPAS flight module indicated, however, that the MIPAS FOV can be more adequately represented using a piecewise linear shape. A tabulated piecewise distribution is in fact the FOV representation presently adopted in the ORM/OFM.

According to these arguments, the effect of field of view can be taken into account in two different ways:

- by using an equivalent observation geometry,
- by performing, for each spectral frequency, the convolution between the spectrum and the antenna pattern (Sect. 4.4.3):

$$S_{FA}\left(\sigma, z_g\right) = S_A\left(\sigma, p\left(z\right)\right) * FOV\left(z_g, z\right). \qquad (6.6.1)$$

Since the equivalent observation geometry is strongly dependent on the molecule, the second option has been chosen.
The standard method used is, therefore, to perform a numerical convolution with the FOV function after repeating forward model calculations for a number of lines of sight that span a user-defined vertical range around the tangent altitude of the sweep to be simulated.
In order to reduce the number of computations, the following optimisations have been implemented:

- convolution of the high resolution spectra with the apodised instrument line shape, before taking into account FOV effects, in order to operate FOV convolution in the coarse frequency grid, instead of the fine grid.
- interpolation of the spectra calculated at the tangent pressures to determine the dependence of the spectra as a function of altitude; the result is used to perform an analytical convolution.

This interpolation is critical: it doesn't seem reasonable to use a high order interpolation extended to remote tangent altitudes, because the spectrum corresponding to a particular layer depends on the value of temperature and VMR profiles at that layer, and these are not necessarily related with those at layers above and below.
For this reason, an improvement in the approximation cannot be obtained increasing the order of interpolation by including spectra at remote tangent altitudes, but must be obtained increasing the number of simulated spectra used for the interpolation between two contiguous tangent altitudes.
Some tests have been performed for determining the minimum number of spectra necessary for performing a correct interpolation.
The critical aspect is given by discontinuities in the rate of change of temperature and of molecule density with the altitude.
The most critical molecules are H_2O and CO_2. H_2O VMR has a strong vertical change rate, in the troposphere. CO_2 is characterised by an almost constant VMR with altitude, however, its emitted lines are strongly affected by changes of temperature near the tropopause.
At higher altitudes the profiles don't show significant changes in the VMR slope, with the only possible exception of O_3 and HNO_3, therefore the FOV effects are expected to be less important.
Tests on CO_2 were performed by comparing the analytical convolution, made using interpolated spectra between three spectra at three contiguous tangent pressures, with a numerical convolution between spectra corresponding to tangent altitudes spaced by 200 metres and the FOV function.
The results of tests on CO_2 are reported in table 6.3, where the error in tangent altitude is shown for different microwindows, computed at various tangent altitudes.

MW TA→ ↓	8 km	11 km	14 km	17 km
12PT37	33	70		
13PT38	20	85	15	
14PT41		85	5	20
15PT44	20	85	5	15

Table 6.3 Results of comparison between reference numerical convolution of field of view and analytical convolution using interpolation with 3 contiguous spectra, for some of the microwindows selected for p-T retrieval. The errors in altitude are expressed in metres.

These errors are acceptable, according to the acceptance criteria reported in section 3. Therefore, for CO_2 and, consequently, for all the other molecules, except water, interpolation can be built from spectra calculated at three contiguous tangent pressures.
In this case, the interpolated spectrum is represented by:

$$S_I\left(\sigma, z_g\right) = cof_1\left(\sigma\right) + cof_2\left(\sigma\right)\cdot z + cof_3\left(\sigma\right)\cdot z^2, \qquad (6.6.2)$$

cof_1, cof_2 , cof_3 are the coefficients of the interpolation calculated, for each frequency, from the values of spectra at the considered tangent pressures.
The spectrum with FOV is given by:

$$S_{FA}\left(\sigma, z_g\right) = \int S_I\left(\sigma, p\left(z\right)\right) FOV\left(z_g, z\right) dz \ , \qquad (6.6.3)$$

The integral can be easily calculated analytically.

Tests on H_2O have shown that at low altitudes, up to the boundary between troposphere and stratosphere, the interpolation with three spectra at three contiguous tangent pressures produces discrepancies between the analytical and numerical ('exact') convolution. These discrepancies can be reduced calculating an additional spectrum at a tangent altitude intermediate between two contiguous tangent altitudes, and hence drawing a quartic order polynomial through five spectra (see Table 6.4).
Because of these results, the retrieval program has been made flexible for the computation of additional spectra in some specific cases. This does not represent a big increase in computing time, because additional spectra have to be calculated only in the troposphere, and only for H_2O.

μWs ↓ TA →	8 km	11 km	14 km
1H2O2B	26	17	21
2H2O3	24	74	21
3H2O4B	20	42	24
4H2O5B	30	17	24
5H2O6B			47
6H2O33	23	116	22

Table 6.4 Results of comparison between reference numerical convolution of field of view and analytical convolution using 5 spectra with tangent heights 1.5 km distant, for some microwindows selected for retrieval of H_2O VMR. The equivalent error in tangent height is expressed in metres.

We underline that, using this approach, the error due to the interpolation is very small when the mean tangent altitude of S_{FA} coincides with that of one of the simulated spectra. The error increases when an offset is introduced.
The final validation of the model for taking into account FOV has been done using RFM spectra.
In Fig. 6.6 the values of the reference spectrum with FOV at a significant frequency at different altitudes is plotted as a function of the corresponding spectrum obtained by analytical convolution. The deviation of the curve from a straight line indicates the presence of a variable error. This variation as a function of the tangent altitude offset indicates the presence of a potential error in the computation of the analytical derivatives with respect to tangent pressure (see below).

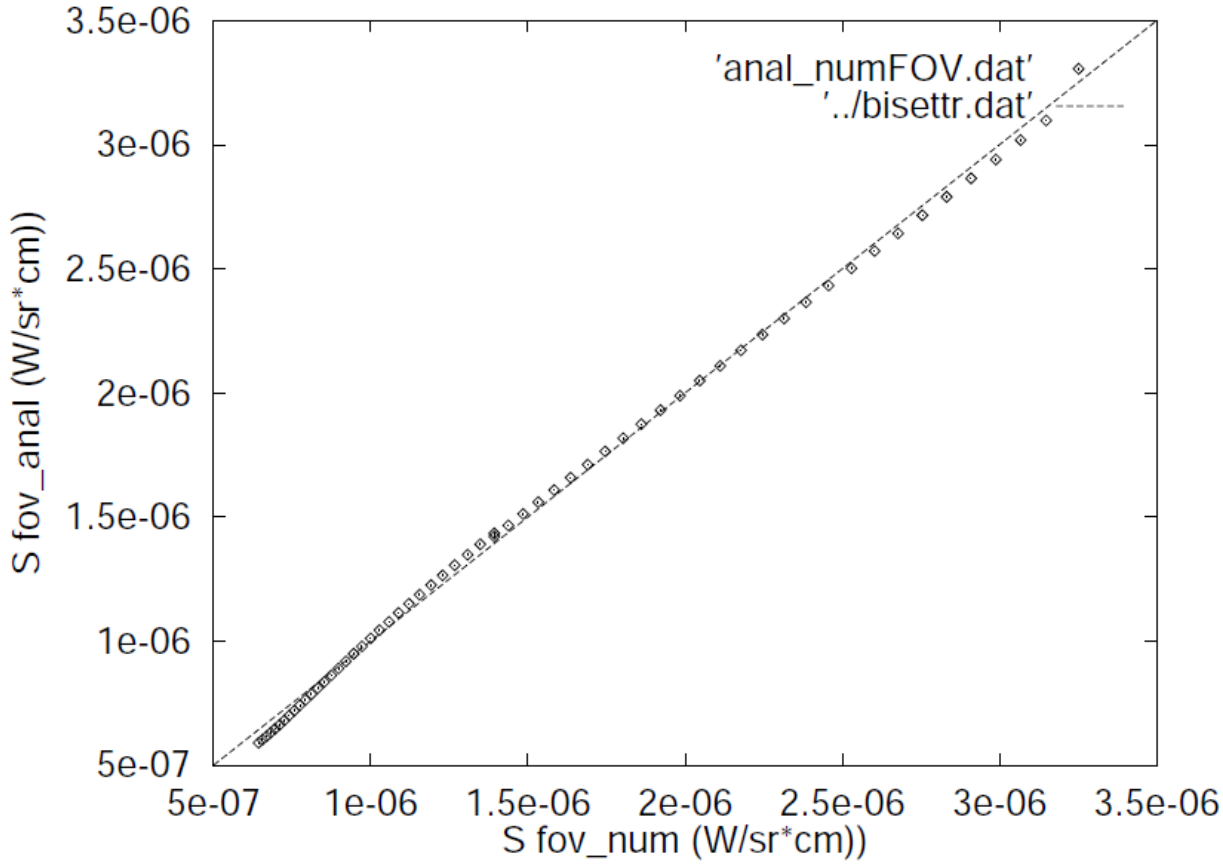

Fig. 6.6 In this plot the values of the spectrum at a significant frequency calculated with a analytical convolution at altitudes between 6.5 km and 12.5 km are plotted as a function of the corresponding values of the spectrum calculated with reference numerical convolution. A microwindow selected for p-T retrieval has been used.

The analytical derivative with respect to tangent pressure, obtained by the following calculation:

$$\frac{dS_{FA}}{dp_{\text{tang}}} = \frac{dS_{FA}}{dz} \cdot \frac{dz}{dp_{\text{tang}}}, \tag{6.6.4}$$

(the relation between z and p is derived by Hydrostatic equilibrium equation) has been compared with the numerical derivative, calculated using two spectra that take into account field of view and are characterised by a difference of 100 m in tangent altitude.

A percentage difference of the order of 10-15 % is obtained (see Fig. 6.7).

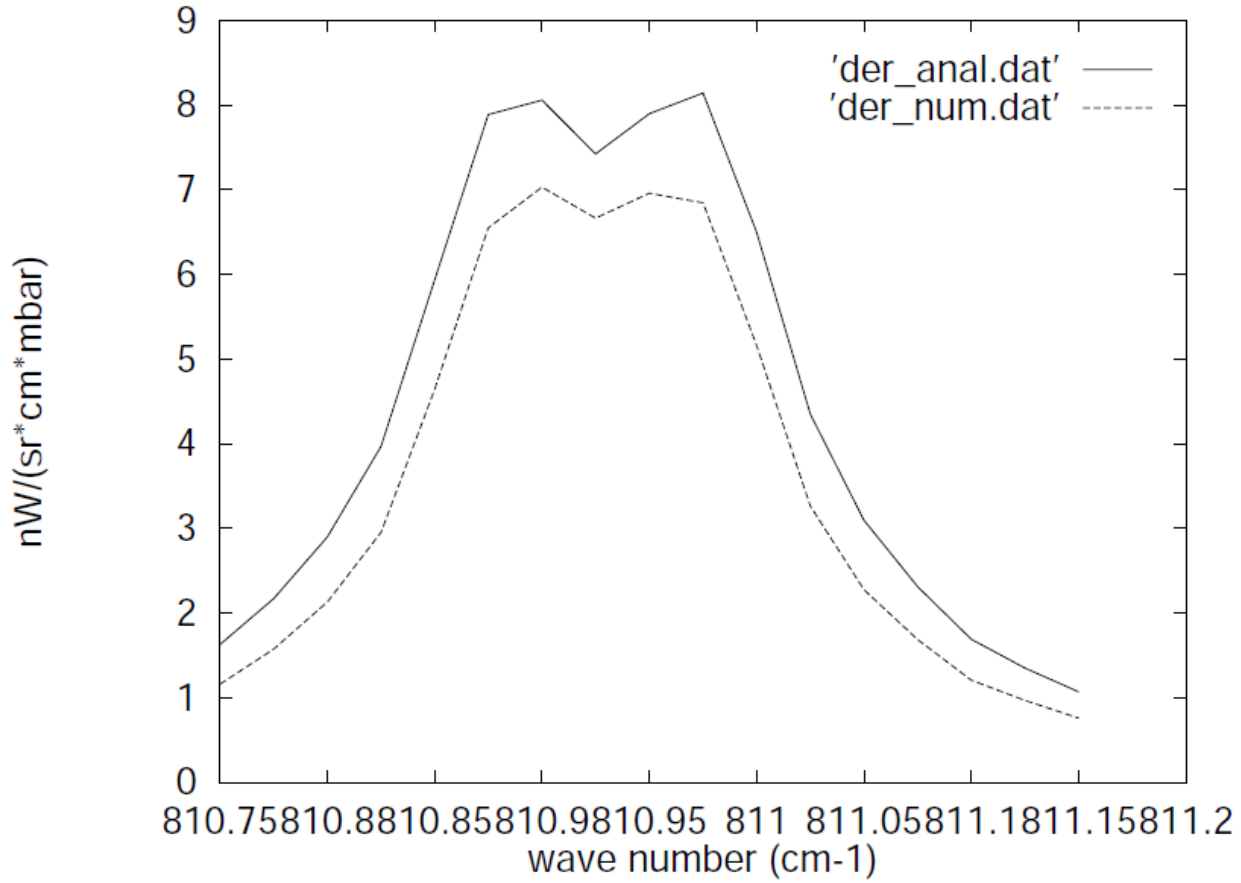

Fig. 6.7 Numerical and analytical derivatives with respect to tangent pressure for a microwindow selected for p-T retrieval, tangent altitude equal to 11 km.

Tests have shown that this error on tangent pressure derivatives does not increase the number of iterations required for reaching the convergence.

6.7 Analytical derivatives

6.7.1 General considerations

In contrast to numeric derivatives for which many reruns of the forward model are necessary, analytical derivatives can be calculated from parameters determined during the forward model calculation. Obviously the use of analytical derivatives makes only sense if the time consumption of their calculation is considerably smaller than the recalculation of the forward model. As a rule of thumb this is the case if the determination of the analytical derivatives avoids the recalculation of the absorption cross sections and if they are sufficiently precise that no extra iteration steps are necessary.

The basic equation of the derivative of the spectrum S with respect to an unknown variable q_r^{ret} (temperature, pressure or volume mixing ratio) on the levels to be retrieved is (for clarity of the equations we omit here the dependence of S on the wavenumber and the tangent altitude and consider only one absorber species, i.e. omit index m on the gases):

$$\frac{dS}{dx_r^{ret}} = \frac{d}{dx_r^{ret}} \sum_{l=1}^{N} B_l(T_l^e) \left[e^{-\sum_{j=1}^{l-1} k_j(T_j^e, p_j^e) C_j} - e^{-\sum_{j=1}^{l} k_j(T_j^e, p_j^e) C_j} \right] \tag{6.7.1}$$

where
N = total number of optical paths used to calculate the radiative transfer in the forward model
T_l^e = equivalent temperature of the layers
p_l^e = equivalent pressure of the layers
C_l = column amount of the absorber species in each layer

$$\begin{aligned}\frac{dS}{dx_r^{ret}} = &\sum_{l=1}^{N} \frac{dB_l(T_l^e)}{dx_r^{ret}} \left[e^{-\sum_{j=1}^{l-1} k_j(T_j^e, p_j^e) C_j} - e^{-\sum_{j=1}^{l} k_j(T_j^e, p_j^e) C_j} \right] \\ &+ \sum_{l=1}^{N} B_l(T_l^e) \left[e^{-\sum_{j=1}^{l-1} k_j(T_j^e, p_j^e) C_j} \sum_{j=1}^{l-1} \left(\frac{-dk_j(T_j^e, p_j^e)}{dx_r^{ret}} C_j + k_j(T_j^e, p_j^e) \frac{-dC_j}{dx_r^{ret}} \right) \right] \\ &- \sum_{l=1}^{N} B_l(T_l^e) \left[e^{-\sum_{j=1}^{l} k_j(T_j^e, p_j^e) C_j} \sum_{j=1}^{l} \left(\frac{-dk_j(T_j^e, p_j^e)}{dx_r^{ret}} C_j + k_j(T_j^e, p_j^e) \frac{-dC_j}{dx_r^{ret}} \right) \right]\end{aligned} \tag{6.7.2}$$

To evaluate this expression, the values that have to be additionally calculated inside the forward model are the derivatives of the Planck function $\frac{dB_l(T_l^e)}{dx_r^{ret}}$, the derivative of the absorption cross sections $\frac{dk_l(T_l^e, p_l^e)}{dx_r^{ret}}$ and the derivatives of the absorber columns $\frac{dC_l}{dx_r^{ret}}$. In order to write these derivatives in a more explicit form, we have to regard that the Curtis-Godson layer values T_l^e, p_l^e and C_l are dependent on the values of temperature, pressure and volume mixing ratio at the levels which are used for the radiative transfer ($T_n^{mod}, p_n^{mod}, \mathrm{X}_n^{mod}$). These are themselves dependent on the levels where the unknowns are retrieved ($T_r^{ret}, p_r^{ret}, \mathrm{X}_r^{ret}$).

$$\begin{aligned}T_l^e &= T_l^e \left[T_n^{mod}(T_r^{ret}, p_r^{ret}), p_n^{mod}(T_r^{ret}, p_r^{ret}), x_n^{mod}(T_r^{ret}, p_r^{ret}, \mathrm{X}_r^{ret}) \right] \\ p_l^e &= p_l^e \left[T_n^{mod}(T_r^{ret}, p_r^{ret}), p_n^{mod}(T_r^{ret}, p_r^{ret}), x_n^{mod}(T_r^{ret}, p_r^{ret}, \mathrm{X}_r^{ret}) \right] \\ C_l &= C_l \left[T_n^{mod}(T_r^{ret}, p_r^{ret}), p_n^{mod}(T_r^{ret}, p_r^{ret}), x_n^{mod}(T_r^{ret}, p_r^{ret}, \mathrm{X}_r^{ret}) \right]\end{aligned} \tag{6.7.3}$$

Finally the derivatives can be written as:

$$\begin{aligned}\frac{dB_l(T_l^e)}{dx_r^{ret}} &= \frac{\partial B_l(T_l^e)}{\partial T_l^e} \frac{dT_l^e}{dx_r^{ret}} \\ \frac{dk_l(T_l^e, p_l^e)}{dx_r^{ret}} &= \frac{\partial k_l(T_l^e, p_l^e)}{\partial T_l^e} \frac{dT_l^e}{dx_r^{ret}} + \frac{\partial k_l(T_l^e, p_l^e)}{\partial p_l^e} \frac{dp_l^e}{dx_r^{ret}} \\ \frac{dC_l}{dx_r^{ret}} &= \frac{dC_l}{dx_r^{ret}}\end{aligned} \tag{6.7.4}$$

with

$$\begin{aligned}
\frac{dT_l^e}{dx_r^{ret}} &= \frac{\partial T_l^e}{\partial T_n^{mod}}\frac{dT_n^{mod}}{dx_r^{ret}} + \frac{\partial T_l^e}{\partial p_n^{mod}}\frac{dp_n^{mod}}{dx_r^{ret}} + \frac{\partial T_l^e}{\partial x_n^{mod}}\frac{dX_n^{mod}}{dx_r^{ret}} \\
\frac{dp_l^e}{dx_r^{ret}} &= \frac{\partial p_l^e}{\partial T_n^{mod}}\frac{dT_n^{mod}}{dx_r^{ret}} + \frac{\partial p_l^e}{\partial p_n^{mod}}\frac{dp_n^{mod}}{dx_r^{ret}} + \frac{\partial p_l^e}{\partial x_n^{mod}}\frac{dX_n^{mod}}{dx_r^{ret}} \\
\frac{dC_l}{dx_r^{ret}} &= \frac{\partial C_l}{\partial T_n^{mod}}\frac{dT_n^{mod}}{dx_r^{ret}} + \frac{\partial C_l}{\partial p_n^{mod}}\frac{dp_n^{mod}}{dx_r^{ret}} + \frac{\partial C_l}{\partial x_n^{mod}}\frac{dX_n^{mod}}{dx_r^{ret}}
\end{aligned} \qquad (6.7.5)$$

and

$$\begin{aligned}
\frac{dT_n^{mod}}{dx_r^{ret}} &= \frac{\partial T_n^{mod}}{\partial T_r^{ret}}\frac{\partial T_r^{ret}}{\partial x_r^{ret}} + \frac{\partial T_n^{mod}}{\partial p_r^{ret}}\frac{\partial p_r^{ret}}{\partial x_r^{ret}} \\
\frac{dp_n^{mod}}{dx_r^{ret}} &= \frac{\partial p_n^{mod}}{\partial T_r^{ret}}\frac{\partial T_r^{ret}}{\partial x_r^{ret}} + \frac{\partial p_n^{mod}}{\partial p_r^{ret}}\frac{\partial p_r^{ret}}{\partial x_r^{ret}} \\
\frac{dX_n^{mod}}{dx_r^{ret}} &= \frac{\partial X_n^{mod}}{\partial T_r^{ret}}\frac{\partial T_r^{ret}}{\partial x_r^{ret}} + \frac{\partial X_n^{mod}}{\partial p_r^{ret}}\frac{\partial p_r^{ret}}{\partial x_r^{ret}} + \frac{\partial x_n^{mod}}{\partial X_r^{ret}}\frac{\partial x_r^{ret}}{\partial x_r^{ret}}
\end{aligned} \qquad (6.7.6)$$

In (6.7.5) and (6.7.6) implicit summations are assumed where a repeated index is present.

6.7.2 Derivative with respect to the volume mixing ratio

The different contributions of the volume mixing ratio derivatives are investigated.
When changing the volume mixing ratio the major effect to the derivative (equation (6.7.2)) is the change of the gas columns in each layer: $\frac{dC_l}{dx_r^{ret}}$. Test calculations have shown that using only this term the residual errors with respect to the total derivatives are about 1-10%, with the largest errors near the tangent level.

These errors are due to neglecting terms $\frac{dB_l(T_l^e)}{dx_r^{ret}}$ and $\frac{dk_l(T_l^e, p_l^e)}{dx_r^{ret}}$ mainly through the dependence of the Curtis-Godson value T_l^e on the volume mixing ratio. Adding the effect of $\frac{dB_l(T_l^e)}{dx_r^{ret}}$ to our previous calculations reduces the errors to about 1-5%.
In order to further improve this derivative a lot of effort is needed: it is necessary to determine

$\frac{dk_l(T_l^e, p_l^e)}{dx_r^{ret}}$, for which (equation 6.7.4), $\frac{\partial k_l(T_l^e, p_l^e)}{\partial T_l^e}$ and $\frac{\partial k_l(T_l^e, p_l^e)}{\partial p_l^e}$ must be calculated:

$$\frac{\partial k_l(T_l^e, p_l^e)}{\partial T_l^e} = \frac{\partial\left[\sum_{li} L_{l,li}(T_l^e) A_{l,li}(T_l^e, p_l^e)\right]}{\partial T_l^e} = \sum_{li}\left[A_{l,li}(T_l^e, p_l^e)\frac{\partial L_{l,li}(T_l^e)}{\partial T_l^e} + L_{l,m}(T_l^e)\frac{\partial A_{l,li}(T_l^e, p_l^e)}{\partial T_l^e}\right] \quad (6.7.7)$$

and

$$\frac{\partial k_l(T_l^e, p_l^e)}{\partial p_l^e} = \frac{\partial \sum_{li}\left[L_{l,li}(T_l^e) A_{l,li}(T_l^e, p_l^e)\right]}{\partial p_l^e} = \sum_{li} L_{l,li}(T_l^e)\frac{\partial A_{l,li}(T_l^e, p_l^e)}{\partial p_l^e} \quad (6.7.8)$$

where li = index for the different lines
$A_{l,li}(T_l^e, p_l^e)$ = line shape of line li
$L_{l,li}(T_l^e)$ = line intensity of line li

It is easy to calculate the derivative of the line intensity with respect to T_l^e but the derivative of the line shape is more problematic. Also if there would be a possibility to calculate it this would not save computation time, since the formula would be more complicated and would need more calculation time than a recalculation of the whole spectrum.
In any case, these calculations have to be done for each single line during the calculation of the absorption cross sections. This needs much more time than the calculation of the quantity $\frac{dC_l}{dx_r^{ret}}$.

Therefore the baseline for the ORM is to compute analytical derivatives which only contain $\frac{dC_l}{dx_r^{ret}}$. In case in future it turns-out that the accuracy of these VMR derivatives is not satisfactory, improvements can be obtained by reducing the layers thickness since this minimises the influence of the other contributions to the whole derivative.

6.7.3 Derivative with respect to temperature

The main contribution to this derivative arises from the derivative of the Planck function $\frac{\partial B_l(T_l^e)}{\partial T_l^e}$ (equation 6.7.4) and the derivative of the line strength $\frac{\partial L_{l,m}(T_l^e)}{\partial T_l^e}$. The larger is the temperature dependence of the line strength, i.e. the bigger E'' and the more important is the latter derivative. Therefore, in our tests, when only taking into account $\frac{\partial B_l(T_l^e)}{\partial T_l^e}$ the errors range from 5-40%. Since, as we said above, the calculation of $\frac{\partial L_{l,m}(T_l^e)}{\partial T_l^e}$ has to be done during the calculation of the absorption cross sections, it requires much more time than $\frac{\partial B_l(T_l^e)}{\partial T_l^e}$. Our baseline is not to calculate the analytical derivatives with respect to the temperature and use numerical derivatives instead.

However, the numerical derivatives are implemented in an optimised form (i.e. the calculation of spectra with the 'T-perturbed' profiles is parallel to the one with the 'original' profile), and not by just recalling the forward model.

6.7.4 Derivative with respect to the atmospheric continuum

The derivative with respect to the atmospheric continuum can be easily calculated since the continuum is taken into account as an absorption cross section which is multiplied by the air column of each path. The Curtis-Godson temperatures, pressures, or the total air column do not change when varying the continuum cross sections. Equation 6.7.1 can be written as:

$$\frac{dS}{dk_r^{cont,ret}} = \frac{d}{dk_r^{cont,ret}} \sum_{l=1}^{N} B_l(T_l^e) \left[\mathrm{e}^{-\sum_{j=1}^{l-1} k_j^{cont,e} C_j^{air}} - \mathrm{e}^{-\sum_{j=1}^{l} k_j^{cont,e} C_j^{air}} \right] \tag{6.7.9}$$

and for 6.7.2 follows:

$$\frac{dS}{dk_r^{cont,ret}} = \sum_{l=1}^{N} B_l(T_l^e) \left[\mathrm{e}^{-\sum_{j=1}^{l-1} k_j^{cont,e} C_j^{air}} \sum_{j=1}^{l-1} \frac{-dk_j^{cont,e}}{dk_r^{cont,ret}} C_j^{air} - \mathrm{e}^{-\sum_{j=1}^{l} k_j^{cont,e} C_j^{air}} \sum_{j=1}^{l} \frac{-dk_j^{cont,e}}{dk_r^{cont,ret}} C_j^{air} \right] \tag{6.7.10}$$

$k_l^{cont,e}$ are the continuum absorption cross sections of the forward model layers and are therefore dependent on the forward model levels ($k_n^{cont,mod}$) which are themselves dependent on the levels where the continuum has to be retrieved ($k_r^{cont,ret}$):

$$\frac{dk_l^{cont,e}}{dk_r^{cont,ret}} = \frac{\partial k_l^{cont,e}}{\partial k_n^{cont,mod}} \frac{\partial k_n^{cont,mod}}{\partial k_r^{cont,ret}} \tag{6.7.11}$$

The baseline is to use these analytical derivatives.

6.7.5 Derivative with respect to the tangent pressure

The main effects of this derivative result from the change of the column, the change of the line shape and the change of the temperature with the tangent pressure. For the modelling of the change of the line shape it is necessary to do calculations in the domain of the absorption cross sections which are very time consuming. Therefore, we decided not to calculate this derivative as given by the formulas above, but to determine it during the convolution with the FOV-function. The spectrum $S_{FA}(\sigma, p)$ is calculated for the field of view function FOV centred at the tangent pressure. Since the convolution with the FOV is an analytical expression, its derivative with respect to the central pressure of the FOV can be easily obtained.
Our baseline is to use this kind of analytical derivatives for the calculation of the derivatives with respect to the tangent pressure.

6.7.6 Independence of retrieved variables

The Jacobian matrix (equation 4.2.6) contains the partial derivatives of the spectrum with respect to the parameters. Therefore, while performing the calculation of the derivatives, one has to take care that either they are partial (if parameters are dependent) or that the parameters are independent ($\partial parameter_i / \partial parameter_j = 0, \forall i \neq j$), so that the partial derivatives are equal to the total ones.
This assumption is clearly fulfilled for the volume mixing ratio retrieval where the parameters are the volume mixing ratios and the continuum cross sections at the tangent levels and the instrumental offset. During the p-T retrieval one has to be more careful since (due to the optimised calculation of the tangent pressure derivatives, cf. 6.7.5) varying the tangent pressure implies also a change of the tangent temperature and of the atmospheric continuum on the tangent levels. This difficulty disappears when we define for each iteration cycle as the fitted parameters the new tangent pressure and the temperature and continuum cross sections at the tangent pressures of the previous iteration. In a subsequent step the new temperatures and continuum cross sections at the previous tangent pressures are interpolated to the new tangent pressures.

6.7.7 New choice of continuum variables in the MIPAS processor starting from V.7.0.

The radiative transfer is a first order differential equation; the solutions are written using exponentials. By combining the emission and absorption phenomena the spectrum is a linear combination of exponentials. The retrieval variables, both for the continuum and the VMR, are located in the exponents of the exponentials. Let $l = 1, \ldots, N$ be the paths defined by the intersections of a given line-of-sight with the defined atmospheric layers. The spectrum reaching the instrument may be written as

$$S(\sigma) = \sum_{l=1}^{N} B(\sigma, T_l^e)(1 - \tau_{l,\sigma}) \prod_{j=1}^{l-1} \tau_{\sigma,j} \qquad (6.7.12)$$

where $\tau_{\sigma,l}$ is the transmittance through the path l at frequency σ. The transmittance of the path l has the following expression:

$$\tau_{\sigma,l} = \exp\left(-\sum_m k_{\sigma,m}(p_l^e, T_l^e) c_{l,m}\right) = \prod_m \exp\left(-k_{\sigma,m}(p_l^e, T_l^e) c_{l,m}\right) \qquad (6.7.13)$$

where m is the gas index, $k_{\sigma,m}$ is the cross-section of that gas at frequency σ, which depends only on the equivalent pressure p_l^e and temperature of that layer. Finally $c_{l,m}$ is the gas column in the in the path, which depends on the gas VMR $x_m(z)$ in the following way:

$$c_{l,m} = \int_l x_m(z) \eta(z) \frac{ds}{dz}(z) dz . \qquad (6.7.14)$$

Here z is the altitude, $\eta(z)$ is the density and ds/dz is the linear element along the line of sight. In the case of the continuum $m = c$ we have $x_c(z) \equiv 1$, so the columns $c_{l,c}$ may be explicitely calculated from the pressure and the temperature of the atmosphere and the knowledge of the line of sight.
On the other hand, the unknowns are the cross-section vertical profile. Being a continuum, within each MW, the cross-section does not depend on the frequency. ORM_SDC versions earlier than 3.0 use the cross-sections $k_i = k(z_i)$ at tangent altitudes z_i, $i = 1, \ldots, n$ as retrieval variables. The cross

section in a given path l is then represented by calculating the average pressure of the path, and interpolating linearly in pressure between the tangent altitudes above and below the layer l. In formulas, if $i(l)$ is the index of the tangent altitude above the path l:

$$k_l = a_l k_{i(l)-1} + b_l k_{i(l)}, \tag{6.7.15}$$

where a_l, b_l are positive constants belonging to the $[0,1]$ interval.

While being physically sound, the retrieval of a linear combination of exponentials from their exponents is unstable, we refer to *Transtrum et al. (2011)* for details. The following example shows the problems linked with the fit of the exponents: it can be readily seen that, given the model function $f(\theta,t) = e^{-\theta_1 t} + e^{-\theta_2 t}$ it is almost impossible to identify the parameters θ_1 and θ_2 given the experimental values of $f(\theta,t_j)$, even for moderately large values of t.
The standard methods to treat this situation, which is called a *sloppy model*, is to modify the minimization method, adjusting the step-length according to some recipe which involves the cost function. At each step, a unidimensional search is therefore necessary along the direction predicted by the descent method (be it the gradient method, or the Gauss-Newton method as in the case of the ORM). This is unacceptable in our case, because this would imply many forward model evaluations, which is very costly in terms of time for the atmospheric model.
As an alternative solution, we changed the retrieval variables in order to eliminate the exponential dependence. Instead of using the k_i from Eq. (6.7.15) we use the new variables

$$\xi_i = \exp(-k_i C) \tag{6.7.16}$$

Where C is a constant. Then the transmission of the continuum of the path l

$$\tau_{l,c} = \exp\left(-(a_l k_{i(l)-1} + b_l k_{i(l)}) c_{l,c}\right) \tag{6.7.17}$$

becomes

$$\tau_{l,c} = \xi_{i(l)-1}^{a_l c_{l,c}/C} \xi_{i(l)}^{b_l c_{l,c}/C} \tag{6.7.18}$$

By choosing a constant $C > c_{l,c}$ for all the paths l, we ensure that the exponents in (6.7.18) are positive and less than 1. We choose $C = 10^{25}$.
There are two consequences of this choice. First, the dependence of the $\tau_{l,c}$ on the ξ_j is of polynomial type. Second, while the permitted values for the k_j were $[0,+\infty)$, the new variables vary in the $[0,1]$ interval. Note that the value $k_j = 0$ (full transparency) in the old variables corresponds to $\xi_j = 1$ in the new variables. Analogously the value $k_j = +\infty$ (complete opacity) in the old variables corresponds to $\xi_j = 0$ in the new variables.
The only two non-vanishing derivatives of the $\tau_{l,c}$ with respect to the new retrieval variables are:

$$\frac{\partial \tau_{l,c}}{\partial \xi_{i(l)-1}} = a_l \frac{c_{l,c}}{C} \xi_{i(l)-1}^{\frac{a_l c_{l,c}}{C}-1} \xi_{i(l)}^{\frac{b_l c_{l,c}}{C}} = a_l \frac{c_{l,c}}{C} \frac{\tau_{l,c}}{\xi_{i(l)-1}} \tag{6.7.19}$$

and

$$\frac{\partial \tau_{l,c}}{\partial \xi_{i(l)}} = b_l \frac{c_{l,c}}{C} \xi_{i(l)-1}^{\frac{a_l c_{l,c}}{C}} \xi_{i(l)}^{\frac{b_l c_{l,c}}{C}-1} = b_l \frac{c_{l,c}}{C} \frac{\tau_{l,c}}{\xi_{i(l)}}. \tag{6.7.20}$$

The ORM calculates the derivatives of the spectrum with respect to the continuum variables by summing the contributions coming from each path *l*, and applying the chain rule:

$$\frac{\partial S}{\partial k_j} = \sum_l \frac{\partial S}{\partial \tau_{l,c}} \frac{\partial \tau_{l,c}}{\partial k_j} \tag{6.7.21}$$

To use the new retrieval variables, we have simply to substitute the last term, thus getting

$$\frac{\partial S}{\partial \xi_j} = \sum_l \frac{\partial S}{\partial \tau_{l,c}} \frac{\partial \tau_{l,c}}{\partial \xi_j} \tag{6.7.22}$$

With this new approach the retrieval variables for the continuum are better identifiable, so that the retrieval is more stable. In this way the regularizing effect of the LM method can be kept weaker. With this approach we were able to reduce the initial value of the LM damping for the continuum variables by a factor of 10.

Tests with real MIPAS observations show that a more stable retrieval is obtained with these new variables. As a consequence, we obtain a reduction in the number of iterations, a smaller minimum of the cost function, and slightly less oscillating profiles. The same modification can be applied also to the VMR retrieval variables. Our tests show, however, that (at least in the present formulation) there is no real advantage connected with this additional change. Further details on this modification can be found in *Ridolfi and Sgheri (2012)* and in *Ridolfi and Sgheri (2013)*.

6.8 Convergence criteria

In Sect. 4.2.4 four possible conditions have been considered for the definition of reached convergence. After several otpimizations based on the analysis of real measurements, the convergence criteria used by the ORM are organized as follows. Let t_1, t_2, t_3, t_4, t_5, t_6 be user-defined, tuned, numerical thresholds. The retrieval is stopped at a macro-iteration "*it*" if at least one of the following conditions is fulfilled:

1. Is $\left(\chi^2(it) - \chi^2_{\mathrm{LIN}}(it)\right) / \chi^2(it) < t_1$ and $\chi^2(it) < t_6$?
2. Is $\left(\chi^2(it) - \chi^2(it-1)\right) / \chi^2(it) < t_2$ and $\chi^2(it) < t_6$?
3. Only in pT retrieval. Is the maximum relative variation of tangent pressure wrt the previous iteration less than t_3 and is the maximum variation of temperature wrt the previous iteration less than t_4 ?
4. Only in VMR retrieval. Is the maximum relative variation of VMR wrt the previous iteration less than t_3 ?
5. Is $\left[\left(\mathbf{x}_{it} - \mathbf{x}_{it-1}\right)^T \mathbf{S}^{-1}_{\mathrm{x},it} \left(\mathbf{x}_{it} - \mathbf{x}_{it-1}\right) / n\right]^{1/2} < t_5$? Where $\mathbf{x}_{it}$ is the retrieved profile at iteration *it*, *n* its number points and $\mathbf{S}_{\mathrm{x},it}$ the estimate of its covariance matrix at the same iteration, i.e.:

$\mathbf{S}_{x,it} = \left(\mathbf{K}_{it}^T \mathbf{S}_y^{-1} \mathbf{K}_{it}\right)^{-1}$.

6. Is *it* < *itmax* ? where *itmax* is the maximum number of allowed iterations.

Condition 6. has no physical rationale, it is only used to limit the computation time and, in normal conditions, it should never be fulfilled. If a retrieval is stopped due to this condition being fulfilled, then the retrieval is said "non-converging" and the corresponding output profile is flagged as invalid.
Conditions from 2. to 5. are more or less equivalent and aim at establishing whether the retrieved profile is changing too little (compared to its error bars) from one iteration to the next, it that case additional iterations would not be worth. When the thresholds t_i are properly tuned, these conditions all ensure that the convergence error is smaller than a suitable fraction of the error due to measurement noise.
Condition 2. checks the relative difference between the actual chi-square and the chi-square evaluated with a linear expansion of the forward model about the current estimate of the state vector. A small value of this difference indicates that the forward model behaves almost linearly, therefore with the current iteration we should have already reached the minimum of the chi-square function.
If the final χ^2 is less than t_6 the retrieved profile is flagged "good" and it is used either as initial guess or as assumed profile in the subsequent retrievals. An exception to this rule is for pT values used in VMR retrievals. VMR retrievals must use pT values retrieved from the same scan, also if pT retrieval terminated with $\chi^2 \geq t_6$. Conditions 1. and 2. are checked only when $\chi^2(it) < t_6$ because we encountered scans with a large χ^2 not changing from one iteration to the next. As a consequence the first part of conditions 2. and 3. could be fulfilled even with such a large χ^2. A check on these scans revealed that applying further iterations would reduce the χ^2 under the t_6 threshold.

A comment to the adopted strategy could be that the above conditions could be erroneously triggered when still far away from the minimum of the χ^2 function, due to occasionally large values of the LM damping parameter λ_M. While in principle this event can occur, we verified that in practice it is very rare (few retrievals over thousands). Of course these occurrences can be detected by checking the final value of λ_M of the retrieval. When the final λ_M is greater than a pre-defined threshold the related profile can be discarded. The thresholds to be used are currently included in the "readme" file accompanying ESA Level 2 products.

Some investigations based on the ESA Level 2 processor IPF v.6, showed that the convergence error achieved with the used convergence thresholds is, on average, of the order of 1/10 of the error due to measurement noise. The results of these investigations can be found in *Ridolfi et al. (2011)*. A document reporting the most recent tests for the selection of the above mentioned criteria is *Ridolfi and Sgheri (2011)*.

6.9 Pre-calculation of line shapes

This item concerns the line shape calculation in the case of HNO_3 lines. Since a lot of lines have to be taken into consideration in HNO_3 microwindows this is a very time consuming part of the VMR-retrieval process. In order to optimise this calculation, we can use the fact that in the HITRAN data base the HNO_3 lines have the same Lorentz half width and the same coefficient of the temperature dependence (equation 4.4.12). Therefore, it is not necessary to calculate the line shape (equation 4.4.15) for each HNO_3 line, this can be calculated for a single line, at the beginning of the cross section calculation for a new path (p_{eq},T_{eq} pair) and used for all other HNO_3 lines of the microwindow. For each transition the pre-calculated line shape is then centred at the central line frequency and interpolated to the wavenumber

grid of the microwindow. This interpolation is performed linearly. The resulting error was determined by test calculations. The maximum difference between exact calculation and use of the interpolated pre-calculated line shape was NESR/88. Due to this small value of the introduced error and to the time saving of 66%, our baseline is to use the pre-calculated HNO_3 line-shapes. Of course, this optimisation is not used when cross-sections are computed from pre-calculated LUTs.

6.10 Different grids during the cross-section calculation

For the calculation of the radiative transfer, absorption cross-sections are required at each grid point of the fine frequency grid at which also the radiative transfer is calculated. Tests have shown that a reasonable and conservative value for the step between two fine grid points can be 5×10^{-4} cm^{-1}. This value, which can in principle be optimised in terms of faster computations, as been adopted as baseline. This results in 4000 points for a 2 cm^{-1} microwindow where cross sections for each transition have to be calculated. Therefore, the run time is directly proportional to the number of grid points. In order to reduce the number of grid points during the calculation of cross sections two methods are used even by accurate line-by-line codes (e.g. Edwards, 1991; Gordley, 1994):

1. far off the line centre the frequency grid can be coarser than near the centre.
2. the grid can be proportional to the half-width of the line, i.e. it can be dependent on the pressure of the layer for which the cross-sections have to be calculated.

These two methods have been implemented into the subroutine for the line-by-line calculation of cross section in the following way: in addition to the constant general fine grid (Δ_{gf} =5×10^{-4} cm^{-1}) two grids, the local coarse (Δ_{lc}) and the local fine grid (Δ_{lf}), are defined for each path where the cross sections are calculated. The grid distances are multiple integers of each other:

$$\Delta_{lf} = n\Delta_{gf}, \Delta_{lc} = m\Delta_{lf} \quad \text{with } n, m \in \mathrm{N}, \text{and } 1 \le n, 1 \le m \qquad (6.11.1)$$

- m, which determines the local coarse grid, is a tunable parameter.
- n is the nearest positive integer value so that $\Delta_{lf} \approx \xi\left(\alpha^{L_m} + \alpha^{D_m}\right)$, where $\alpha^{L_m}, \alpha^{D_m}$ are the Lorentz and the Doppler half width of the target gas transition with the largest intensity, and ξ is a second optimisation parameter that determines the period of the local fine grid.
- The third parameter ζ defines the distance $\zeta\left(\alpha^{L_m} + \alpha^{D_m}\right)$ of the transition between local fine and local coarse grid from the line centre.

After the calculation of the cross sections for all lines of the microwindow both grids are linearly interpolated to the general fine grid. Run time tests with this implementation showed a considerable time saving for the calculation of the absorption cross sections of more than 50%. Again, also this optimisation is used only when absorption cross-sections are computed with the line-by-line approach, it is not exploited when cross-sections are computed from pre-calculated LUTs.

6.11 Cross-section look-up tables

The use of pre-computed look-up tables (LUTs) is an alternative method to the explicit line-by-line calculation of absorption cross sections (equation 4.4.6). The basic idea of this method is to pre-calculate

for each frequency grid point the absorption cross sections of each gas for a set of different pressures and temperatures within the range of the atmospheric variability. These data are stored in files which are read at the beginning of each retrieval. Then they are interpolated to the equivalent pressure and temperature of the atmospheric paths (p_{eq}, T_{eq} pairs). Since the frequency grid in which the cross sections have to be calculated is rather fine (5×10^{-4} cm^{-1}, see Sect. 6.10) the amount of data is large.
In order to reduce the amount of data contained in the look-up tables and their reading time, a compression procedure has been studied at University of Oxford (see Morris (1997)). The algorithm used to build compressed look-up tables and procedure for the decompression are based on the matrix singular value decomposition applied to the cross-sections and is described in Strow et al., (1998).
Since version 2.3, the ORM code is able to handle these compressed look-up tables, including cases in which the look-up tables are available only for a sub-set of the operational microwindows and / or for a sub-set of the gases contributing to the emission in each microwindow.
The importance of time savings obtained using LUTs instead of line-by-line calculations depends very much on the considered retrieval. Largest savings are obtained in the case of HNO_3 retrieval (38% reduction of forward model runtime), less significant savings (15% reduction of forward model runtime) are obtained in the cases of O_3 and CH_4. In other cases the use of compressed LUTs provides no time savings (N_2O) or an increase of computing time like in p,T and H_2O retrievals.
LUTs represent a very efficient optimisation only when irregular frequency grids (see Sect. 6.12) are used in combination.

6.12 Variable frequency grids for radiative transfer computation

Limb radiance spectra contain spectral features on a range of scales varying from the narrow, isolated, Doppler-broadened line centers at high altitudes, to wide, overlapping, Lorentz-broadened line wings from low altitudes.
Therefore, a minimum subset of spectral grid points (irregular grid) can be determined that are sufficient to reconstruct full radiance spectra, applicable over a range of tangent altitudes and atmospheres. Full radiative transfer calculations are then only required for this subset of points, the remaining fine grid points are obtained using a pre-determined interpolation scheme. The irregular grid is a function of the microwindow boundaries, the chosen interpolation scheme and the spectral convolution by the Instrument Line Shape.
Typically, it is found that only 5-10 % of the full resolution grid is required for reconstruction of the spectra. When combined with the Look-Up Tables, this also means that absorption cross-section only has to be reconstructed at the same fraction of grid points resulting in even more efficient optimization.
On the other hand, the use of irregular grids does not reduce the computation time of the algorithm for line-by-line evaluation of the cross-section. This algorithm in fact already uses its own internal, line-specific, irregular grid (see Sect. 6.10) and takes little advantage from the externally provided optimized grids.
The ORM code is able to exploit externally provided, microwindow-specific irregular grids. Due to the very significant time savings obtained with the combined use of LUTs and irregular grids (a factor of 10 in the computing time required for the full retrieval chain) and to the small size of the introduced inaccuracies (< NESR / 10 in spectral radiances), the ORM baseline is to use both LUTs and irregular grids in operational retrievals.
Both LUTs (see Sect. 6.11) and irregular grids optimized for MIPAS microwindows are currently calculated by a dedicated algorithm developed at Oxford University (see Morris, (1997) and Wells, (1997)). A summary description of this algorithm is reported in Appendix D.

References

Barrell, H. and Sears, J. E.: The refraction and dispersion of air for the visible spectrum, Philos. T. Roy. Soc. A, 238, 1–62, 1939.

Bennett, V. L., A. Dudhia and C. D. Rodgers, *Microwindow Selection for MIPAS using Information Content*, ESAMS'99 Proceedings, 18-22 January 1999, Noordwijk, NL.

Born, M., E. Wolf, *'Principles of Optics',* Oxford, Pergamon Press, 5th edition, 1975.

Carli, B.,'*Document on the choice between retrieval of profile at fixed levels and at tangent altitude levels*', Action item from 24th MIPAS SAG Meeting of 15 November 1995, 4 December 1995.

Carli, B., B.M.Dinelli, P.Raspollini, M.Ridolfi, '*Discrete representation and resampling in the case of limb-sounding measurements*', Appl. Optics, Vol. 40, No. 8, p. 1261-1268, (2001).

Carlotti M., '*Global-fit approach to the analysis of limb-scanning atmospheric measurements'*, Appl. Optics, 27, 3250-3254, (1988).

Carlotti, M., B.Carli, '*Approach to the design and data analysis of limb-scanning atmospheric measurements'*, Appl. Optics, 33, 15, 3237-3249, (1994)

Carlotti, M., G. Paruolo, F. Alboni, B. Carli, F. Mencaraglia, M. Ridolfi, *'Determination of atmospheric pressure and temperature distributions from MIPAS limb emission line spectra',* ESA contract report No. 142956, 1995.

Carlotti, M., B.M.Dinelli, P.Raspollini, M.Ridolfi, '*Geo-fit approach to the analysis of satellite limb-scanning measurements'*, Appl. Optics, Vol. 40, No. 12, p. 1872 – 1875, (April 2001).

Castelli E., Marco Ridolfi, Massimo Carlotti, Michael Kiefer, Bjorn-Martin Sinnhuber, Investigations on horizontal inhomogeneities issue: Outcome of WP 9000, Tech. Note output of WP9000 of the study Support to MIPAS L2 product validation, Issue 1.0, 22 February 2014.

Castelli, E., Ridolfi, M., Carlotti, M., Sinnhuber, B.-M., Kirner, O., and Dinelli, B. M.: Errors induced by different approximations in handling horizontal atmospheric inhomogeneities in MIPAS/ENVISAT retrievals, Atmos. Meas. Tech., doi:10.5194/amt-2016-68, 2016.

S. Ceccherini, *'Analytical determination of the regularization parameter in the retrieval of atmospheric vertical profiles'*, Optics Letters, **30**, 2554-2556, (2005).

S. Ceccherini, C. Belotti, B. Carli, P. Raspollini and M. Ridolfi, *'Technical Note: Regularization performances with the error consistency method in the case of retrieved atmospheric profiles'*, Atmos. Chem. Phys., **7**, 1435-1440, (2007).

S. Ceccherini and M. Ridolfi, *Technical Note: Variance-covariance matrix and averaging kernels for the Levenberg-Marquardt solution of the retrieval of atmospheric vertical profiles*, Atmos. Chem. Phys., **10**, 3131-3139 (2010).

Ciddor, P. E.: Refractive index of air: new equations for the visible and near infrared, Appl. Optics, 35, 1566–1573, 1996.

Clarmann T., '*Untersuchungen zur Strahldichteberechnung mit Linie - für - Linie - Computerprogrammen*', Diplomarbeit für Meteorologie, Universität München, Meteorologisches Institut, 1986.

Clough, S. A., F. X. Kneizys, L. S. Rothman, and W. O. Gallery, *'Atmopspheric spectral transmission and radiance: FASCOD1B'*, SPIE 277, 152-166, 1981.

Clough, S. A., F. X. Kneizys and R. W. Davies, *'Line shape and the water vapor continuum'*, Atmospheric Research, 23 229-241, 1989.

Cousin, C., R. Le Doucen, C. Boulet, and A. Henry, *'Temperature dependence of the absorption in the region beyond the 4.3 μm band head of CO_2. 2: N_2 and O_2 broadening'*, Appl. Opt., 24, 3899-3907, 1985.

Defense Mapping Agency, '*WGS84 Ellipsoidal Gravity Formula and Gravity Anomaly Conversion Equations':* DMA Aerospace Center, St. Louis p. 10.

Delbouille, L., G. Roland, *'Assessement of finite field-of-view effects on MIPAS ILS & Review of resolution enhancement techniques',* Answer to ESA NTO/ME/1573.

Dinelli, B.M., E.Battistini, B.Carli, '*MIPAS-B2 data analysis'* TN-ISM-0002, (2000).

Doicu, A., Trautmann, T. and Schreier, F., *Numerical regularization for atmospheric inverse problems* (Springer, Berlin, 2010).

Drayson, S. R., *'Rapid computation of the Voigt profile'*, J Quant. Spectr. Radiat. Transfer, 16, 611-614, 1976.

Dudhia, P. E. Morris and R. J. Wells, *Acceleration of Radiative Transfer Calculations* ESAMS'99 Proceedings, 18-22 January 1999, Noordwijk, NL.

Dudhia, A., '*MIPAS ultimate retrieval accuracy'*, final report, 19 June 2000 (a).

Dudhia, A., '*MIPAS ultimate retrieval accuracy'* appendix to the final report, 7 December 2000 (b).

Dudhia, A., '*Latitude-dependence of MIPAS microwindow selection*', report of task 5.7 of the CCN5 of the ESA contract 11717/95/NL/CN, 12 February 2001.

Edlén, B.: The refractive index of air, Metrologia, 2, 71–80, 1966.

Edwards, D. P., *'GENLN2 a general line-by-line atmospheric transmittance and radiance model'* Version 3.0 Description and Users Guide, 1992.

Flaud, J.-M., C.Piccolo, B.Carli, *'Update A of the spectroscopic Database for MIPAS'*, TN-LPM-IROE-01, draft, (May 2001).

Gordley, L. L., B. T. Marshall, D. A.. Chu, *LINEPAK: algorithms for modelling spectral transmittance and radiance',* J Quant. Spectr. Radiat. Transfer, 52, 563-580, 1994.

Hase, F. and Höpfner, M.: Atmospheric ray path modeling for radiative transfer algorithms, Appl. Optics, 38, 3129–3133, doi:10.1364/AO.38.003129, 1999.

Hobiger, T., Ichikawa, R., Koyama, Y., and Kondo, T.: Fast and accurate ray-tracing algorithms for real-time space geodetic applications using numerical weather models, J. Geophys. Res., 113, D20302, doi:10.1029/2008JD010503, 2008.

Hollweg, H.D., V.S. Kostsov, G. Schlussel, P. Schlussel, Y.M. Timofeyev, *Interaction at MM and Optical Frequencies,* ESA Interim Report Contract 10603/93/NL/NB, 1994.

Humlicek, J., *'Optimized computation of the Voigt and complex probability functions'*, J. Quant. Spectr. Radiat. Transfer, 27, 437-444, 1982.

Isaacson, E.: Analysis of Numerical Methods, Courier Dover Publications, 1994.

Kiefer, M., Arnone, E., Dudhia, A., Carlotti, M., Castelli, E., von Clarmann, T., Dinelli, B. M., Kleinert, A., Linden, A., Milz, M., Papandrea, E., and Stiller, G.: Impact of temperature field inhomogeneities on the retrieval of atmospheric species from MIPAS IR limb emission spectra, Atmos. Meas. Tech., 3, 1487-1507, doi:10.5194amt-3-1487-2010, 2010.

Lafferty, W..J., A.M.Solodov, A.Weber, W.B.Olson, J.-M.Hartmann: *'Infrared collision-induced absorption by N_2 near 4.3 μm for atmospheric applications: measurements and empirical modelling'*, Appl. Opt., 35, 5911-5917, (1996).

Levenberg, K.: A method for the solution of certain problems in least squares, Quart. Appl. Math., 2, 164-168, 1944.

List R. J. ed.: *Smithsonian Meteorological Tables,* Sixth Revised Edition, Washington, D.C., 1963.

Marquardt D. W.: An algorithm for the least-squares estimation of nonlinear parameters, SIAM J. Appl. Math., 11, 431-441, 1963.

Mathar, R. J.: Calculated refractivity of water vapor and moist air in the atmospheric window at 10 μm, Appl. Optics, 43, 928–932, 2004.

Morris P., '*Generation of compressed cross-section look-up tables for NRT MIPAS retrievals'*, ESA report PO-TN-OXF-GS-0011, (1997).

F. Niro, G. Brizzi, M. Carlotti, E. Papandrea, and M. Ridolfi, Precision improvements in the geo-fit retrieval of pressure and temperature from MIPAS limb observations by modeling CO2 line-mixing. Journal of Quantitative Spectroscopy and Radiative Transfer, 103(1), 14-26, (2007).

C. Piccolo, M. Prosperi, M. Ridolfi, V. Tenna, '*Level 2 Algorithm Characterization and Validation Plan'*, prog. doc. n. TN-IROE-GS0101, (2001).

Press, W. H., S. A. Teukolsky, W. T. Wetterling, B. P. Flannerly: '*Numerical Recipes in Fortran'*, Second Edition Cambridge University Press 1992.

P. Raspollini, C. Belotti, A. Burgess, B. Carli, M. Carlotti, S. Ceccherini, B. M. Dinelli, A. Dudhia, J.-M. Flaud, B. Funke, M. Hoepfner, M. Lopez-Puertas, V. Payne, C. Piccolo, J. J. Remedios, M. Ridolfi and R. Spang, *'MIPAS level 2 operational analysis'*, Atmos. Chem. Phys., **6**, 5605-5630, 2006

P.Raspollini and M.Ridolfi, '*Mapping of Temperature and Line-of-Sight Errors in Constituent Retrievals for MIPAS / ENVISAT Measurements*', Atmospheric Environment, Vol. **34**, Nos. 29 – 30, p. 5329 – 5336 (2000).

Raspollini, P., Carli, B., Carlotti, M., Ceccherini, S., Dehn, A., Dinelli, B. M., Dudhia, A., Flaud, J.-M., López-Puertas, M., Niro, F., Remedios, J. J., Ridolfi, M., Sembhi, H., Sgheri, L., and von Clarmann, T.: *Ten years of MIPAS measurements with ESA Level 2 processor V6 – Part I: retrieval algorithm and diagnostics of the products*, Atmos. Meas. Tech. Discuss., 6, 461-518, doi:10.5194/amtd-6-461-2013, (2013).

Remedios, J. J., Leigh, R. J., Waterfall, A. M., Moore, D. P., Sembhi, H., Parkes, I., Greenhough, J., Chipperfield, M. P., and Hauglustaine, D.: MIPAS reference atmospheres and comparisons to V4.61/V4.62 MIPAS level 2 geophysical data sets, Atmos. Chem. Phys. Discuss., 7, 9973–10017, https://doi.org/10.5194/acpd-7-9973-2007, 2007.

Ridolfi M., B.Carli, M.Carlotti, T.v.Clarmann, B.M.Dinelli, A.Dudhia, J.-M.Flaud, M.Hoepfner, P.E.Morris, P.Raspollini, G.Stiller, R.J.Wells, 'Optimized forward model and retrieval scheme for MIPAS near-real-time data processing' *Appl. Optics*, Vol. **39**, No. 8, p. 1323 – 1340 (10 March 2000).

Ridolfi, M. and Sgheri, L.: A self-adapting and altitude-dependent regularization method for atmospheric profile retrievals, Atmos. Chem. Phys., 9, 1883-1897, (2009).

Ridolfi, M., Carli, B., Carlotti, M., Ceccherini, S., Dinelli, B.M., Raspollini, P. and Sgheri, L.: Diagnostics and convergence in the ORM and GEOFIT Levenberg-Marquardt retrievals - rebuttal report -, Technical Note, Issue 1, October 2011.

Ridolfi, M. And Sgheri, L., Improvement of the ORM convergence criteria: test of performance and implementation details, Technical Note, May 2011.

Ridolfi, M. and Sgheri, L.: Iterative Variable Strength (IVS) regularization for MIPAS retrievals, Technical Note, 7 July 2011.

Ridolfi, M. and Sgheri, L.: Iterative approach to self-adapting and altitude-dependent regularization for atmospheric profile retrievals, Opt Express 19, 26696-26709 (2011).

Ridolfi, M. and Sgheri, L.: New retrieval variables for the continuum profile, July 2012 (technical note).

Ridolfi, M. and Sgheri, L.: On the choice of retrieval variables in the inversion of remotely sensed atmospheric measurements, Optics Express, 21(9), 11465 - 11474, (2013).

Ridolfi, M. and Sgheri, L., Characterization of model errors in the calculation of tangent heights for atmospheric infrared limb measurements, Atmospheric Measurement Techniques, 7(12), 4117 - 4122, (2014).

Ridolfi, M., Sgheri, L., Cartelli, E., Dinelli, B.-M., Technical note: testing the horizontal gradient model implemented in the ORM v8, delivery of the study "Support to MIPAS Level 2 processor verification and validation - Phase F", 23 May 2017.

Rodgers C. D. '*Retrieval of Atmospheric Temperature and Composition from Remote Measurements of Thermal Radiation*', Reviews of Geophysics and Space Physics, Vol. 14 N. 4, p.609, 1976.

Rodgers C. D., '*Inverse Methods for Atmospheric Sounding: Theory and Practice'*, Series on Atmospheric, Oceanic and Planetary Physics – Vol. 2, World Scientific, (2000).

Rosenkranz, P. W., *'Shape of the 5 mm oxygen band in the Atmosphere',* IEEE Trans. Antennas Propag. 23, 498-506, 1975.

Schreier, F., *'The Voigt and complex error function: a comparison of computational methods'*, J Quant. Spectr. Radiat. Transfer, 48, 743-762, 1992.

Sgheri, L. and Ridolfi, M., Tech Note: Implementation of the Horizontal Gradients in the ORM V8, delivery of the study "Support to MIPAS Level 2 processor verification and validation - Phase F", Issue 1.0, 19 April 2018.

Sterne T. E. '*An Introduction to Celestial Mechanics',* Interscience publishers Ltd, London, 1960.

Strow, L.L., Motteler H.E., Benson R.G., Hannon S.E. and De Souza-Machado S. *'Fast Computation of monochromatic infrared atmospheric transmittances using compressed look-up tables'*. J. Quant. Spectrosc. Radiat. Transfer, 59, p481-493, (1998).

Thayer, G. D.: A rapid and accurate ray tracing algorithm for a horizontally stratified atmosphere, Radio Sci., 1, 249–252, 1967.

Thibault, F., V.Menoux, R.Le Doucen, L.Rosenmann, J.-M.Hartmann, Ch.Boulet: *'Infrared collision-induced absorption by O_2 near 6.4 μm for atmospheric applications: measurements and empirical modelling'*, Appl. Opt., 36, 563-567, (1997).

Tikhonov, A., *'On the solution of incorrectly stated problems and a method of regularization'*, Dokl. Acad. Nauk. SSSR, 151, 501-504, 1963.

Transtrum M.K., Machta B.B. and Sethna J.P.: *Geometry of nonlinear least squares with applications to sloppy models and optimization*, Phys. Rev. E, 83, 036701, 2011.

Turner, D. S., *'Absorption coefficient estimation using a two-dimensional interpolation procedure',* J. Quant. Spectrosc. Radiat. Transfer, 55, 633-637, 1995.

Young, A. T.: Refractivity of air, available at: http://mintaka.sdsu.edu/GF/explain/atmos_refr/air_refr.html (last access: 22 August 2019), 2011.

Valeri, M., Carlotti, M., Flaud, J.-M., Raspollini, P., Ridolfi, M., and Dinelli, B. M.: Phosgene in the UTLS: seasonal and latitudinal variations from MIPAS observations, Atmos. Meas. Tech., 9, 4655-4663, 2016.

Wells, R., '*Generation of optimized spectral grids',* Technical report for ESA study 11886/96/NL/GS, document: PO-TN-OXF-GS-0010, (14th July 1997).

Appendix A: Determination of the VCM of engineering tangent heights in MIPAS

Based on a memorandum prepared by M. Ridolfi and B. Carli, (22 July 1999)

A1. Introduction

The ORM code uses engineering pointing information in p,T retrieval. This information is included in the retrieval using the optimal estimation method, therefore also a realistic variance-covariance matrix (VCM) is needed for a proper weighting of engineering data by the inversion algorithm (see Sect. 4.2.6). Since the MIPAS pointing system is characterized only by very general engineering specifications, some assumptions must be made and an algorithm must be set up to build a realistic VCM of the engineering tangent altitudes, starting from the specified pointing performance. In this Appendix we present the algorithm used by the ORM for this purpose.

A2. MIPAS pointing performance

The VCM of pointing is built on the basis of some pieces of information provided by British Aerospace (BAe) which is responsible for the platform and for compiling the pointing budgets. BAe reports MIPAS pointing stability for 4.0 and 75 s time intervals for the three satellite axes (*x*-axis being the most critical for MIPAS pointing accuracy). *x*-axis stability, in terms of tangent altitude, is:

- 230 m for 4 s stability
- 660 m for 75 s stability

BAe provides also the total pointing accuracy:

- 2000 m is the total accuracy

The reported values have a confidence level of 95.4%, meaning that the above values are not exceeded in 95.4% of the cases. The errors are not purely gaussian because they include e.g. linear drifts due to temporary unavailability of the stars used by the satellite star sensors. However, in order to exploit the formalism of the statistics, we will consider these errors as gaussian with standard deviation equal to **half** of the above reported figures (Note: we are assuming that the stability provided by BAe is an excursion from an average value, a quarter should be used if the provided value is a peak-to-peak excursion).
BAe informs also that for time intervals between 4 and 75 s no analyses have been made, however in these cases, the best approximation is to linearly interpolate between the above reported figures. This approximation will not be exploited in the proposed algorithm because it does not provide realistic stability figures for time intervals much shorter than 4s and much longer than 75s. In Sect.A3 a more sophisticated interpolation scheme is proposed.
Another assumption we will use in the following is about the speed of MIPAS interferometer. We assume that MIPAS will be always operated at a 5 cm/s speed independently of the adopted spectral resolution. Furthermore we will assume the 'turn-around' time, i.e. the time required for speed inversion and positioning of the limb-scanning mirror, to be equal to 0.45 s. Scans with altitude step greater than 10 km characterized by a turn-around time greater than 0.45 s will not be considered here. In this hypothesis, the time Δt required for measuring a sweep with resolution identified by MPD is given by:

- $\Delta t_s = \frac{MPD(cm)}{5cm/s} + 0.45s$

A3. Algorithm

From the above figures, the total pointing error ($\sigma_{tot} = 1000$ m) can be intended as absolute error of the individual tangent heights, while the stability specifications can be exploited (as it will be explained) to derive the correlations between tangent heights.
Let's calculate explicitly the correlation $c_{i,k}$ between two generic tangent heights z_i and z_k, assuming that they have been measured at times t_i and t_k. The general expression of the correlation provides:

$$c_{i,k} = \frac{\sum_{j=1}^{N}(z_i(j) - \bar{z}_i)(z_k(j) - \bar{z}_k)}{\left[\left(\sum_{j=1}^{N}(z_i(j) - \bar{z}_i)^2\right)\cdot\left(\sum_{j=1}^{N}(z_k(j) - \bar{z}_k)^2\right)\right]^{\frac{1}{2}}} \quad \text{(A1)}$$

where $\bar{z}_i$ is given by:

$$\bar{z}_i = \sum_{j=1}^{N}\frac{z_i(j)}{N} \quad \text{(A2)}$$

and the index j ranges over an hypothetical set of N measurements of the tangent heights z_i and z_k with i,k =1, 2, …, N_{LS} (N_{LS} = number of sweeps in the considered limb-scanning (LS) sequence).
Let's indicate:

$$\varepsilon_i(j) = (z_i(j) - \bar{z}_i) \quad \text{(A3)}$$

$\varepsilon_i(j)$ is the error on $z_i(j)$ in the sense that it is the deviation of $z_i(j)$ from its 'true' value which is represented by the average of equation (A2).
If the two tangent heights z_i and z_k have been measured at times t_i and t_k such that $\Delta t = |t_i - t_k|$, their errors cannot differ too much due to the stability specifications of the pointing. In particular we will have:

$$\varepsilon_k(j) = \varepsilon_i(j) + \delta_{\Delta t}(j) \quad \text{(A4)}$$

where $\delta_{\Delta t}(j)$ is a random term with standard deviation $\sigma_{\Delta t}$. In order to calculate $\sigma_{\Delta t}$ from the specified short- and long- term stability we will use the following function:

$$\sigma_{\Delta t} = \sigma_{tot}\cdot\left(1 - \exp\left(-\alpha\cdot(\Delta t)^{\beta}\right)\right) \quad \text{(A5)}$$

with α and β constants determined imposing $\sigma_{\Delta t=4s} = \sigma_{4s}$ and $\sigma_{\Delta t=75s} = \sigma_{75s}$, where σ_{4s} = 115 m and σ_{75s} = 330 m are the standard deviations associated respectively to the 4s and to the 75 s specified stability. Please note that, as it is logically required, expression (A5) provides $\sigma_{\Delta t} \Rightarrow 0$ for $\Delta t \Rightarrow 0$ and $\sigma_{\Delta t} \Rightarrow \sigma_{tot}$ for $\Delta t \Rightarrow \infty$. The behavior of $\sigma_{\Delta t}$ as a function of Δt is plotted in Fig.A1.

The standard deviation of ε_k (equation (A3)) can be expressed as:

$$\frac{1}{N}\sum_{j=1}^{N}\varepsilon_k^2(j)=\frac{1}{N}\sum_{j=1}^{N}[\varepsilon_i(j)+\delta_{\Delta t}(j)]^2=$$
$$\frac{1}{N}\sum_{j=1}^{N}\varepsilon_i^2(j)+\frac{2}{N}\sum_{j=1}^{N}\varepsilon_i(j)\delta_{\Delta t}(j)+\frac{1}{N}\sum_{j=1}^{N}\delta_{\Delta t}^2(j)= \tag{A6}$$
$$\sigma_{tot}^2+\frac{2}{N}\sum_{j=1}^{N}\varepsilon_i(j)\delta_{\Delta t}(j)+\frac{1}{N}\sum_{j=1}^{N}\delta_{\Delta t}^2(j)$$

Now, since ε_k must have standard deviation equal to σ_{tot}, from equation (A6) we get:

$$\sum_{j=1}^{N}\varepsilon_i(j)\delta_{\Delta t}(j)=-\frac{1}{2}\sum_{j=1}^{N}\delta_{\Delta t}^2(j) \tag{A7}$$

Substituting expressions (A3) and (A7) in (A1) we obtain:

$$c_{i,k}=\frac{\sum_{j=1}^{N}\varepsilon_i(j)[\varepsilon_i(j)+\delta_{\Delta t}(j)]}{N\sigma_{tot}^2}=1-\frac{\sum_{j=1}^{N}\delta_{\Delta t}^2(j)}{2N\sigma_{tot}^2}\equiv 1-\frac{\overline{\delta_{\Delta t}^2}}{2\sigma_{tot}^2} \tag{A8}$$

where in the second step we have used:

$$\sigma_{tot}^2=\frac{\sum_{j=1}^{N}\varepsilon_i^2(j)}{N} \tag{A9}$$

Considering that:

$$\overline{\delta_{\Delta t}^2}=\sigma_{\Delta t}^2+\bar{\delta}_{\Delta t}^2 \tag{A10}$$

and that, from heuristic considerations, it should be:

$$\bar{\delta}^2=2\sigma_{tot}^2-\sigma_{\Delta t}^2-2\sigma_{tot}\sqrt{\sigma_{tot}^2-\sigma_{\Delta t}^2} \tag{A11}$$

equation (A8) becomes:

$$c_{i,k}=\sqrt{1-\frac{\sigma_{\Delta t}^2}{\sigma_{tot}^2}} \tag{A12}$$

From a more qualitative point of view, this very simple result can also be justified as follows. The tangent height z_k has two error components: the first component (σ_1) is linked to the measurement of the

neighboring tangent height z_i, the second component $\sigma_{\Delta t}$ does not depend on previous measurements. The two components must satisfy:

$$\sqrt{\sigma_{\Delta t}^2 + \sigma_1^2} = \sigma_{tot} \tag{A13}$$

since the error associated to z_i is σ_{tot}, the correlation between tangent heights z_i and z_k is by definition:

$$c_{i,k} = \frac{\sigma_1}{\sigma_{tot}} = \frac{\sqrt{\sigma_{tot}^2 - \sigma_{\Delta t}^2}}{\sigma_{tot}} = \sqrt{1 - \frac{\sigma_{\Delta t}^2}{\sigma_{tot}^2}} \tag{A14}$$

where the value for σ_1 has been extracted from equation (A13).
Equation (A12), together with expression (A5) provides the tool for calculating the correlation between two generic tangent heights z_i and z_k. This tool can be exploited for computing the VCM **S** of the tangent heights whose elements $s_{i,k}$ are given by:

$$s_{i,k} = \sigma_{tot}^2 \cdot c_{i,k} \tag{A15}$$

The VCM $\mathbf{V}^z$ relating to the differences between tangent heights (whose inverse is used by the ORM) can be obtained through the transformation:

$$\mathbf{S}_z = \mathbf{J}_\Delta \mathbf{S} \mathbf{J}_\Delta^T \tag{A16}$$

where $\mathbf{J}_\Delta$ is the jacobian matrix that represents the linear transformation leading from tangent heights to differences between tangent heights. If we indicate with $\Delta z_i \equiv z_{i+1} - z_i$, the jacobian $\mathbf{J}_\Delta$ contains the derivatives:

$$\left(J_\Delta\right)_{i,k} = \frac{\partial(\Delta z_i)}{\partial z_k} = \begin{cases} -1 & \text{if } i = k \\ 1 & \text{if } i = k-1 \\ 0 & \text{in the other cases} \end{cases} \tag{A17}$$

with $i = 1, \ldots, N_{LS}$ -1 and $k = 1, \ldots, N_{LS}$.

A4. Software module

A very simple software module has been implemented that computes the VCMs **S** and $\mathbf{S}_z$ of MIPAS pointing system using the explained algorithm. Beside the parameters defining pointing performances described in Sect.A2, the only inputs of this tool are the max. path difference and the number of sweeps of the limb-scanning sequence for which we want to calculate the VCM of pointings. The outputs of this program are:

- ✓ correlation matrix of tangent heights
- ✓ VCM of tangent heights
- ✓ correlation matrix of differences between tangent heights
- ✓ errors on differences between tangent heights
- ✓ VCM of differences between tangent heights
- ✓ inverse of VCM of differences between tangent heights

A5. Results

Figure A2 shows the correlations between different tangent heights for a scan of 16 sweeps and MPD = 20 cm as a function of the sweep index. Figure A3 shows the correlations of differences between tangent heights for the same scan of Fig. A2 as a function of the sweep index. The same quantities are reported in Fig's A4 and A5 respectively, for a scan of 16 sweeps and MPD = 5 cm (reduced resolution). In the adopted approach, the absolute errors of both tangent heights and differences between tangent heights are constant with altitude. The errors on differences between tangent heights depend however on the selected MPD. The dependence of these errors on the MPD is shown in Fig. A6. General comments are:

- the absolute error on tangent heights is a constant (does not depend on MPD)
- the correlation between tangent heights increases when decreasing the resolution (i.e. decreasing MPD)
- decreasing the resolution, in consequence of the increased correlations, the errors on the differences between tangent heights decrease (see Fig. A6).

A6. Adopted strategy for handling pointings VCM in Level 2

The quantity required in input to the ORM is the inverse of the VCM of the differences between tangent heights. Given the invariance of the obtained results with respect to the sweep index, the following approach has been adopted for storage / handling of pointing VCM in Level 2 framework, up to IPF version 7. The file 'PI_VCM.DAT' (defined in the ICD document, PO-IF-DOG-GS-0002, Issue 1c) contains VCMs of the tangent heights tabulated as a function of max. path difference. The tabulated VCMs refer to a scan with a maximal number N_{max} of sweeps (e.g. N_{max} = 30 sweeps). Given a scan with N_{sw} (with $N_{sw} < N_{max}$) sweeps to be analyzed and max. path difference MPD = xx, a block matrix of dimension N_{sw} x N_{sw} is extracted from the VCM relating to OPD = xx. Rows and columns relating to corrupted sweeps are then removed from this block. The remaining rows and columns are transformed according to equation (A16) and the resulting matrix is inverted and provided in input to Level 2 processor.
The ORM version 8 includes, in the pre-processing section, the software module presented in this appendix. This function is called when the actual value of MPD and the sets of limb views to be processed for each scan are already known and consolidated. In this way, the required inverse VCM of the pointing increments can be computed directly for each scan, without need of establishing a pre-tabulated set of VCMs of tangent heights, as it was done in earlier Level 2 versions.
Despite the differences existing between the algorithm presented here and the old algorithm developed during the first MIPAS pT retrieval study (ESTEC Purchase Order No: 142956 terminated in Sept.'95) for the calculation of pointing VCMs, the results of the two algorithms agree in the case of MPD = 20 cm. The old algorithm could not be used any further as it was limited to the case of constant spectral resolution. The analytical expression presented in this memorandum provides a more simple and flexible calculation tool.

Fig. A1 a: Stability error as a function of time. Log-scale x

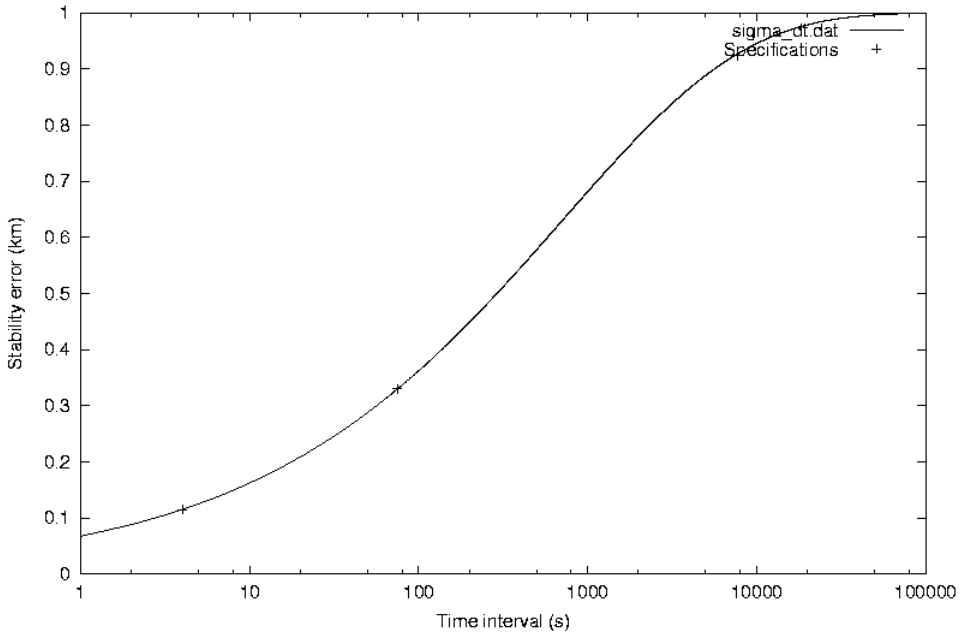

Fig. A1 b: Stability error as a function of time. Linear scale x

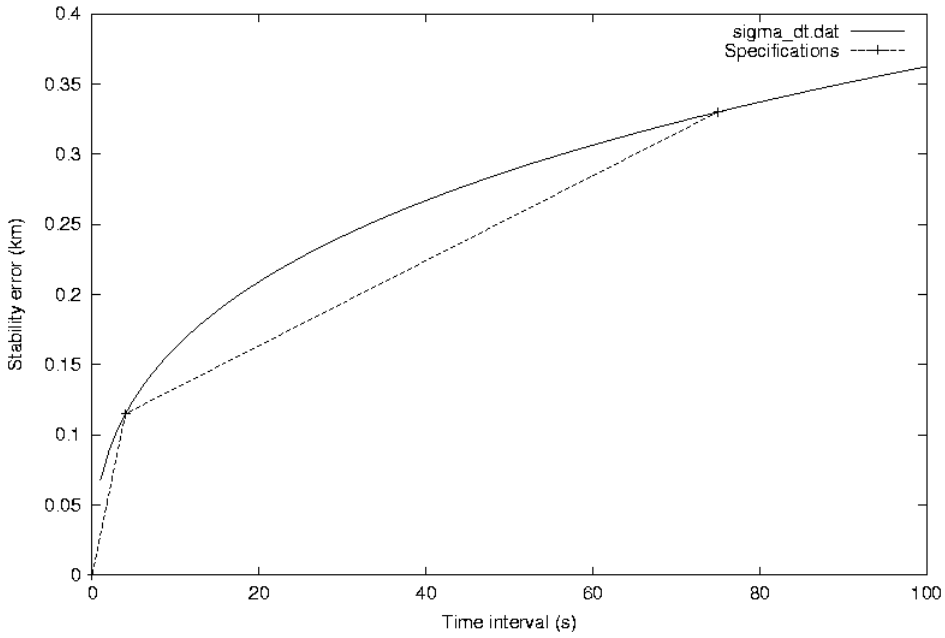

Fig. A2: Correlations between Z, OPD = 20 cm, N. of sweeps = 16

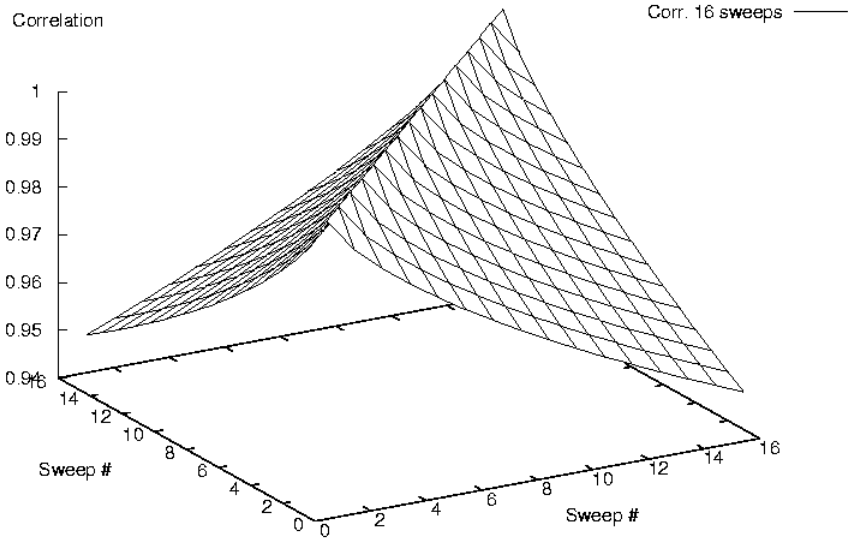

Fig. A3: Correlations between dZ, MPD = 20 cm, N. of sweeps = 16

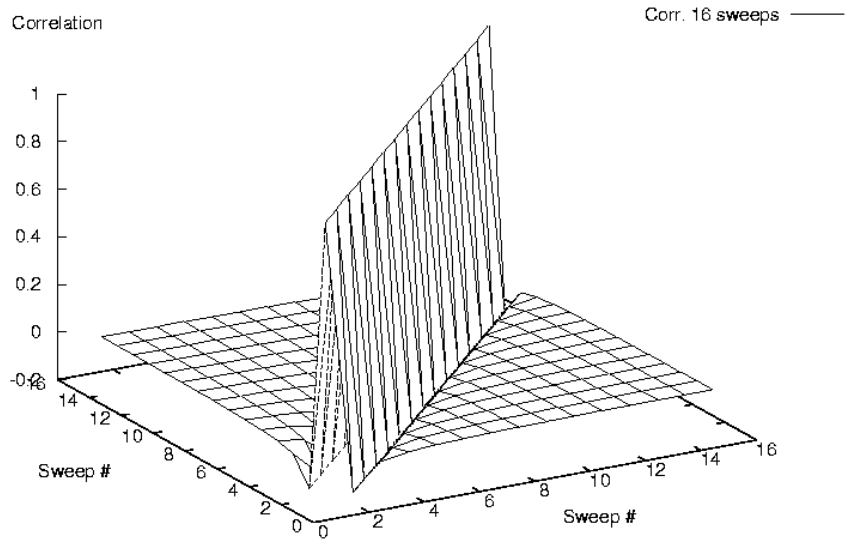

Fig. A4: Correlations between Z, OPD = 5 cm, N. of sweeps = 16

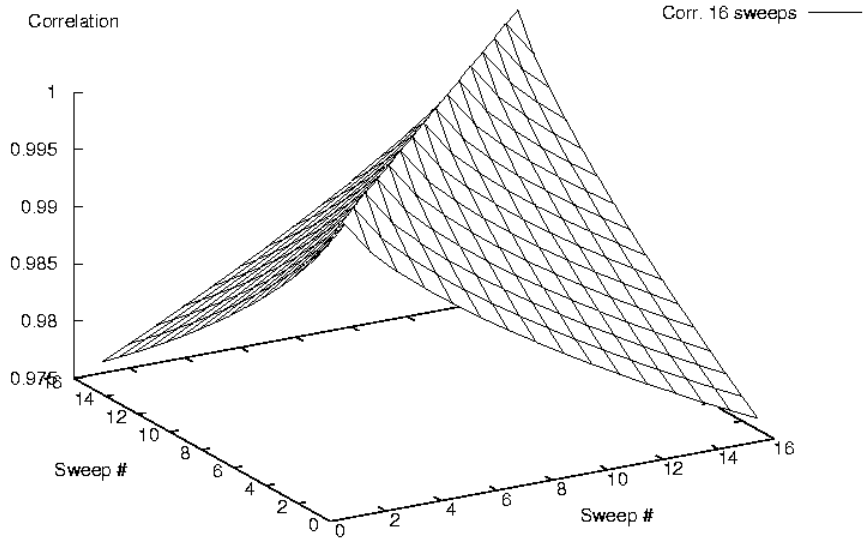

Fig. A5: Correlations between dZ, MPD = 5 cm, N. of sweeps = 16

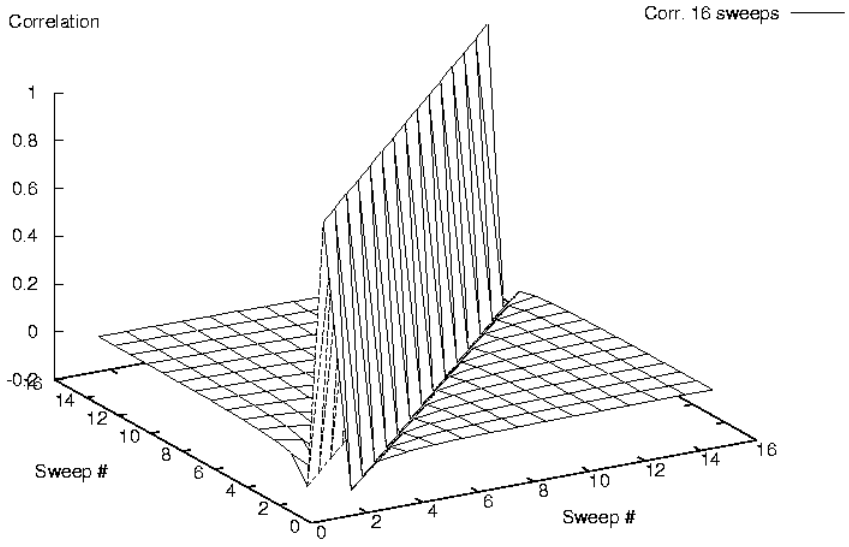

Fig. A6: Errors on dZ for different MPDs. Errors do not depend on sweep.

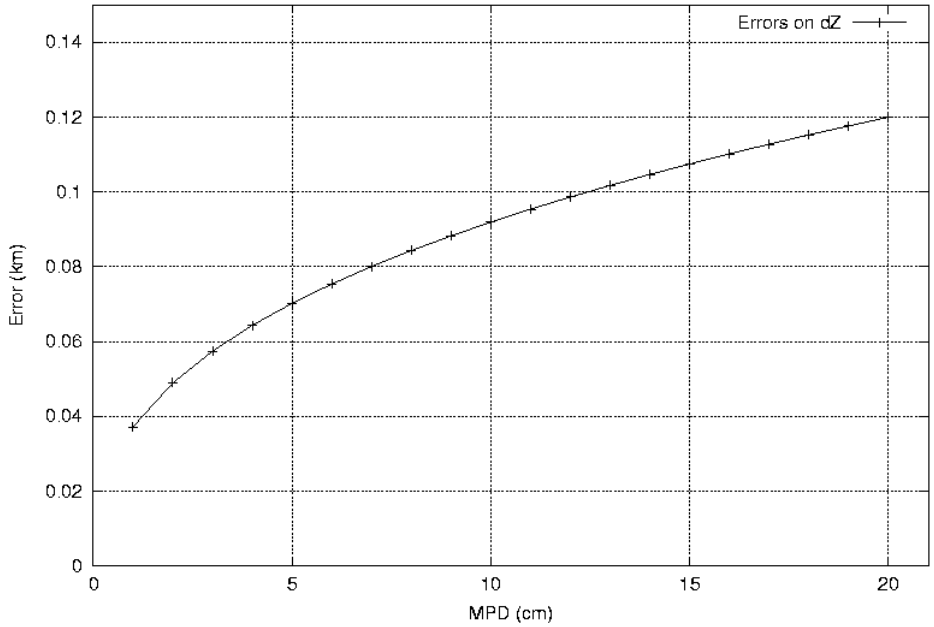

Appendix B: Evaluation of retrieval error components and total error budget

The recommendations arising from the 30th MIPAS Scientific Advisory Group meeting (ESTEC, 25th and 26th June 1998) regarding total retrieval error (see SAG minutes MIN-MIPAS-0030), can be summarized by the following statements:

- the random error affecting the retrieved profiles has two components:

  ⇒ The first random component is due to measurement noise. This component is evaluated as part of the inversion procedure (Gauss-Newton method) by the retrieval program. The ORM output files already contain the retrieved profile(s) variance-covariance matrix obtained from measurement noise (derived in Level 1b processing) without scaling by the actual χ^2 of the fit. This variance-covariance matrix is included in Level 2 products.

  ⇒ The second random component of profiles error is due to pressure and temperature error propagation in VMR retrievals. This component is evaluated, on-line, by a function implemented in Level 2 processor and is also included in Level 2 products.

- Systematic error on the retrieved profiles has several components:

  ⇒ **Contaminants**: this error component is due to imperfect assumption of the contaminant profiles in the forward model.

  ⇒ **Horizontal homogeneity error**: due to horizontal homogeneity assumption in the forward model (this error component is applicable only to Level 2 products version 7 and older)

  ⇒ **Spectroscopic errors**: are due to errors in spectroscopic data used by the forward model.

  ⇒ **Instrumental errors**. Due to imperfect (frequency and intensity) calibration of the observed spectra, imperfect knowledge of the ILS (and of the FOV).

  ⇒ **Model errors**. These are purely systematic errors biasing the simulated observations. For the moment only errors arising from neglecting Non-LTE and using LUTs and IGs in the forward model are expected to belong to this group.

Systematic errors in contaminant profiles, model assumptions, horizontal homogeneity, and instrument may have some 'random' character in the sense that, in principle, their value may vary from retrieval to retrieval. For this reason, the rule with which they combine may vary as a function of the application. This prevents the calculation of a total error budget valid in general.

The evaluation of the total systematic errors affecting the retrieved profiles is not a task of the Level 2 processor. A database has been developed at Oxford University containing systematic error profiles relating to Temperature and VMR profiles retrieved by the Level 2 processor. The database can be freely accessed from this link: http://eodg.atm.ox.ac.uk/MIPAS/err/ .

The retrieval error due to the mapping of the measurement noise into the solution of the retrieval is described by the random error covariance matrix included in the Level 2 products, calculated as described in Sect. 4.2.7.

Here below we describe how the Level 2 processor computes the random error component on the retrieved VMR profiles due to the propagation of the random error on the retrieved tangent pressures and temperature profile.

B1. Temperature and pressure induced errors in VMR retrievals

A generic retrieved VMR profile **x** is obtained through the inversion formula:

$$\boldsymbol{\Delta}_x = (\mathbf{K}^T\mathbf{S}_m\mathbf{K})^{-1}\mathbf{K}^T\mathbf{S}_m\boldsymbol{\Delta}_S \qquad \text{(B1.1)}$$

where $\boldsymbol{\Delta}_s$ is the residuals vector, $\mathbf{S_m}$ is the VCM of the observed spectra and **K** is the jacobian of the VMR retrieval. An uncertainty $\Delta(\mathbf{p},\mathbf{T})$ on the assumed tangent pressures and temperatures, translates into an error $\Delta_{\Delta S}$ on the simulated spectra and therefore into an error Δ_x on the retrieved profile equal to:

$$\boldsymbol{\Delta}_x = \mathbf{G}\boldsymbol{\Delta}_{\Delta S} = \mathbf{GC}\Delta(p,T) \qquad \text{(B1.2)}$$

where **C** is the matrix accounting for p,T error propagation in the simulated spectra of VMR retrieval and contains the derivatives:

$$C_{i,j} = \frac{\partial S_i}{\partial \begin{pmatrix} P \\ T \end{pmatrix}_j} \qquad \text{(B1.3)}$$

The index '*i*' identifies the fitted spectral points (as a function of frequency for all the microwindows and all the tangent altitudes) and the index '*j*' identifies the retrieved tangent altitudes. In equation (B1.2) we have assume **G** as locally independent of p,T (always true for small errors $\Delta(\mathbf{p},\mathbf{T})$).
In our case, the error on the retrieved p,T is described by a VCM $\mathbf{S}_{p,T}$, the corresponding VCM $\mathbf{S}_{x'}$ relating to $\boldsymbol{\Delta}\mathbf{x}$ and due to p,T error is given by:

$$\mathbf{S}_{x'} = \mathbf{GCS}_{p,T}(\mathbf{GC})^T = \mathbf{ES}_{p,T}\mathbf{E}^T \qquad \text{(B1.4)}$$

where we have defined **E** = **GC**. **E** is the matrix transforming p,T error into VMR error. The order of magnitude of the size of this matrix is (e.g. for FR measurements):

E: (17 VMR retrieved points) x (34 p,T retrieved points) x (4 bytes/datum) ≈ 2.3 Kb
In principle, matrix **E** depends on:

- current atmospheric status (p,T and VMR)
- set of adopted MWs in VMR retrieval (Occupation Matrix)

These dependencies have been studied with full details in Raspollini and Ridolfi, (2000). The strategy adopted in the Level 2 processor to calculate pT error propagation in VMR retrievals consists in:

- creating a database of **E** matrices: since matrix **E** depends on the chosen set of MWs (occupation matrix), we compute as many **E** matrices as many occupation matrices are defined for VMR retrievals. Matrices **E** are calculated by means of sensitivity tests.
- Modeling of a first order dependence of **E** on the atmospheric state is foreseen, via coefficients calculated with sensitivity tests. These coefficients, however, have never been used so far.
- $\mathbf{S}_{x'}$ is evaluated using equation (B1.4).

Appendix C: Generation of MW Databases and Occupation matrices

Microwindow selection is performed by an algorithm which simulates the propagation of random and systematic errors through the retrieval and attempts to maximise the information content (Bennett et al, 1999). The information content of a microwindow increases as the "log" of the determinant of the total covariance decreases, total covariance being the sum of the random and various systematic error covariances. Broadly speaking, 1 `bit' of information is equivalent to a factor 2 reduction in the uncertainty at one profile altitude.

Microwindows are created by first selecting a number of single measurements, identified by location in the spectral and tangent altitude grids, as starting points. Adjacent measurements are added to each until the information content no longer improves or the maximum width of 3 cm^{-1} is reached. The best of these trial microwindows is selected, the retrieval covariance modified, and the process repeated for a new set of measurements as starting points. The procedure of growing microwindows also allows for measurements within microwindows to be `masked', i.e., excluded from the retrieval. This usually applies to measurements where the associated systematic errors such as the uncertainty in modelling a contaminant, outweigh any benefit in the reduction of the random error when considering the total covariance.

Initially, a set of typically 10 microwindows, or 10000 measurements (whichever occurs first) is selected based on the assumption that spectra for all MIPAS bands are available. Further microwindows are then selected to maximise information retrieved in situations where data from different bands may be unavailable. This set of 20-30 microwindows constitutes the database.

Occupation matrices represent subsets of microwindows to be used under different retrieval circumstances, and these are constructed using the same approach: selecting the microwindows from the database (rather than growing new microwindows) in the sequence which maximises the retrieved information. A number of these OMs are pre-computed, corresponding to different band-availabilities, and associated with each of these is a single figure-of-merit representing the information content.

Further details of the algorithm used to grow optimised spectral microwindows are included in Dudhia, (2000 a), Dudhia, (2000 b) and in Dudhia, (2001).

From the above description it is clear that a side product of this algorithm is the total error affecting the retrieved profiles as a function of altitude. By operating the algorithm without constraints limiting the maximum number of observations included in the analysis, it is possible to obtain ultimate accuracy figures for the parameters retrieved from MIPAS measurements.

For each of the measurement scenarios of the two mission phases (FR and OR, see Appendix F) and each target retrieval parameter, an occupation matrix has been established. The various error components evaluated by the algorithm illustrated above are shown in the following web page maintained at the University of Oxford: http://eodg.atm.ox.ac.uk/MIPAS/err/ .

Figures C1 and C2 show, for the highest priority retrieval parameters and the two mission phases, the ultimate retrieval accuracy. The estimation of the retrieval accuracy for the profiles of the Optimized Resolution (OR) part of the mission (after January 2005) does not take into account the regularization applied. This is because the regularization strength is self-adapting and, therefore, changes on the basis of the actual atmospheric state. As a consequence, the accuracy reported in Fig. C2 should be regarded as an upper bound for the actual profile accuracy.

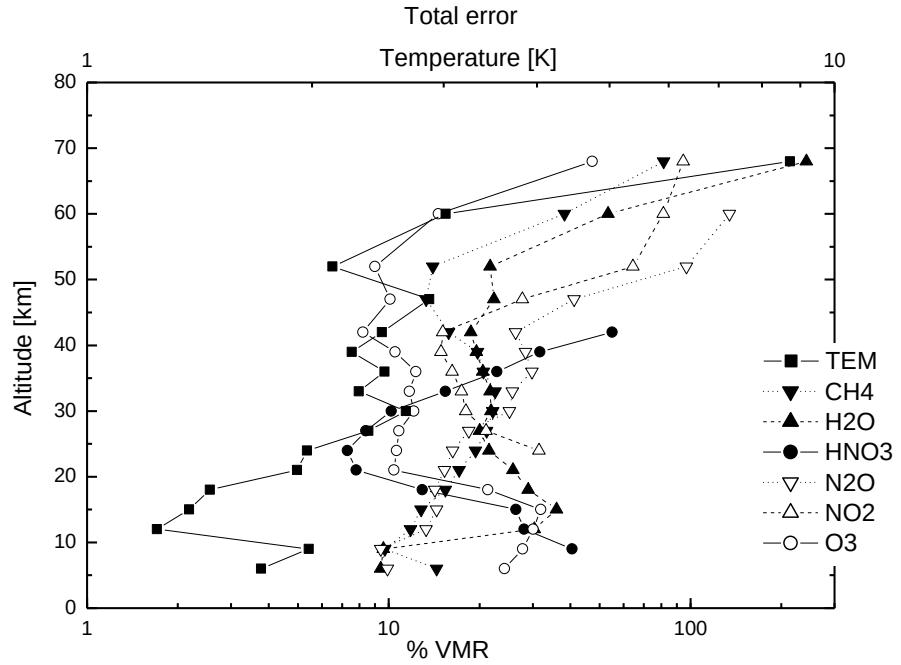

Fig. C1: Ultimate accuracy of the highest priority retrieval targets for the Full Resolution measurements (acquired before January 2005).

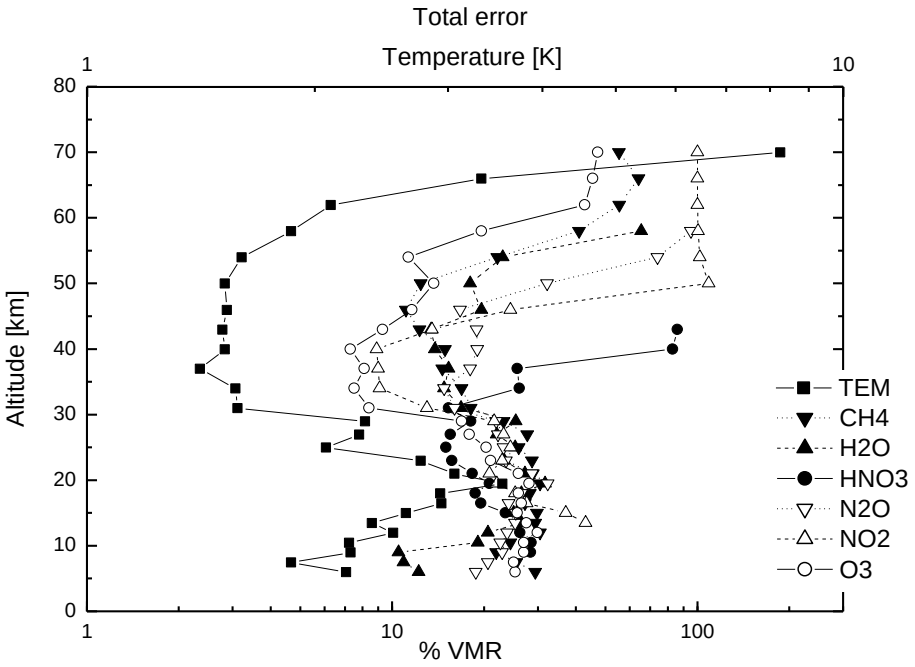

Fig. C2: Ultimate accuracy of the highest priority retrieval targets for the Optimised Resolution measurements (acquired after January 2005).

Appendix D: Generation of LUTs and Irregular frequency Grids (IG)

The creation of lookup tables and the irregular grids for spectral calculations is a process consisting of four stages (Dudhia et al, 1999).

The first stage is to determine the significant absorbers for each microwindow. The maximum radiance for all potential absorbers is assessed considering atmospheres containing just that absorber in isolation with its maximum concentration. Any absorber contributing more than 10% of the NESR is considered significant and added to the absorber list for the microwindow.

The second stage is to establish the tabulation axis increments in temperature and ln[pressure] for the absorber look-up tables. Large tables (i.e., small axis increments) of monochromatic absorption coefficient are initially created for all microwindow absorbers. MIPAS radiances are modelled for three different atmospheres (representing nominal, minimum and maximum absorber concentrations) using these tables and compared with line-by-line calculations for the same cases. The tabulation axis increments are iteratively increased for each absorber until the maximum discrepancy reaches NESR/30.

The third stage is to perform the singular value decomposition (SVD) of these tables. Initially, each absorber table is SVD-compressed, retaining 30 singular values. MIPAS radiances are modelled using the SVD-compressed tables for the three atmospheres as in the previous stage, and compared with the same line-by-line calculations. The number of singular values for each absorber table is iteratively reduced until the maximum discrepancy reaches NESR/15.

The fourth stage is to determine the irregular grid for spectral integration. This starts with the MIPAS radiances calculated with the SVD-compressed LUTs in the previous stage, which are determined on a regular fine grid (0.0005 cm^{-1} spacing) prior to the AILS convolution. Grid points are then selectively removed until the maximum discrepancy compared to a line-by-line on the full spectral grid reaches NESR/10.

Appendix E: Generation of MW-dedicated spectral linelists

By feeding a given line-by-line radiative transfer forward model only with the spectral lines actually needed for the microwindows and measurement geometry under consideration, a lot of computation time can be saved. This lines selection can be performed either online, i.e. during the run of radiative transfer codes or offline. Off-line, spectroscopic data preselection offers the advantage, that the importance of a certain transition can be more easily assessed on the basis of the related radiance signal rather than by means of absorption cross sections. This is particularly important for nonlinear radiative transfer in the case of a non-isothermal atmosphere.

Each transition in the MIPAS-specific spectroscopic database (HITRAN_MIPAS_PFxx) within 25 cm^{-1} of the microwindow boundaries is examined, while lines outside this margin are assumed to be parametrized by a continuum model. The effect of neglecting a line in radiance calculations is estimated for each nominal MIPAS tangent altitude between 5 and 83 km and for each predefined microwindow and forms the basis of the decision whether a line should be included or excluded. For reasons discussed below, the contribution of a spectral line has to be assessed within an iterative loop. Therefore, a simple and quick approach to estimate the contribution of a transition is needed, in order to reduce computation time to tolerable limits. A common and simple approach for this purpose is to neglect convolution by any lineshape function and to approximate the contribution of a spectral line, L as

$$S_l = B(T^{CG}) \times (1 - \exp(-S_{li}\ (T^{CG}) \times M^{ip})) \qquad \text{(E1)}$$

for a homogeneous atmosphere where

S_l = radiance
T^{CG} = Curtis-Godson mean value of temperature over whole path,
B = Planck function
S_{li} = line intensity
$M^{ip}{}_i$ = integrated mass of the gas along the optical path.

This approach is equivalent to the so-called $S \times M$ spectra which are commonly used to estimate the radiance contribution of a transition. This approximation, however, which avoids both layer-by-layer calculation and evaluation of the line shape, while being favourable with respect to computational expenses, turned out not to be satisfactory in terms of accuracy. We found, that for tangent altitudes below the stratopause, the homogeneous and optically thin approximation is not sufficient, because higher and thus warmer layers in the atmosphere significantly contribute to the spectrum. Furthermore, due to pressure broadening and spectral apodization, signal from other lines is imported to the signal at a particular line center. Therefore, we had to account for more realistic line shapes.
A more sophisticated approach describes the monochromatic radiative transfer through the atmosphere by a two-layer model which supports temperature inhomogeneities:

$$\begin{aligned} S_l = {} & B(T_1^{CG}) \times (1 - \exp(-k_1^{acs}(T_1^{CG}, p_1^{CG}) \times M_1^{ip})) \times \exp(-k_2^{acs}(T_2^{CG}, p_2^{CG}) \times M_2^{ip}) \\ & + B(T_2^{CG}) \times (1 - \exp(-k_2^{acs}(T_2^{CG}, p_2^{CG}) \times M_2^{ip})) \end{aligned} \qquad \text{(E2)}$$

with:

$p^{CG}{}_1$, $p^{CG}{}_2$ = Curtis-Godson mean values of pressure in layers 1 and 2, respectively,
$T^{CG}{}_1$, $T^{CG}{}_2$ = Curtis-Godson mean values of temperature in layers 1 and 2, respectively,
$M^{ip}{}_1$, $M^{ip}{}_2$ = slant path column amounts in layers 1 and 2, respectively,

k_1^{acs}, k_2^{acs} = absorption cross sections in layers 1 and 2, respectively.

The optimal layering turned out to be such that the slant path absorber amount in the tangent layer M_1 is about 96% of the total slant path column amount $M^{ip}{}_1 + M^{ip}{}_2$.
The line shape is modelled by the Voigt function. The radiance spectra are convolved with a triangular (in frequency space) apodization function leading to a spectral resolution of 0.05 cm^{-1} in terms of FWHM (= full width at half maximum). The frequency grid is set up using 5 gridpoints within each HWHM (= half width at half maximum) of each line, and a coarser grid in the gaps between the lines.
By this model, the contribution of other lines are explicitly considered at the center of one particular line under consideration. However, continua (aerosols etc.) and no gases for which only absorption cross-sections but no spectroscopic line data are available (CFCs etc.) are not taken into account. This simplified model provides reasonably accurate radiance spectra within a tolerable amount of computing time. For all cases checked, it was within 10 - 20% of the "true" radiance usually providing an overestimate of the true radiance. It should be mentioned again that the purpose of this simplified radiance modelling is only to assess the importance of a certain transition within a line rejection loop.
Due to non-linearity of radiative transfer and the contribution of overlapping lines to the radiance at a particular line position, and since the contribution of each line considered for exclusion depends on the signal of lines still to be included, this approach requires an iterative processing. Starting with the spectrum of all lines, the radiance spectrum of lines considered for exclusion is compared to an error threshold. By checking the spectrum of neglected lines only rather than the difference between all-lines and selected-lines spectra, it is guaranteed not to underestimate the contribution of any line in a potentially saturated spectrum. Within each iteration step, the lines contributing most to this 'error spectrum' are re-included in the list of transitions to be considered.
Selection criteria are based on the expected apodized noise equivalent spectral radiance (NESR) of the MIPAS instrument. The error threshold to fall below in any case is set to NESR/10. In a first step, lines from outside the microwindows are selected according to their radiance contribution within the microwindow. Those lines remaining in the linelist for a microwindow will therefore provide a sufficiently accurate estimate of the overall contribution from outside lines. Due to non-linearity in radiative transfer, this continuum-like contribution has to be taken into account when selecting the lines lying inside the microwindow.
The treatment of lines outside the microwindow is performed as follows: Only HITRAN_MIPAS_PF_xx lines less than 25 cm^{-1} from the microwindow boundaries are considered for further investigation. First, lines are sorted according to the criterion:

$$\alpha \times S_{li} \times \left(M_l^{ip}\right)^2 \times \left(\frac{\partial k^{acs}}{\partial \nu}|_{\nu_1} - \frac{\partial k^{acs}}{\partial \nu}|_{\nu_2}\right) \qquad \text{(E3)}$$

where

S = line intensity of candidate transition
α = Lorentzian half width of the candidate transition
M_l^{ip} = mass in tangent layer
$\frac{\partial k^{acs}}{\partial \nu}|_{\nu_1}$ = wavenumber derivative of absorption coefficient at microwindow boundary ν_1
$\frac{\partial k^{acs}}{\partial \nu}|_{\nu_2}$ = wavenumber derivative of absorption coefficient at microwindow boundary ν_2

This expression weights the contribution of the considered line to the radiance of a far wing continuum brought in by lines from outside the microwindow. Furthermore, it gives less weight to weakly

frequency-dependent contributions, reflecting the fact that in the OFM/ORM the continuum-like signal is not modelled on a line-by-line basis.
Beginning with the weakest ones, according to this criterion, lines are excluded as long as the apodized radiances of the excluded lines at the microwindow boundaries do not exceed a pre-defined threshold which depends on the apodized noise equivalent spectral radiance and the radiance of all lines at the microwindow boundary under consideration:

a) $T_a = 0.07$ NESR if $L_b \geq 0.7$ NESR
b) $T_a = 0.1\ L_b$ if 0.7 NESR $> L_b \geq 0.07$ NESR
c) $T_a = 0.007$ NESR if $L_b \leq 0.07$ NESR.

For exclusion of lines inside the microwindow, the threshold for the maximum allowed radiance signal of removed lines is calculated from the maximum radiance of all lines.

a) T_i = NESR/10 if $L_{max} \geq$ NESR,
b) $T_i = L_{max}/10$ if $L_{max} <$ NESR.

If at any spectral gridpoint ν inside the microwindow the radiance signal of excluded lines exceeded the threshold, T_i, the line which contributed most at this spectral gridpoint and is centered within a predefined interval $\nu \pm \Delta\nu/2$ where $\Delta\nu$ = apodized spectral resolution = 0.05 cm^{-1}, is re-included to the linelist. This step is repeated iteratively as long as the threshold is no longer exceeded at any spectral gridpoint. In order to avoid endless loops, lines once re-included are never again excluded. Typically after 5 to 10 iterations the error threshold is no longer reached at any spectral gridpoint within the microwindow. By checking the radiance spectrum of the potentially negligible lines instead of checking the residual spectrum between full calculation and calculation with a reduced linelist, a conservative estimate of the contribution of the neglected lines is achieved.
The remaining lines are compiled in a database which is organized microwindow by microwindow and contains, beside spectroscopic data, the following table entries:

- tangent altitude range where a line has to be considered
- a flag indicating whether the line shape has to be evaluated on a fine grid or if a coarse grid is sufficient

The suitability and appropriateness of the produced linelists is checked by FASCOD2 reference calculations. FASCOD2 radiance spectra were calculated with the full HITRAN_MIPAS_PF_xx database and the selected linelist for more than 70 cases. These test calculations proved that the radiance difference due to neglecting lines is always significantly below the MIPAS NESR, thus justifying the two-layer approach for the purpose of lines selection.
The efficiency of line reduction is very high due to the optimized iterative selection scheme. The number of lines outside a microwindow (corresponding to a 25 cm^{-1} interval around the microwindow) that need to be considered is reduced to 0.15 - 1.8% of the full set in HITRAN_MIPAS_PF_xx for low tangent heights (< 20 km) while for tangent heights above 40 km it is less than 0.03%. Inside the microwindows, 17 - 77% of the full HITRAN_MIPAS_PF_xx lines contribute considerably below 20 km, and 1.3 - 18% have to be used above 40 km (see Table 1). The resulting reduction of computational time for the line-by-line absorption coefficient calculation is directly proportional to the line number reduction.

Target gas	Number of mw's	Average number of HITRAN lines	Reduced number of lines (target and contaminant gases) in the linelist [% of full HITRAN]					
O3	121	Out: 23331 In: 255	1.1 53	0.73 42	0.26 31	0.032 18	0.003 8.7	0 5.1
p-T	130	Out: 23309 In: 111	1.8 44	0.67 40	0.17 30	0.034 15	0.001 6	0.001 2.5
H_2O	101	Out: 9107 In: 152	0.302 24	0.145 18	0.034 11	0.001 4.4	0 2.1	0 1.4
CH_4	57	Out: 22562 In: 230	0.66 53	0.31 41	0.048 20	0.001 2.9	0 2.2	0 1.8
N_2O	45	Out: 15209 In: 116	0.63 34	0.23 24	0.033 12	0 5	0 4.9	0 4.2
HNO_3	47	Out: 27349 In: 729	0.9 77	0.78 72	0.16 36	0.001 15	0 9.5	0 4.6

Table 1: Averaged line reduction efficiency for the 6 target gases.

Appendix F: MIPAS observation modes

In the first two years of the mission, most of the MIPAS measurements were acquired in the nominal mode consisting of 17 sweeps per scan, with tangent heights ranging from 6 to 68 km, at steps of 3 km from 6 to 42 km, of 5 km from 42 to 52 km and of 8 km from 52 to 68 km. A small number of measurements were acquired in *special modes*.

The special mode measurements performed before January 2005 are defined as:

S1 Polar Chemistry and Dynamics:
rear view; tangent heights = 7-55 km, height step = 2-10 km,
horizontal spacing = 420 km.

S2 Stratosphere/troposphere exchange, troposphere chemistry:
rear view, tangent heights = 5-40 km, height step = 1.5-10 km,
horizontal spacing = 420 km.

S3 Impact of Aircraft emission:
side view; tangent heights = 6-40 km, height step = 1.5-10 km,
horizontal spacing = 330 km.

S4 Stratospheric Dynamics:
rear view; tangent heights = 8-53 km, height step = 3 km,
horizontal spacing = 390 km.

S5 Diurnal changes:
side views; tangent heights =15-60 km, height step = 3 km,
horizontal spacing = 480 km.

S6 Upper troposphere / Lower stratosphere:
rear view, altitude range 6-35 km, height step 7-2 km, horizontal spacing = 120 km.

S7 Upper atmosphere:
rear view; tangent heights = 20-160 km, height step = 3-8 km,
horizontal spacing = 800 km.

After January 2005 (in the so called Optimized Resolution mission) both nominal and special modes have been redefined. For the nominal observation mode a floating altitude-sampling grid is adopted in order to roughly follow the tropopause height along the orbit, with the requirement to collect at least one spectrum within the troposphere but to avoid too many cloud-affected spectra which are hard to analyse. The following formula provides the lowest tangent altitude as a function of the tangent point latitude:

$$\text{minimum\_tangent\_altitude} = C - D * \cos(90° - |\text{tangent\_point\_latitude}|)$$

with C=12 km and D=7 km

Table F1 provides a detailed description of the nominal observation mode adopted after January 2005.

Table F1. Nominal observation mode adopted after January 2005.

Mode	**NOM**		
Floating altitude grid	yes		
# of altitude grid points	27		
Approx. along track sampling (km)	410		
Sample Latitude	90°	45°	0°
Tangent altitudes (km)			
	5	7.05	12
	6.5	8.55	13.5
	8	10.05	15
	9.5	11.55	16.5
	11	13.05	18
	12.5	14.55	19.5
	14	16.05	21
	15.5	17.55	22.5
	17	19.05	24
	18.5	20.55	25.5
	20	22.05	27
	22	24.05	29
	24	26.05	31
	26	28.05	33
	28	30.05	35
	30	32.05	37
	33	35.05	40
	36	38.05	43
	39	41.05	46
	42	44.05	49
	45	47.05	52
	49	51.05	56
	53	55.05	60
	57	59.05	64
	61	63.05	68
	65.5	67.55	72.5
	70	72.05	77

The special mode measurements defined for the mission phase after January 2005:

UTLS-1	Upper Troposphere Lower Stratosphere (primary UTLS mode)
UTLS-2	Upper Troposphere Lower Stratosphere (Test mode for 2-D retrievals)
MA	Middle Atmosphere
NLC	Middle/Upper atmosphere in summer (Noctilucent clouds)
UA	Upper Atmosphere
AE	Aircraft Emissions

For the UTLS-1 mode a floating altitude-sampling grid is adopted, according to the following formula which provides the lowest tangent altitude as a function of the tangent point latitude:

minimum_tangent_altitude = A + B * cos (2*tangent_point_latitude)

with A=8.5 km and B=3 km

Table F2 provides a detailed description of the special observation modes adopted after January 2005.

A schematic summary of MIPAS measurement modes, as well as the related "mission plan" documents are available at the following web-pages maintained by A.Dudhia at University of Oxford:

- FR modes: http://www.atm.ox.ac.uk/group/mipas/frmodes.html (years 2002-2004)
- OR modes: http://www.atm.ox.ac.uk/group/mipas/rrmodes.html (years 2005 - onward)

Table F2. Special observation modes adopted after January 2005.

Mode	UTLS-1		UTLS-2	MA	NLC	UA	AE
Floating altitude grid	yes		no	no	no	no	no
# of altitude grid points	19		11	29	25	35	12
Approx. along track sampling (km)	290		180	430	375	515	n.a.
Sample Latitude	90°	0°	0-90°	0-90°	0-90°	0-90°	Sector *
Tangent altitudes (km)							
	5.5	11.5	12	18	39	42	7
	7	13	14	21	42	45	8.5
	8.5	14.5	16	24	45	48	10
	10	16	18	27	48	51	11.5
	11.5	17.5	20	30	51	54	13
	13	19	23	33	54	57	15
	14.5	20.5	26	36	57	60	17
	16	22	29	39	60	63	20
	17.5	23.5	33	42	63	66	24.5
	19	25	37	45	66	69	29
	21	27	42	48	69	72	33.5
	23	29		51	72	75	38
	25	31		54	75	78	
	28	34		57	78	81	
	31	37		60	79.5	84	
	35.5	41.5		63	81	87	
	40	46		66	82.5	90	
	44.5	50.5		69	84	93	
	49	55		72	85.5	96	
				75	87	99	
				78	90	102	
				81	93	107	
				84	96	112	
				87	99	117	
				90	102	122	
				93		127	
				96		132	
				99		137	
				102		142	
						147	
						152	
						157	
						162	
						167	
						172	

* Latitude-longitude sector covered by AE mode for the North-Atlantic flight corridor: 30-70° Latitude North, 80°W-20°E Longitude.